Analysis of Tow-Placed, Variable-Stiffness Laminates

Chris Waldhart

Thesis submitted to the Faculty of the
Virginia Polytechnic Institute and State University
in partial fulfillment of the requirements for the degree of

MASTER OF SCIENCE
IN
ENGINEERING MECHANICS

Approved:
Zafer Gürdal, Chair
Calvin Ribbens
Robert M. Jones

June 5, 1996
Blacksburg, Virginia

Keywords: Variable-stiffness laminates, curvilinear fibers, tow placement machine, buckling

Design of Tow-Placed, Variable-Stiffness Laminates

Chris Waldhart

(Abstract)

It is possible to create laminae that have spatially varying fiber orientation with a tow placement machine. A laminate which is composed of such plies will have stiffness properties which vary as a function of position. Previous work had modelled such variable-stiffness laminae by taking a reference fiber path and creating subsequent paths by shifting the reference path. This thesis introduces a method where subsequent paths are truly parallel to the reference fiber path. The primary manufacturing constraint considered in the analysis of variable-stiffness laminates was limits on fiber curvature which proved to be more restrictive for parallel fiber laminae than for shifted fiber. The in-plane responses of shifted and parallel fiber variable-stiffness laminates to either an applied uniform end shortening or in-plane shear were determined. Both shifted and parallel fiber variable-stiffness laminates can redistribute the applied load thereby increasing critical buckling loads compared to traditional straight fiber laminates. The primary differences between the two methods is that parallel fiber laminates are not able to redistribute the loading to the degree of the shifted fiber. This significantly reduces the increase in critical buckling load for parallel fiber variable-stiffness laminates over straight fiber laminates.

Acknowledgements

I would like to express gratitude to my advisor, Dr. Zafer Gürdal, and Dr. Calvin Ribbens for making the time to answer the seemingly endless line of questions I had during the past couple of years. I would also like to thank Dr Robert M. Jones for being on my advisory committee. Finally, I would like to acknowledge the financial support offered by NASA Langley Research Center under grant NAG-1-643, Boeing Defense and Space Group, and the NASA Multidisciplinary Analysis and Design Fellowship Program.

Contents

List of Figures

List of Tables

Chapter 1

Introduction

Composite materials are being used in an effort to create efficient structures which are tailored to specific applications. By combining layers with various fiber orientation, material properties, or thickness, it is possible to have a laminate which responds favorably to a prescribed loading condition. Traditional design considers these lamina properties to be constant throughout the entire ply. In many applications, the traditional design methods will produce quite satisfactory results. However, it is desirable to consider ways to further tailor the design of composite materials so that the resulting structures will offer an advantage over current practices (such as lighter weight, reduced manufacturing cost, better thermal properties, and so on). One concept which has been utilized in expanding the tailorability of the design of composite structures is the idea of variable-stiffness composite laminates.

1.1 Methods of Creating Variable-Stiffness Composite Laminates

There are many ways to create a variable-stiffness composite laminate including, but not limited to, dropping plies in the laminate, varying the fiber volume fraction in a ply, and changing the fiber orientation within a lamina. In each case, the resulting structure will have spatially varying properties. By having a structure which changes its properties as a function of position, it becomes possible to redistribute an applied loading so that a more favorable loading condition is encountered in a critical region of the structure. This section will review previous research which was able to improve upon a design using the concept of variable-stiffness laminates.

A typical method to change the thickness of a laminate is to drop a ply. An example of a laminate with a dropped ply is shown in Figure 1.1. This laminate is initially composed of four plies at $x = 0$. In order to reduce the laminates thickness at $x = a$ while still maintaining a flat, continuous surface on the lower edge, the ply on the upper surface is terminated after $x = a$. Dropping this ply causes the laminate to have its stiffness properties changing as a step function at $x = a$. For the laminate presented in Figure 1.1, the section of the laminate from $x = 0$ to $x = a$ has a $[0/\pm 45/90]$ layup and after $x = a$ has a $[\pm 45/90]$ stacking sequence.

DiNardo and Lagace have researched the effect of internal dropped plies on the buckling of compressively loaded plates [1]. Dropping a ply will change the elastic properties of the structure as well as introduce an eccentricity in loading. The result of these changes is that bending and twisting of the laminate will occur when the plate is only under applied in-plane loading. In Reference [1], three types of plates are examined: a typical flat plate, a plate having internally dropped plies, and laminates with plies that have sudden changes in fiber orientation angles. When considering the reduction in buckling loads for laminates with dropped plies, it is convenient to define a longitudinal

bending stiffness ratio between the region with the dropped ply and the undropped section. A linear relationship appears, both experimentally and numerically, between the ratio of the buckling loads for a laminate with and without dropped plies and the longitudinal bending stiffness ratio. The conclusion from portion of the study is that a reduction in the D_{11} term of the laminate having a dropped ply was proportional to the reduction in critical buckling load relative to an initial laminate having uniform thickness. A similar trend was found for laminates which had plies with sudden changes in fiber orientations. However, this relation was more complicated than the dropped ply case because the variation in critical buckling load took into account the relative magnitude of fiber orientation change between the two sections. Over all, the changes in buckling of laminates with either dropped plies or sudden changes in fiber orientation are primarily dependent upon the change in stiffness experienced by the laminate and not from the loading eccentricity due to the change in the laminate midplane.

Still another technique which results in a structure which has variable properties is to vary the fiber volume fraction as a function of position. An example of varying fiber volume fraction is provided in Figure 1.2 where a ply with a fixed cross section has the fiber volume fraction increasing from the left edge to the right. This will cause an increase in stiffness towards the right edge since the fibers are much stiffer compared to the matrix.

Leissa and Martin have solved the vibration and buckling of a rectangular composite ply composed of variably spaced straight and parallel fibers [2]. When dealing with a varying fiber spacing, it becomes necessary to treat the material as being nonhomogeneous on both the macroscopic and microscopic levels. The resulting stress-strain relationship can be expressed in terms of the engineering constants for both the fiber and matrix properties through the law of mixtures. In this case, the stiffness properties will not be constant as they are for uniformly spaced fiber laminae.

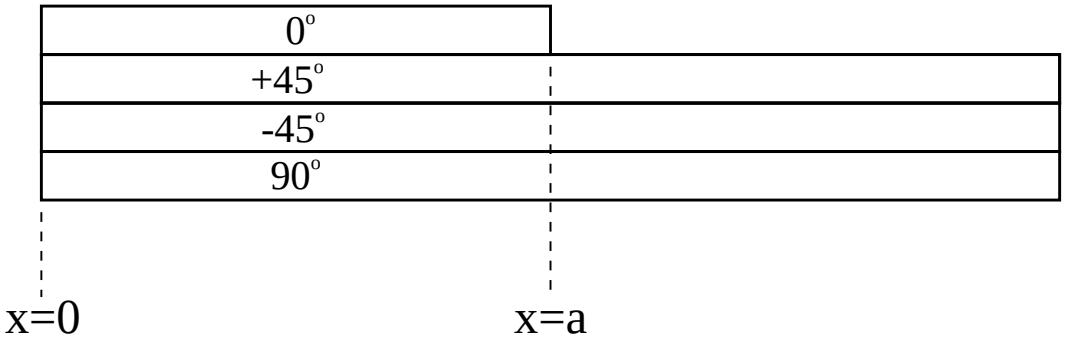

Figure 1.1: Laminate with a dropped ply.

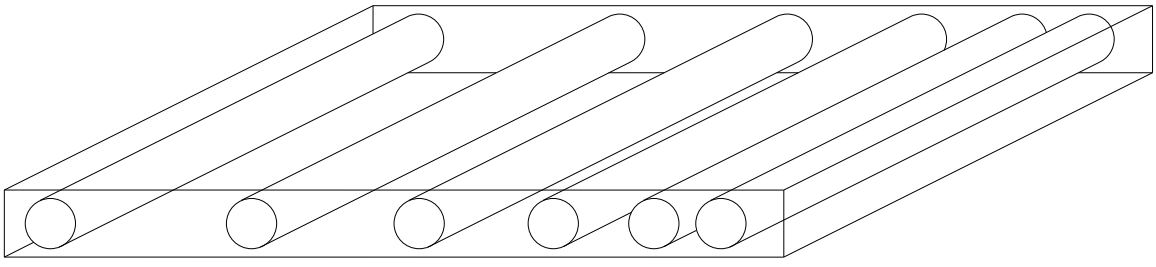

Figure 1.2: Lamina with variable fiber volume fraction.

Since fiber spacings were assumed to only vary in the x direction, the lamina stiffness properties will only be functions of the x location. This results in having variable coefficients in the governing equations which greatly complicates the in-plane solution. The Ritz method was used to solve the resulting in-plane elasticity problem. This solution was then utilized in the vibration and buckling analyses which again employed the Ritz method. By varying the fiber spacing in the x direction, several cases were able to significantly increase both the critical buckling load and the fundamental frequency of vibration. While improvements were found for several spacing variations, cases were also present which lowered both parameters.

The final example of a variable property composite structure is a ply that has its fiber orientation varying as a function of position, Figure 1.3. The properties of a given ply are dependent on the fiber orientation relative to the geometric axis of the panel. By varying this orientation with position, the ply will have properties which also change with position.

One example of research dealing with spatially varying fiber orientation is the work by Hyer and Charette [3]. The goal of this work was to increase the failure load of a composite plate with a circular hole under tensile loading by varying the fiber orientation with respect to position. The goal was to orient the fibers so that they were somewhat aligned with the principal stress directions over a given region of the panel. This was modelled iteratively using a finite element analysis in which the fiber direction is assumed to be constant within a given element but changed in discrete steps from one element to another. The initial fiber orientations were such that for a given element, the fibers were oriented along the larger principal stress direction of an isotropic plate. A new stress distribution was found using the prescribed fiber orientations which was in turn used to determine the principal stress directions. The fiber orientation of an element was then aligned with the new principal stress directions. This procedure was repeated until only a slight change in an element's

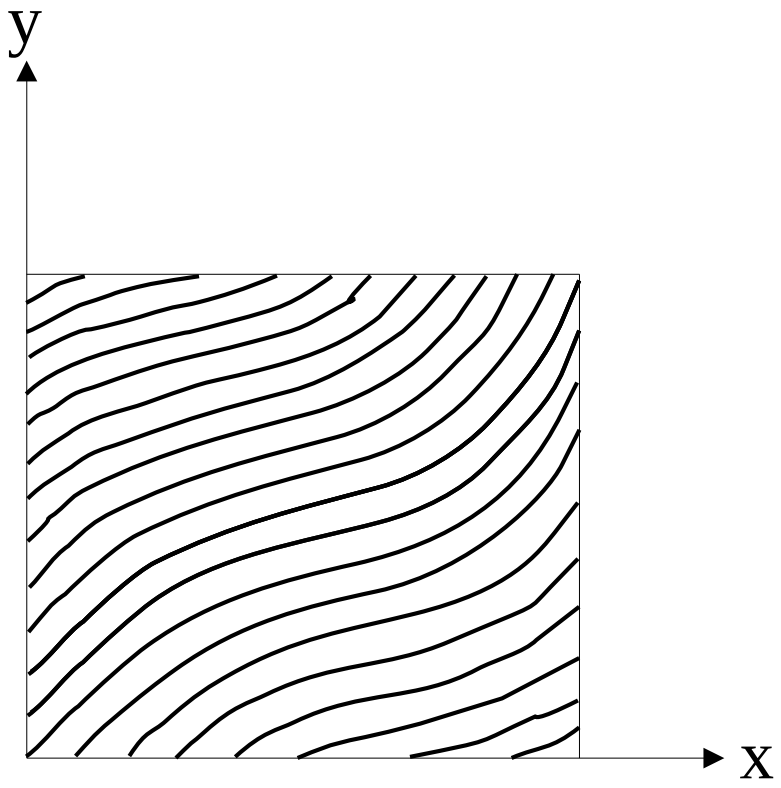

Figure 1.3: Lamina with fiber orientation varying with position.

fiber orientation occurred between successive iterations. The result was that both the failure load and location could be changed by using different combination of plies with spatially varying fiber orientation in conjunction with traditional straight fiber plies. While larger failure loads compared to traditional straight fiber laminates were achieved, the buckling loads for these variable-stiffness laminates were smaller than the base straight fiber laminate.

1.2 Design of Curvilinear Fiber Laminates

The thrust of this research is to create improved performance of composite laminates by varying the fiber orientation continuously within single laminae. It is necessary to first describe the method which would be used to manufacture these variable-stiffness laminates. This will be followed by a description of previous attempts at modelling laminates with spatially varying fiber orientation. Finally, a brief outline of this current research effort will be provided.

1.2.1 Manufacturing of Curvilinear Fiber Laminates

Advances in manufacturing techniques such as the tow placement machine make it possible to spatially vary the fiber orientation within a single lamina. This capability is not present in either filament winding or tape layup machines. Since this machine has yet to be used extensively, a brief overview of the workings of a tow placement machine will be provided. Evans, Vanigila, and Hopkins [4] have provided a review of a tow placement machine manufactured by Cincinnati Milacron. A similar tow placement machine manufactured by Hercules, Inc. has been described by Barth [5]. While these tow machines are not identical to one another, it is reasonable to assume that they exhibit traits which are inherent in tow placement machines. Assuming that these two machines are representative of tow placement machines in general, it is possible to describe the

features of a typical tow placement machine.

In general, the tow placement machine is a computer controlled, multi-axis fiber placement system. Three different components account for a total of seven degrees of freedom - a sled, a fiber delivery head, and a mandrel. Figure 1.4, taken from Reference [5], shows these seven axes of motion. The delivery head accounts for three degrees of freedom by being attached to a robotic wrist which can rotate about three axes. The delivery head is positioned on a platform which can move two directions with a rotation about one axis. The seventh degree of freedom is obtained by rotating the mold in a mandrel. The key benefits of the tow placement machine over alternative manufacturing techniques lie in the actual fiber placement process. In order to examine this process more closely, it is necessary to examine the delivery head in detail.

The fibers are passed through a delivery head which is attached to a three axis, robotic wrist. At this point the benefits of the system becomes apparent. Several individual tows, ranging from 8 to 32 depending upon the design of the delivery head, are passed through the delivery head. The speed at which each tow passes through the head is individually controlled. This is termed differential tow payout. This differential tow payout is vital in producing curved paths. In order to trace a curved path, one end of the delivery head will create a path which is longer than the other. Considering Figure 1.5, path A is longer than B. This requires that the head be able to dispense tows at different rates. In addition to individually controlling the rate at which tows are placed, the head has the capability to cut an individual tow while continuing the placement of the remaining tows and then to restart the cut tow later. Figure 1.6 shows the cutting and restarting of the middle tow (the omitted portion of the tow is shaded grey for ease of viewing). The last major feature of the delivery head is that a roller compacts a tow onto either the mold or previous tow paths. This compaction helps reduce both entrapped air and gaps between the tows and aids

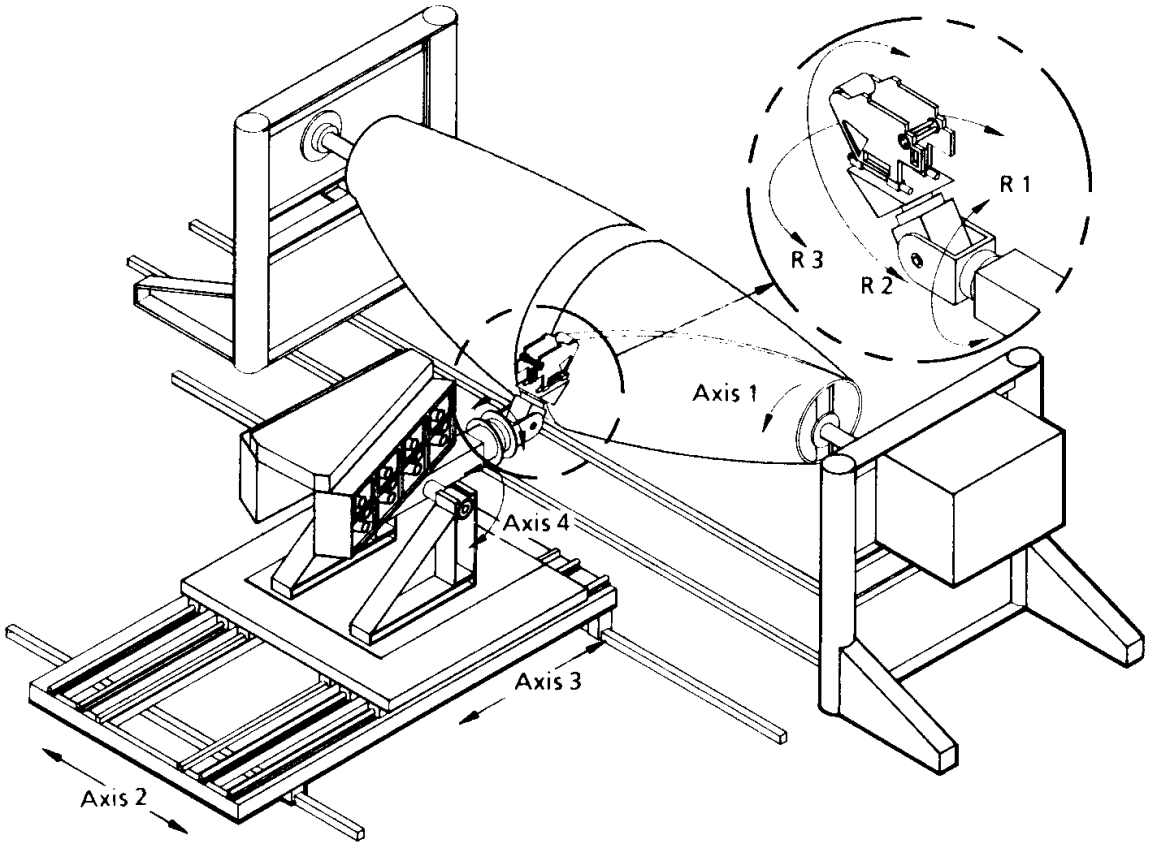

Figure 1.4: Hercules, Inc tow placement machine, taken from J. R. Barth [5].

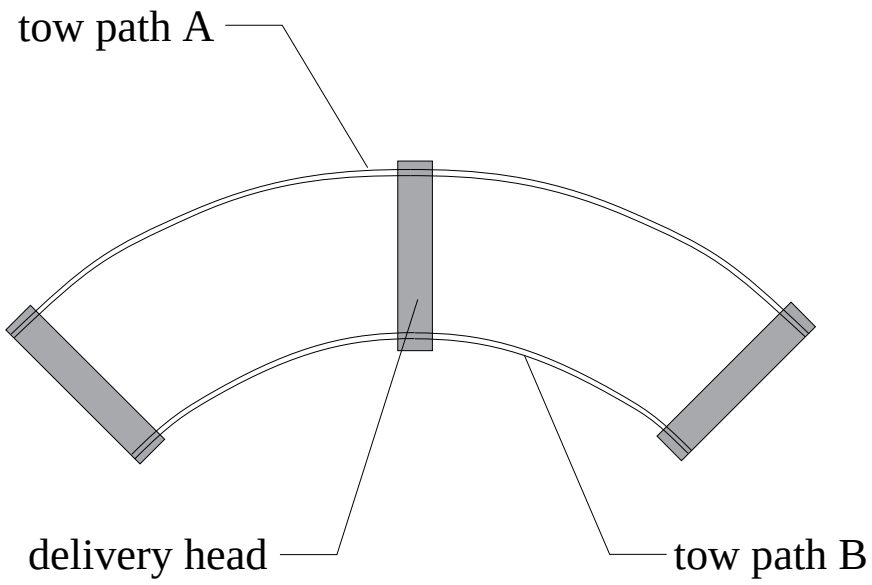

Figure 1.5: The creation of curved fiber paths by the tow placement machine.

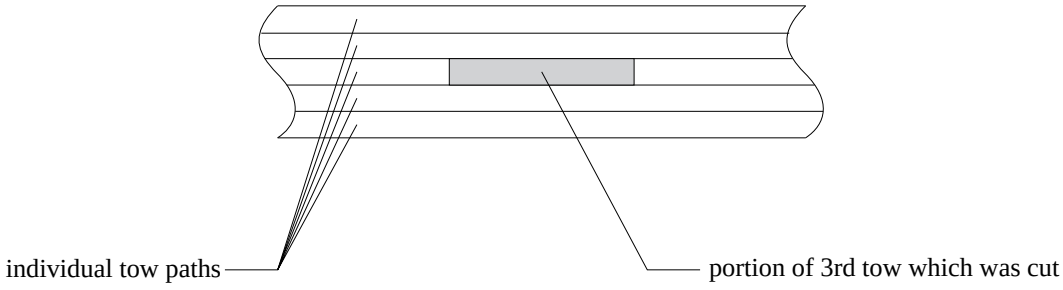

Figure 1.6: Ability of a tow placement machine to cut and then restart individual tow paths.

in making structures which have more consistent properties.

As previously mentioned, the tow placement machine is computer controlled. The information used by this numerical controller is created by the user off-line. First, the basic geometry of a part is determined. Next, the actual ply orientations and boundaries are determined using a path generator software. These fiber paths are then incorporated into a manufacturing simulation package which ensures that the prescribed paths are acceptable for the tow placement machine. Finally, the control information is fed into the tow placement machine and the part is created.

When considering tow placement machines it is reasonable to compare them to several alternative manufacturing methods: filament winding machines, tape laying machines, and manual tape laying. Aspects of this comparison have been included in works by Evans, Vanigila, and Hopkins [4], Barth [5], Bullock, Kowalski, and Young [6], and Enders and Hopkins [7]. The tow placement machine can be thought of as combining the best aspects of both the filament winding and tape layup machines.

Both tow placement and filament winding machines create a structure by positioning individual fiber tows on a surface. However, the filament winding machine can not do concave surfaces since the tension in the fibers will cause them to simply bridge the concave region. The tow placement machine uses the compaction pressure to directly place the tows onto the concave surface. Another shortcoming of a filament winding machine is that it is only able to produce stable fiber paths where the friction between adjacent fiber paths keeps them in place. This limits a structure to having only geodesic fiber paths. Again, the compaction of the tow placement process allows the fibers to be curved in the plane that they are being laid in regardless of the surface of the mold with the limitation on this being the actual wrinkling of the material as it is curved. Still another advantage of the tow placement machine over filament winding is that it can locally reinforce a

structure. Since the tows do not need to be continuous over the entire structure, it is possible to place individual tows in the desired region by using the compaction process in conjunction with the control of individual tow length.

Tape layup and tow placement machines are similar in that both use compaction to position a given width of material onto a surface. They also can cut the material as it is being laid. The differences between these two methods lie primarily in the ability of the tow placement machine to control individual tows. The tape layup requires that a fixed width of tape be used. The tow placement machine, on the other hand, affords the capability to reduce the bandwidth by simply cutting undesired tows, thus reducing the width of the material being laid. Also, the tape layup machine can not create non-geodesic paths since this would require one edge of the tape to have a different length than the other edge. The tow placement machine does not have this drawback since it uses differential payout in the placement of the individual tows.

The primary difference between tow placement and the manual layup of a composite part is a result of the automation of the manufacturing process. By automating the layup procedure, the process repeatability is greatly improved. A part which can be produced by a machine, whether it be filament winding, tape layup, or tow placement, can also more accurately follow the design compared to manual layup. The time to produce complicated parts by an automated method such as tow placement will be significantly less than that of a manual layup.

While the use of tow placement machines is still relatively new, it has been shown that it can produce large and complicated structures. Hercules, Inc. has shown that their machine can produce parts ranging from wing spars to primary fuselage structures [5]. The aft fuselage section of the Bell Boeing V-22 Osprey is created using a tow placement machine manufactured by Cincinnati Milacron [8]. By designing it with the intention of manufacturing it with a tow placement machine,

an initial design of nine skin panels and over 150 stiffeners was reduced to a single piece component with seventeen continuous, co-cured J-stringers. The improved design should reduce labor by over 50% and offer savings of $45 million for a production run of 614 aircrafts (saving over $73,000 per aircraft). The use of a tow placement machine also reduced the mismatch between aircraft frame and skins. The tow-placed design offered a lighter structure due to better precision in reproducing the desired fiber orientations. These examples show the versatility of the tow placement machine which might allow it to eventually supersede other methods in manufacturing of complicated composite structures.

1.2.2 Previous Research into the Modelling of Curvilinear Fiber Paths

Several different approaches have been used in the creation of curvilinear fiber paths by a tow placement machine. The motivation in each case is that by spatially varying the fiber paths within a ply it might be possible to improve the performance of a composite structure. There are several possibilities on how to develop these curved fiber paths. Hyer and Charette modelled fiber paths in finite elements which were piecewise continuous and oriented in the principal stress directions [3]. A drawback to this technique is that the fiber paths are not continuous and fiber orientation angles are constant within each element. Two different efforts have focussed on the modelling of complete fiber paths. In work done by Parthasarathy, Kodiyalam, and Davis [9], a fiber path was defined by using a series of control points and then passing a curve through them from which the fiber orientation was then obtained. Another method of defining curvilinear fiber paths was suggested by Gürdal and Olmedo [10, 11] in which a linear fiber orientation variation is used to define a path.

The research by Parthasarathy, Kodiyalam, and Davis in [9] was an effort to increase design performance by spatially varying the fiber paths of a structure. The optimization procedure converted

manufacturing limitations of a Cincinnati Milacron tow placement machine, such as minimum fiber length and fiber curvature, into numerical constraints. They defined a single path using a series of basis shapes. By varying the influence of a basis curve, different fiber paths could be created. Once the design path was determined, subsequent paths were made parallel to it until the entire model surface had been generated. The resulting fiber paths were then imported to a finite element mesh generator which proceeded to determine the fiber orientation of an element to be the orientation at the centroid of each element (variation of the fiber orientation over the element was not taken into account). One of the examples that they explored was the maximization of the critical buckling load of a flat plate with a circular hole under uniaxial loading. After several iterations, the buckling load of a laminate with curvilinear fibers had 1.9 times the buckling load of the base straight fiber laminate. In this case, using spatially varying fiber paths significantly increased the performance of the composite plate.

The response of laminates composed of layers with fiber orientation varying along one direction to uniform end shortening has been studied earlier by Gürdal and Olmedo [10, 11]. In those studies, first a reference fiber path which passed through the center of the panel and had fiber orientation varying linearly along a geometric axis of the panel was created. Subsequent fiber paths were obtained by shifting the reference path in a direction perpendicular to its axis of fiber orientation variation. The results from this work indicate that variable-stiffness laminates offer significant performance improvements compared to traditional straight fiber laminates in terms of both buckling load and axial stiffness.

These two methods provide different ways to tailor a structure by using the capabilities of a tow placement machine to create variable-stiffness structures. These approaches are by no means the only way to vary the fiber orientation of a single ply. Another approach would be to create

fiber paths which simply conform to the desired geometry. An example of this would be to steer the fiber paths around a hole in a panel. However, regardless of the design methodology used, the goal is still to improve performance by tailoring a structure through the use of curved fiber paths. Therefore the benefits and drawbacks of using one of these methods to create a variable-stiffness laminate need to be examined on a case by case basis.

1.3 Focus of This Research into Variable-Stiffness Composite Laminates

The term "variable-stiffness laminate" in this work will be used to define a laminate which has spatially varying stiffness properties due to the use of curvilinear fiber paths as defined by Gürdal and Olmedo [10, 11]. As explained previously, a tow placement machine can be used to spatially vary the fiber orientation of continuous fibers within a single ply. This research will examine the design of curvilinear fiber paths defined by fiber orientation parameters, taking manufacturing aspects of the tow placement machine into account. While the use of variable-stiffness laminates in [10, 11] did improve the critical buckling load, the fiber paths described by these laminates are not truly parallel. Although the types of laminates studied earlier may be buildable by using tow placement machines, certain features of the tow placement machine lend themselves to manufacturing layers with parallel fibers. Since the tows will tend to wrinkle if they are curved too much, it is necessary to place a limit on fiber curvature. This research will attempt to expand the previous work by applying the variable-stiffness concept in a manner which reflects these manufacturing considerations.

First the creation of the reference fiber path will be reviewed. This path will be present in all of the variable-stiffness laminates presented herein. Next, the creation of paths for the shifted

fiber method utilized in [10, 11] will be described. Then, a new method to model parallel fiber paths will be presented. After defining how variable-stiffness laminates are modelled using both the shifted and parallel fiber methods, the in-plane analysis procedure for these laminates will be outlined. This will be followed by a description of the strength and curvature constraints being imposed on the laminates in this thesis. A comparison between the in-plane responses of traditional straight fiber laminates and the shifted and parallel fiber variable-stiffness laminates under uniaxial compression and applied in-plane shear deformation will be made. These in-plane comparisons will be followed by a comparison of the critical buckling loads and equivalent stiffnesses of the various laminates. Finally, a brief series of conclusions and suggestions for future work will be provided.

Chapter 2

Creation of Variable-Stiffness Laminates

The creation of a variable-stiffness lamina begins with the description of a reference fiber path. This reference fiber path will serve as the basis for creating other fiber paths that together will form a single ply. After defining the reference fiber path for a given lamina, it is necessary to describe the other fiber paths. Currently two different methods have been utilized to perform this. The first consists of producing the remaining fiber paths by shifting the reference fiber path along the y' axis. The other method which is introduced during this study creates fiber paths by defining sets of points that are fixed distances from the reference curve. The subsequent paths created by this method are truly parallel to the reference fiber path.

2.1 Description of the Reference Fiber Path

Unlike conventional straight fiber plies, curvilinear fiber paths can not be described by a single orientation angle. A convention has been adopted [11] that offers a wide range of freedom in describing the variable-stiffness fiber orientation. It is assumed that the fiber orientation of the reference fiber path varies linearly from one value at the center of the panel to another at a specified distance. The angle at the center of the panel is denoted as T_0. The other angle, T_1, will represent the fiber orientation at a distance $a/2$ from the origin where a is a characteristic dimension of the panel. In the present work, only rectangular laminates are considered so this characteristic dimension will be the panel width. The linear variation is said to take place along the x direction. Therefore the orientation of a single curvilinear fiber path can be denoted using "$\langle T_0|T_1\rangle$." The reference fiber path and corresponding fiber orientation for a $\langle 0|45\rangle$ fiber can be seen in Figure 2.1. Since a ply is made of fibers oriented similarly to the reference fiber path, the description of the reference fiber path will also serve to describe the ply. A $\pm$ sign in front of this term means that there are two adjacent layers with equal and opposite T_0 and T_1 angles.

A more general fiber path definition can be achieved by rotating the axis of fiber orientation by an angle, ϕ, from the geometric axis of the panel. This rotation angle defines a new coordinate system denoted by x' and y'. The fiber path defined by "$\phi\langle T_0|T_1\rangle$" will vary linearly along the x' direction from T_0 at the center to T_1 at the characteristic dimension of the panel. A $\pm$ sign in front of the rotation angle, ϕ, means that the reference fiber paths for two successive layers are rotated equal and opposite amounts. The addition of ϕ to the fiber path defined by $\langle 0|45\rangle$ can be seen in Figure 2.2. The rotation of the x' axis relative to the panel geometry is the only difference between the three fiber paths. To summarize, the components used in defining the reference fiber path for

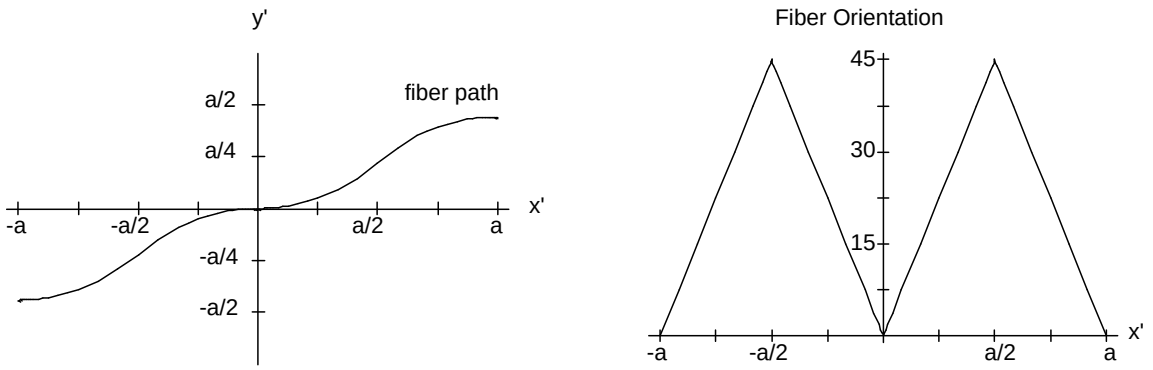

Figure 2.1: $\langle 0|45\rangle$ fiber path and orientation.

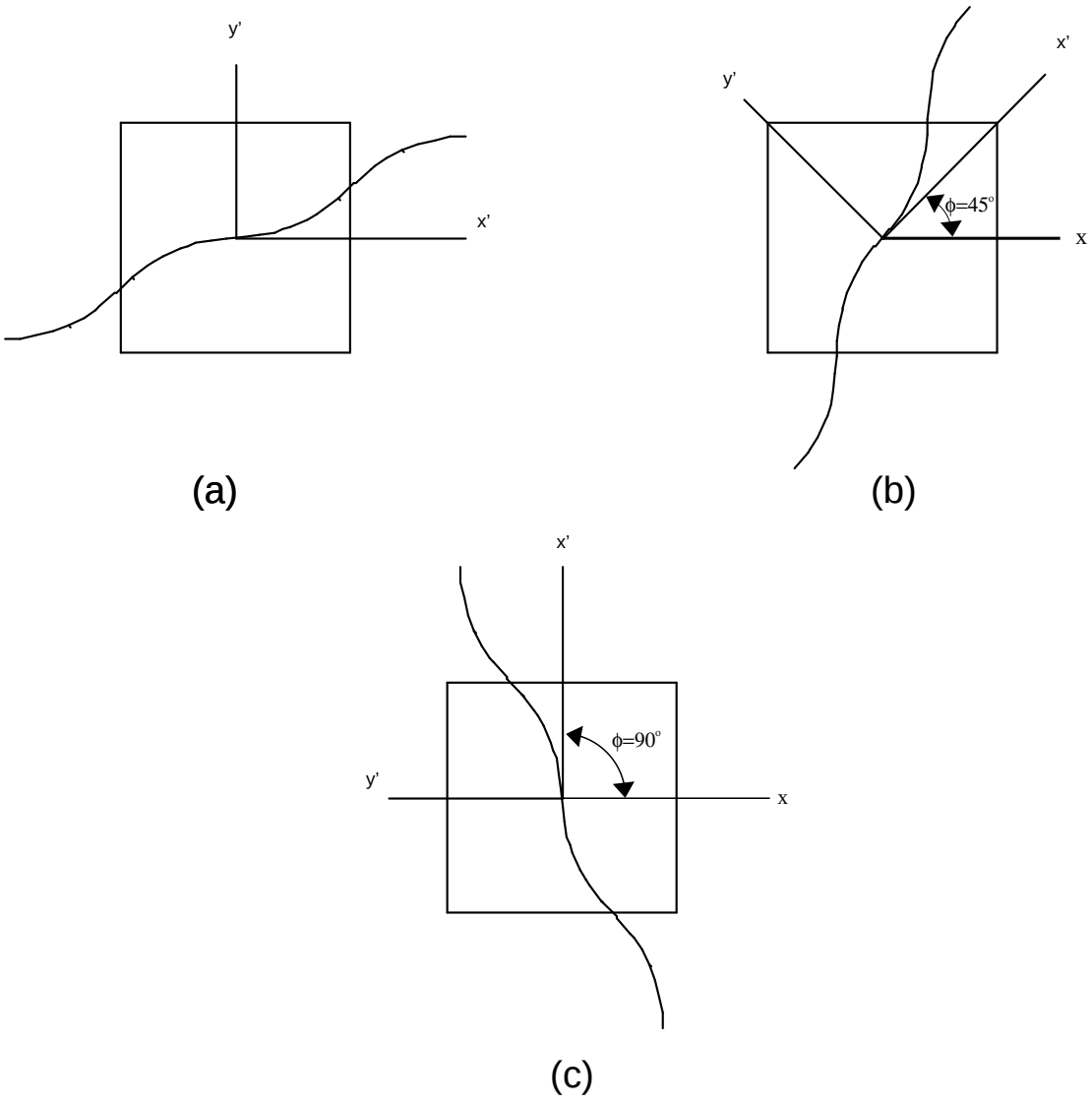

Figure 2.2: Effect of adding $\phi =$ (a)0^o, (b)45^o, and (c) 90^o to $\langle 0|45\rangle$ reference fiber path.

a give ply are shown in Figure 2.3. The resulting reference fiber path equation, $y'(x')$, and fiber path orientation, $\theta(x')$, can be determined in terms of ϕ, T_0, T_1 and x':

$$y'(x') = \begin{cases} \frac{a}{2(T_0-T_1)}\left\{\ln\left[\cos T_0\right] - 2\ln\left[\cos T_1\right] + \ln\left[\cos\left(-T_0+2T_1+\frac{2(T_1-T_0)}{a}x'\right)\right]\right\}, \\ \qquad\qquad\qquad\qquad\qquad\qquad\qquad\qquad \text{for } -a \le x' \le -\frac{a}{2} \\ \frac{a}{2(T_1-T_0)}\left\{-\ln\left[\cos T_0\right] + \ln\left[\cos\left(T_0+\frac{2(T_0-T_1)}{a}x'\right)\right]\right\}, \\ \qquad\qquad\qquad\qquad\qquad\qquad\qquad\qquad \text{for } -\frac{a}{2} \le x' \le 0 \\ \frac{a}{2(T_0-T_1)}\left\{-\ln\left[\cos T_0\right] + \ln\left[\cos\left(T_0+\frac{2(T_1-T_0)}{a}x'\right)\right]\right\}, \\ \qquad\qquad\qquad\qquad\qquad\qquad\qquad\qquad \text{for } 0 \le x' \le \frac{a}{2} \\ \frac{a}{2(T_1-T_0)}\left\{\ln\left[\cos T_0\right] - 2\ln\left[\cos T_1\right] + \ln\left[\cos\left(-T_0+2T_1+\frac{2(T_0-T_1)}{a}x'\right)\right]\right\}, \\ \qquad\qquad\qquad\qquad\qquad\qquad\qquad\qquad \text{for } \frac{a}{2} \le x' \le a \end{cases} \tag{2.1}$$

$$\theta(x') = \begin{cases} \phi + \frac{2}{a}(T_1 - T_0)x' + T_0 - 2(T_0 - T_1), & \text{for } -a \le x' \le -\frac{a}{2} \\ \phi + \frac{2}{a}(T_0 - T_1)x' + T_0, & \text{for } -\frac{a}{2} \le x' \le 0 \\ \phi + \frac{2}{a}(T_1 - T_0)x' + T_0, & \text{for } 0 \le x' \le \frac{a}{2} \\ \phi + \frac{2}{a}(T_0 - T_1)x' + T_0 - 2(T_0 - T_1), & \text{for } \frac{a}{2} \le x' \le a \end{cases} \tag{2.2}$$

$$\text{where} \quad x' = x\cos\phi + y\sin\phi\,. \tag{2.3}$$

2.2 Shifted Fiber Paths

The shifting of the reference fiber path along the y' axis to create the remaining paths is straight forward. The first fiber path created is the reference fiber path. The next fiber path is made by

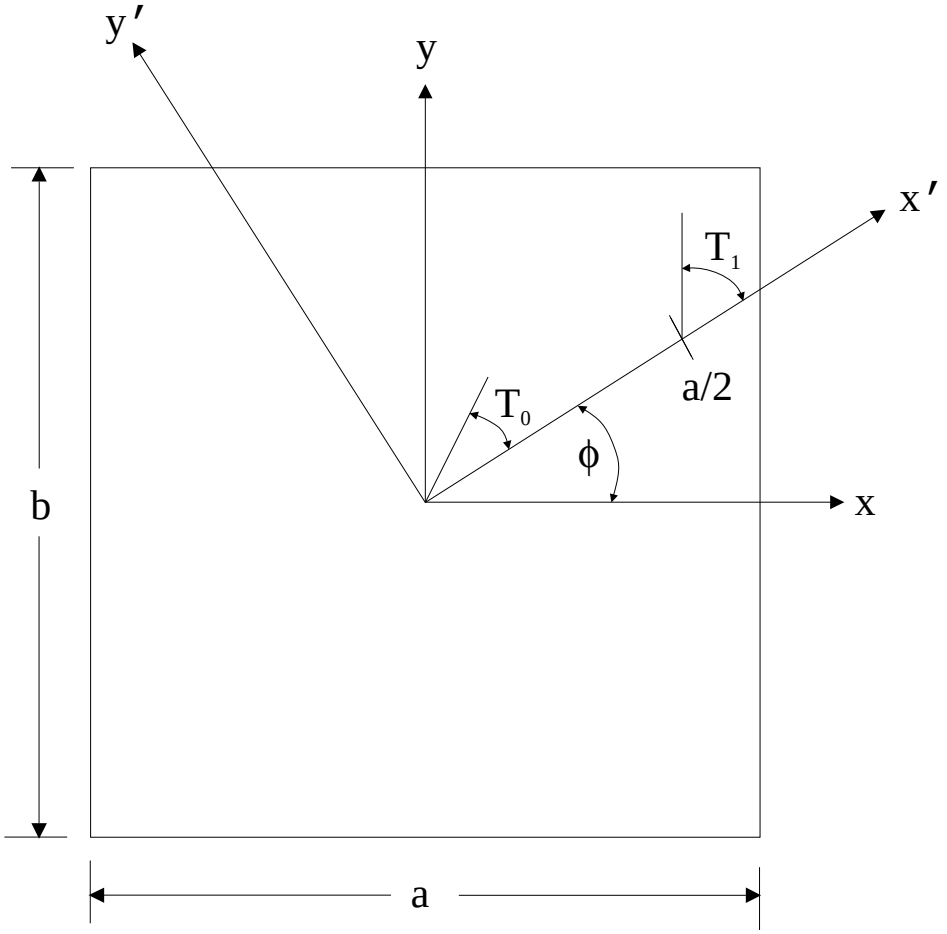

Figure 2.3: Components used in definition of reference fiber path.

shifting the reference fiber path a fixed amount in the y' direction. The remaining fiber paths for the lamina are made in the same manner, with the only difference being the amount that each path is shifted along the y' axis. The completed shifted fiber $0\langle 0|45\rangle$ lamina can be seen in Figure 2.4. Note that the change in fiber orientation only takes place along the x' axis.

2.3 Parallel Fiber Paths

The other method used to define the remaining fiber paths is the parallel fiber method. This method creates fiber paths so that each path is defined as a set of points lying a constant distance from the reference curve. As opposed to the shifted fiber case where an analytical expression exist for each individual fiber path, parallel fiber paths are generated through a numerical scheme which simulates the process for creating any curve parallel to another curve. Information required to create a curve parallel to a reference curve is provided in Figure 2.5. The reference fiber path A in this case is defined by an infinite number of points, A_i. The path B parallel to it is defined by a set of points, B_i. These points lay at a fixed distance from the reference fiber path, measured along the normal to the reference path, $\hat{n}_{A_i}$, so that

$$|\overline{A_1B_1}| = |\overline{A_2B_2}| = |\overline{A_3B_3}| = \cdots = |\overline{A_iB_i}|. \tag{2.4}$$

Assuming that B_i satisfies Equation (2.4), then curve B is parallel to curve A. Repeating this procedure creates a lamina with truly parallel fibers. A similar method, described in Section 3.8, is employed to determine the fiber orientation of a point along a path.

A $0\langle 0|45\rangle$ lamina made of parallel fibers is shown in Figure 2.6. Unlike the shifted fiber $0\langle 0|45\rangle$, two points, P and Q, which have the same x' coordinate no longer have identical fiber orientations. In this case, point P has a fiber orientation of approximately 0^o while Q is almost 45^o. Therefore,

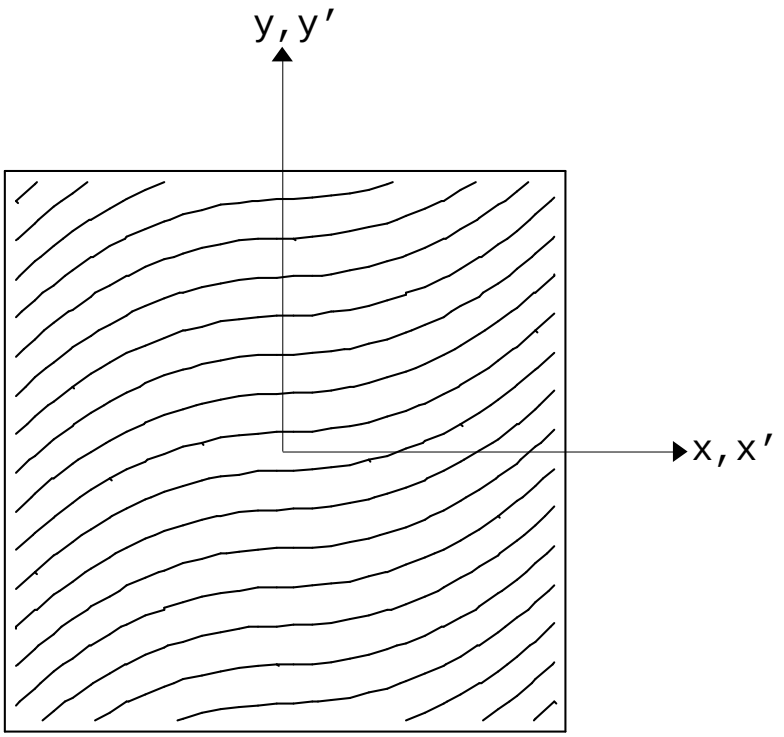

Figure 2.4: A $0\langle 0|45\rangle$ lamina made by the shifted fiber method.

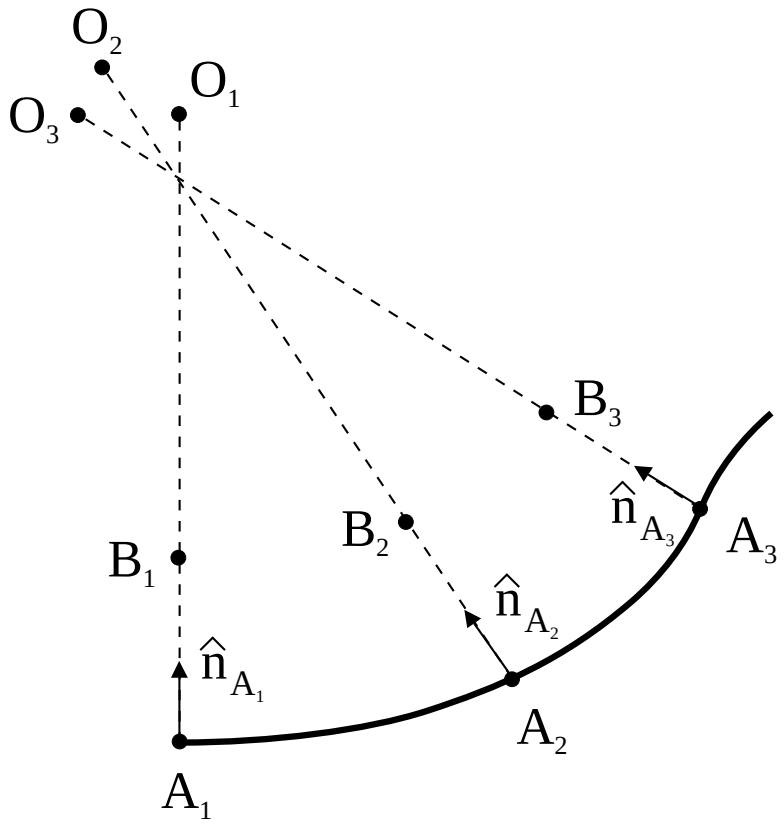

Figure 2.5: Creation of two parallel curves.

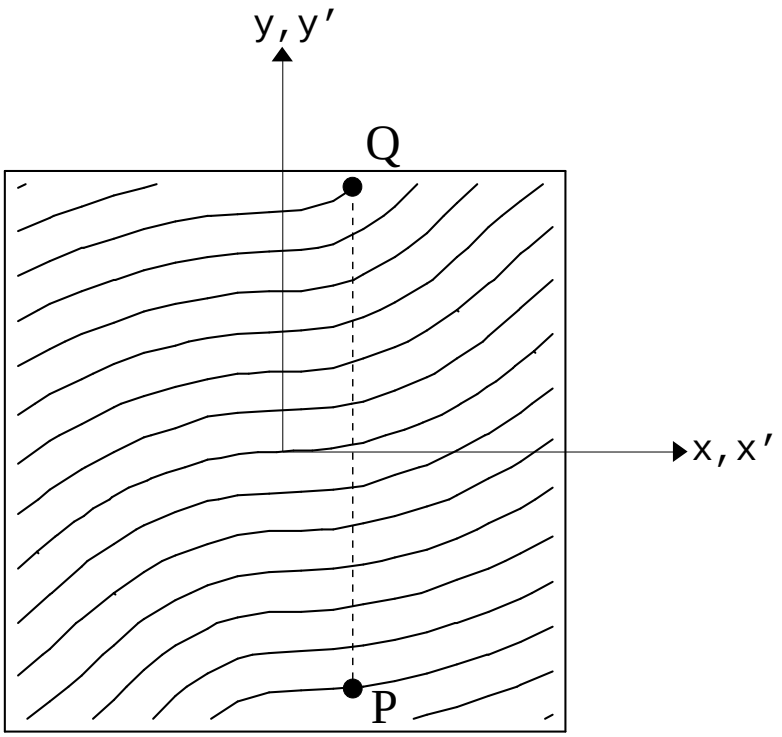

Figure 2.6: A $0\langle 0|45\rangle$ lamina created by the parallel fiber method.

fiber orientation of the parallel fiber $0\langle 0|45\rangle$ lamina varies in both the x' and y' directions.

2.4 Comparison of Laminae Made By the Shifted and Parallel Fiber Methods

Both methods used to model the placement of fiber paths define subsequent paths as sets of points a fixed distance from the reference path. The difference between the two methods is in how this distance is measured. The shifted fiber method defines this distance to be along the y' axis while the parallel method defines the distance to be along the normal to the reference curve. Therefore, the amount that a lamina created by the two methods differ is dependent upon the differences between the y' axis and the normal to the reference curve. As such, variations between the two methods do not depend upon the rotation angle in any manner. Therefore, the only parameters that will change the relationship of y' to the normal lines of the reference curve are the orientation angles at the center and edge of the panel, T_0 and T_1, respectively.

The effect that varying the fiber orientation angle from T_0 to T_1 has on the fiber paths created by the two methods is shown in Figures 2.7 and 2.8. When the difference between T_0 and T_1 is relatively small, 10^o in Figure 2.7, the two methods produce very similar fiber paths. However, with larger changes in orientation angle between the center and edge of the panel, 75^o for Figures 2.8(a) and (b), come considerable differences between the shifted and parallel fiber methods. For the shifted fiber $0\langle 0|75\rangle$ lamina, Figure 2.8(a), the fibers will tend to either bunch together or spread apart reflecting a fiber volume fraction variation as a function of the location in the panel. This variation would appear as a change in panel thickness as a function of location. Currently, this fiber volume fraction variation is neglected altogether in this analysis. Again, it is clear from

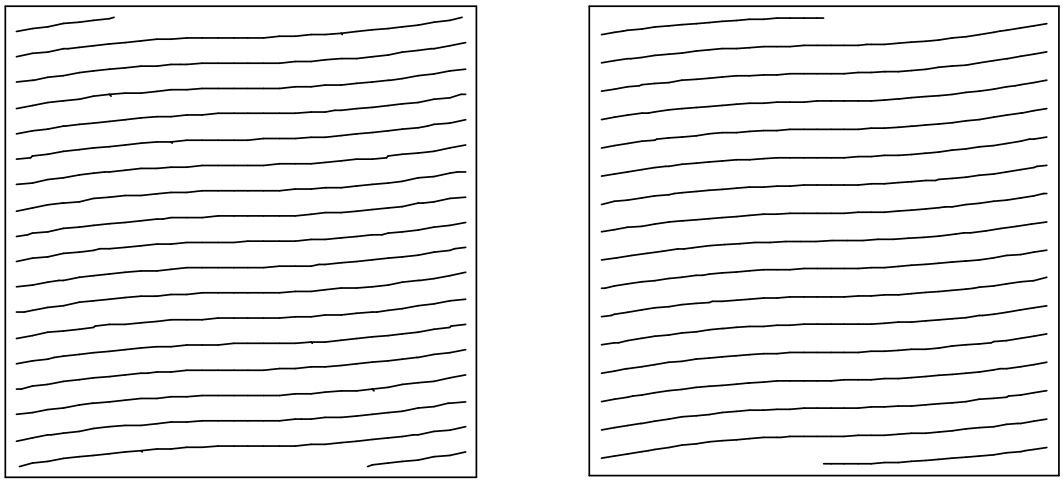

(a) (b)

Figure 2.7: A $0\langle 0|10\rangle$ lamina created (a) shifted fiber method and (b) parallel fiber method.

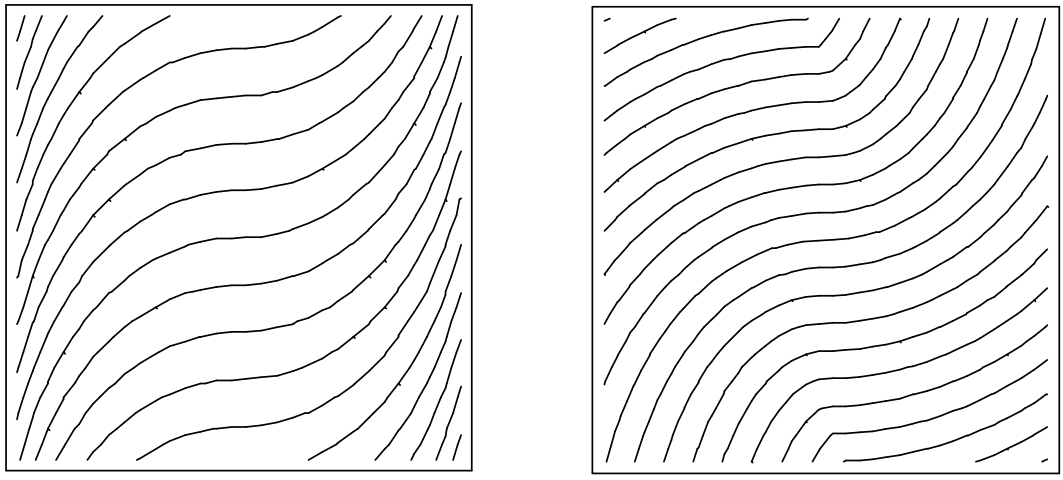

(a) (b)

Figure 2.8: A $0\langle 0|75\rangle$ lamina created (a) shifted fiber method and (b) parallel fiber method.

Figure 2.8(b) that the fiber orientation of the parallel fiber lamina varies with respect to both the x and y directions. Also, the large change in fiber orientation for the parallel fiber $0\langle 0|75\rangle$ lamina created kinks in the fiber paths in the vicinity of $(0, \pm b/2)$. Similar kinks will occur whenever a fiber path passes sufficiently close to the reference fiber path's centers of curvature. A manufacturing constraint on fiber curvature described in Section 4.2 will disqualify a lamina in which a fiber path kinks in this manner by limiting the acceptable curvature of a fiber path. In conclusion, despite producing very similar laminae for small changes in T_0 and T_1, the laminae created by the two methods will only be identical when they are describing a straight fiber laminate.

Chapter 3

In-Plane Response of Variable-Stiffness Laminated Plates

In order to understand the behavior of a laminated plate, it is necessary to grasp the response of a single lamina. Once this is achieved, the response of a laminated structure can be determined. This section will provide this progression from a single straight fiber ply to a variable-stiffness laminate beginning with the generalized Hooke's Law and how it is applicable to the analysis of composite laminates. Then the analytical formulation of composite laminates will be determined. Finally, the response of composite plates using Classical Lamination Theory (CLT) will be developed. Once this has been formulated, the procedure for performing the analysis of variable-stiffness laminates will be described.

3.1 Generalized Hooke's Law for Composite Laminae

It is possible to represent the generalized Hooke's Law using a stiffness matrix, C_{ij}, and a contracted notation as follows:

$$\begin{aligned} \sigma_i = C_{ij}\epsilon_j \quad & i,j = 1,2,\ldots,6 \\ \text{where} \quad & \sigma_1 = \sigma_{11}, && \epsilon_1 = \epsilon_{11}, \\ & \sigma_2 = \sigma_{22}, && \epsilon_2 = \epsilon_{22}, \\ & \sigma_3 = \sigma_{33}, && \epsilon_3 = \epsilon_{33}, \\ & \sigma_4 = \sigma_{23} = \tau_{23}, && \epsilon_4 = \gamma_{23} = 2\epsilon_{23}, \\ & \sigma_5 = \sigma_{31} = \tau_{31}, && \epsilon_5 = \gamma_{31} = 2\epsilon_{31}, \\ & \sigma_6 = \sigma_{12} = \tau_{12}, && \epsilon_6 = \gamma_{12} = 2\epsilon_{12}. \end{aligned} \tag{3.1}$$

It is necessary to note that for $i \neq j$, γ_{ij} is the engineering shear strain while ϵ_{ij} is the shear strain tensor. The difference between the two shear strain representations is that the engineering shear strain is simply twice as large as the shear strain tensor.

For elastic materials, the stiffness matrix will become symmetric, $C_{ij} = C_{ji}$. This reduces the number of independent constants in 3.1 from 36 to 21. The resulting generalized Hooke's Law for anisotropic materials, materials having no symmetry planes for material properties, is the following:

$$\begin{Bmatrix} \sigma_1 \\ \sigma_2 \\ \sigma_3 \\ \sigma_4 \\ \sigma_5 \\ \sigma_6 \end{Bmatrix} = \begin{bmatrix} C_{11} & C_{12} & C_{13} & C_{14} & C_{15} & C_{16} \\ C_{12} & C_{22} & C_{23} & C_{24} & C_{25} & C_{26} \\ C_{13} & C_{23} & C_{33} & C_{34} & C_{35} & C_{36} \\ C_{14} & C_{24} & C_{34} & C_{44} & C_{45} & C_{46} \\ C_{15} & C_{25} & C_{35} & C_{45} & C_{55} & C_{56} \\ C_{16} & C_{26} & C_{36} & C_{46} & C_{56} & C_{66} \end{bmatrix} \begin{Bmatrix} \epsilon_1 \\ \epsilon_2 \\ \epsilon_3 \\ \epsilon_4 \\ \epsilon_5 \\ \epsilon_6 \end{Bmatrix}. \tag{3.2}$$

For orthotropic materials which have two planes of symmetry, the number of independent

constants is reduced from the 21 in the anisotropic case down to 9. In this case, the generalized Hooke's Law simplifies to

$$\begin{Bmatrix} \sigma_1 \\ \sigma_2 \\ \sigma_3 \\ \sigma_4 \\ \sigma_5 \\ \sigma_6 \end{Bmatrix} = \begin{bmatrix} C_{11} & C_{12} & C_{13} & 0 & 0 & 0 \\ C_{12} & C_{22} & C_{23} & 0 & 0 & 0 \\ C_{13} & C_{23} & C_{33} & 0 & 0 & 0 \\ 0 & 0 & 0 & C_{44} & 0 & 0 \\ 0 & 0 & 0 & 0 & C_{55} & 0 \\ 0 & 0 & 0 & 0 & 0 & C_{66} \end{bmatrix} \begin{Bmatrix} \epsilon_1 \\ \epsilon_2 \\ \epsilon_3 \\ \epsilon_4 \\ \epsilon_5 \\ \epsilon_6 \end{Bmatrix}. \tag{3.3}$$

The 9 independent constants are $E_1,\ E_2,\ E_3,\ G_{12},\ G_{13},\ G_{23},\ \nu_{12},\ \nu_{13},$ and ν_{23}. The values for the remaining Poisson's ratios, $\nu_{21}, \nu_{31},$ and ν_{32}, can be found using using the following relations

$$\frac{\nu_{ij}}{E_i} = \frac{\nu_{ji}}{E_j}. \tag{3.4}$$

C_{ij} can now be expressed in terms of these engineering constants

$$\begin{aligned} C_{11} &= \left(1 - \nu_{23}^2 \frac{E_3}{E_2}\right) \frac{E_1}{O}\,, \\ C_{12} &= \left(\nu_{12} + \nu_{13}\nu_{23} \frac{E_3}{E_2}\right) \frac{E_2}{O}\,, \\ C_{13} &= \left(\nu_{13} + \nu_{12}\nu_{23}\right) \frac{E_3}{O}\,, \\ C_{22} &= \left(1 - \nu_{13}^2 \frac{E_3}{E_1}\right) \frac{E_2}{O}\,, \\ C_{23} &= \left(\nu_{23} + \nu_{12}\nu_{13} \frac{E_2}{E_1}\right) \frac{E_3}{O}\,, \\ C_{33} &= \left(1 - \nu_{12}^2 \frac{E_2}{E_1}\right) \frac{E_3}{O}\,, \\ C_{44} &= G_{23}\,, \\ C_{55} &= G_{13}\,, \\ C_{66} &= G_{12}\,, \end{aligned} \tag{3.5}$$

$$\text{where } O = 1 - \nu_{12}\left(\nu_{12}\frac{E_2}{E_1} + 2\nu_{23}\nu_{13}\frac{E_3}{E_1}\right) - \nu_{13}^2\frac{E_3}{E_1} - \nu_{23}^2\frac{E_3}{E_2}\,. \tag{3.6}$$

3.2 Stress-Strain Relations for Orthotropic Material Using a Plane Stress Condition

A representation of a typical orthotropic material, shown as a fiber reinforced lamina, is provided in Figure 3.1. Imposing a plane stress condition on such a material requires

$$\begin{aligned} &\sigma_3 = 0, \text{ and} \\ &\tau_{23} = \tau_{31} = 0. \end{aligned} \tag{3.7}$$

The resulting stress-strain relation, using the reduced stiffness matrix, Q_{ij}, becomes

$$\begin{Bmatrix} \sigma_1 \\ \sigma_2 \\ \tau_{12} \end{Bmatrix} = \begin{bmatrix} Q_{11} & Q_{12} & 0 \\ Q_{12} & Q_{22} & 0 \\ 0 & 0 & Q_{66} \end{bmatrix} \begin{Bmatrix} \epsilon_1 \\ \epsilon_2 \\ \gamma_{12} \end{Bmatrix} \tag{3.8}$$

$$\begin{aligned} \text{where} \quad Q_{11} &= \frac{E_1}{1-\nu_{12}\nu_{21}}, & Q_{22} &= \frac{E_2}{1-\nu_{12}\nu_{21}}, \\ Q_{12} &= \frac{\nu_{12}E_2}{1-\nu_{12}\nu_{21}} = \frac{\nu_{21}E_1}{1-\nu_{12}\nu_{21}}, & Q_{66} &= G_{12}. \end{aligned} \tag{3.9}$$

It is desirable to determine the stress-strain relation for the x-y plane. Let the 1-2 system be rotated by an angle θ from the x-y system, as shown in Figure 3.2. The resulting stresses and strains in the x-y plane is found using the stresses and strains in the 1-2 system through a transformation matrix, T, which only depends upon the angle θ

$$\begin{Bmatrix} \sigma_x \\ \sigma_y \\ \tau_{xy} \end{Bmatrix} = [T]^{-1} \begin{Bmatrix} \sigma_1 \\ \sigma_2 \\ \tau_{12} \end{Bmatrix} \quad \text{and} \quad \begin{Bmatrix} \epsilon_x \\ \epsilon_y \\ \gamma_{xy}/2 \end{Bmatrix} = [T]^{-1} \begin{Bmatrix} \epsilon_1 \\ \epsilon_2 \\ \gamma_{12}/2 \end{Bmatrix} \tag{3.10}$$

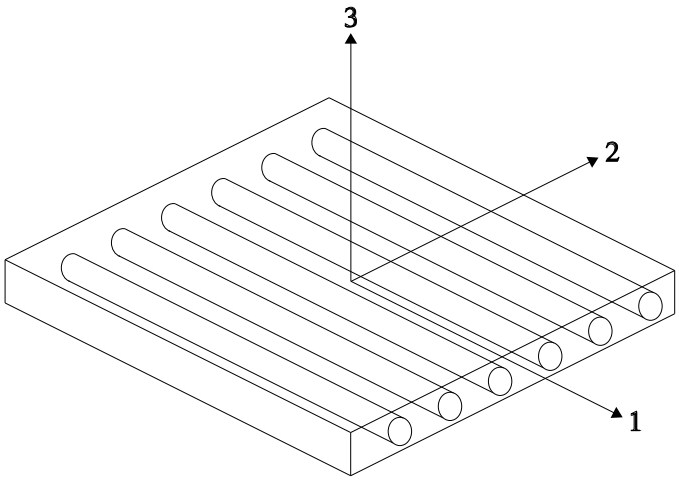

Figure 3.1: Coordinate system for fiber reinforced laminae.

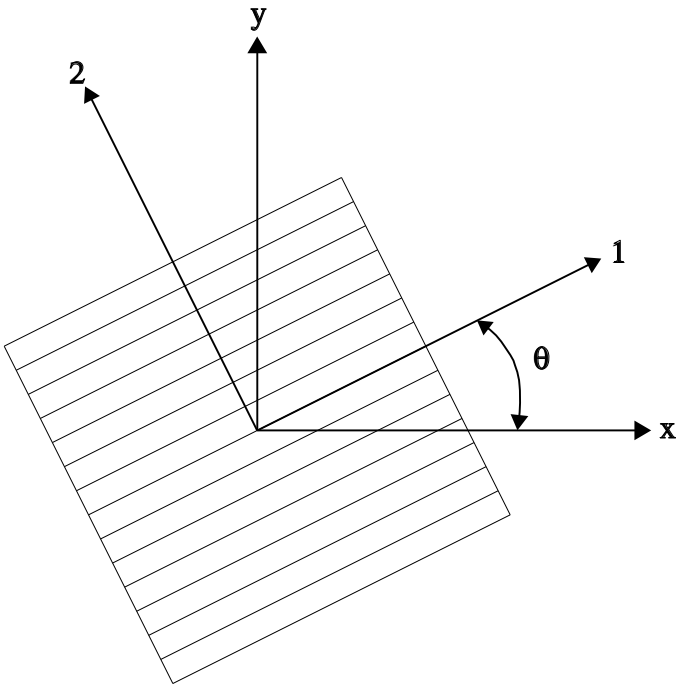

Figure 3.2: Transforming 1-2 properties into x-y coordinates.

$$\text{where } [T] = \begin{bmatrix} \cos^2\theta & \sin^2\theta & 2\sin\theta\cos\theta \\ \sin^2\theta & \cos^2\theta & -2\sin\theta\cos\theta \\ -\sin\theta\cos\theta & \sin\theta\cos\theta & \cos^2\theta - \sin^2\theta \end{bmatrix}. \tag{3.11}$$

It is then possible using the transformations in Equation (3.10) in conjunction with stress-strain relationship in the 1-2 system, Equation (3.8), to express the stress strain relationship in the x-y plane as follows

$$\begin{Bmatrix} \sigma_x \\ \sigma_y \\ \tau_{xy} \end{Bmatrix} = \begin{bmatrix} \overline{Q}_{11} & \overline{Q}_{12} & \overline{Q}_{16} \\ \overline{Q}_{12} & \overline{Q}_{22} & \overline{Q}_{26} \\ \overline{Q}_{16} & \overline{Q}_{26} & \overline{Q}_{66} \end{bmatrix} \begin{Bmatrix} \epsilon_x \\ \epsilon_y \\ \gamma_{xy} \end{Bmatrix}. \tag{3.12}$$

The $\overline{Q}$ matrix is the transformed reduced stiffness matrix and is determined from the stiffness matrix, Q, and the fiber orientation angle, θ,

$$\begin{aligned} \overline{Q}_{11} &= Q_{11}\cos^4\theta + 2(Q_{12} + 2Q_{66})\sin^2\theta\cos^2\theta + Q_{22}\sin^4\theta\,, \\ \overline{Q}_{12} &= (Q_{11} + Q_{22} - 4Q_{66})\sin^2\theta\cos^2\theta + Q_{12}(\sin^4\theta + \cos^4\theta)\,, \\ \overline{Q}_{22} &= Q_{11}\sin^4\theta + 2(Q_{12} + 2Q_{66})\sin^2\theta\cos^2\theta + Q_{22}\cos^4\theta\,, \\ \overline{Q}_{16} &= (Q_{11} - Q_{12} - 2Q_{66})\sin\theta\cos^3\theta + (Q_{12} - Q_{22} + 2Q_{66})\sin^3\theta\cos\theta\,, \\ \overline{Q}_{26} &= (Q_{11} - Q_{12} - 2Q_{66})\sin^3\theta\cos\theta + (Q_{12} - Q_{22} + 2Q_{66})\sin\theta\cos^3\theta\,, \\ \overline{Q}_{66} &= (Q_{11} + Q_{22} - 2Q_{12} - 2Q_{66})\sin^2\theta\cos^2\theta + Q_{66}(\sin^4\theta + \cos^4\theta)\,, \end{aligned} \tag{3.13}$$

3.3 Classical Lamination Theory

A laminate is composed of several laminae that each satisfy the generalized Hooke's Law,

$$\begin{Bmatrix} \sigma_x \\ \sigma_y \\ \tau_{xy} \end{Bmatrix}_k = \begin{bmatrix} \overline{Q}_{11} & \overline{Q}_{12} & \overline{Q}_{16} \\ \overline{Q}_{12} & \overline{Q}_{22} & \overline{Q}_{26} \\ \overline{Q}_{16} & \overline{Q}_{26} & \overline{Q}_{66} \end{bmatrix}_k \begin{Bmatrix} \epsilon_x \\ \epsilon_y \\ \gamma_{xy} \end{Bmatrix}_k \tag{3.14}$$

where the subscript k indicates the k^{th} ply in the laminate. It is evident from Equation (3.14) that the stiffnesses of a laminate will now vary through the thickness of the laminate, depending on which ply is being considered.

Classical Lamination Theory (CLT) uses a series of assumptions and approximations to simplify the analysis of the loading of a composite laminate. One simplification is that the bonds between adjacent laminae are perfect and infinitesimally thin. This will cause the displacements to be continuous between plies. So despite being composed of laminae with varying stiffnesses, the resulting laminate will respond as if it were a single layer.

If the laminate is thin relative to either its length or width, then the Kirchhoff hypothesis can be employed. This states that if a line is straight and perpendicular to the midplane of the laminate before deformation, then it is straight, has the same length, and is normal to the midplane after deformation as well. By imposing the straight and normal conditions after deforming the laminate, the analysis is neglecting the shear in the z direction, $\gamma_{xz} = \gamma_{yz} = 0$. Also, requiring the length of the line to remain constant is the same as ignoring the strain in the z direction, $\epsilon_z = 0$. As a result of using the Kirchhoff hypothesis, the u and v displacements become a linear functions in terms of the midplane strains, u^0 and v^0, the z coordinate, and the slope of the midplane in the x and y directions, $\frac{\partial w^0}{\partial x}$ and $\frac{\partial w^0}{\partial y}$, respectively. Note that the superscript 0 denotes a midplane value. As a result of requiring $\epsilon_z = 0$, the displacement in the z direction will only be a function of x and y. Therefore, the w displacement is identical throughout the thickness, $w^0 = w = w(x, y)$. The resulting u and v displacements can be expressed as:

$$u = u^0 - z\frac{\partial w}{\partial x} \text{ and} \tag{3.15}$$

$$v = v^0 - z\frac{\partial w}{\partial y} . \tag{3.16}$$

Using the strain-displacement relations, the strains in the x-y plane can be expressed as

$$\epsilon_x = \epsilon_x^0 + z\kappa_x \ , \tag{3.17}$$

$$\epsilon_y = \epsilon_y^0 + z\kappa_y \ , \tag{3.18}$$

$$\gamma_{xy} = \gamma_{xy}^0 + z\kappa_{xy} \ , \tag{3.19}$$

$$\text{where} \quad \epsilon_x^0 = \frac{\partial u^0}{\partial x} \ , \qquad \epsilon_y^0 = \frac{\partial v^0}{\partial y} \ , \qquad \gamma_{xy}^0 = \frac{\partial u^0}{\partial y} + \frac{\partial v^0}{\partial x} \ ,$$

$$\kappa_x = -\frac{\partial^2 w}{\partial x^2} \ , \quad \kappa_y = -\frac{\partial^2 w}{\partial y^2} \ , \quad \kappa_{xy} = -\frac{\partial^2 w}{\partial x \partial y} \ .$$

3.4 Stress and Moment Resultants

Stress and moment resultants are expressions which are convenient in describing the equilibrium equations for laminated plates. The stress and moment resultants are obtained by integrating the stresses through the thickness of the laminate. Performing this integration provides quantities which represent a force per unit length and a bending moment per unit length. Since each laminate is composed of several plies, the stress and moment resultants for a laminate can be found by summing the stress and moment resultants acting on the individual plies. The resulting equations for the stress and moment resultants of an N ply laminate can be shown to be

$$\begin{Bmatrix} N_x \\ N_y \\ N_{xy} \end{Bmatrix} = \sum_{k=1}^{N} \int_{z_{k-1}}^{z_k} \begin{Bmatrix} \sigma_x \\ \sigma_y \\ \tau_{xy} \end{Bmatrix} dz \ , \tag{3.20}$$

$$\begin{Bmatrix} M_x \\ M_y \\ M_{xy} \end{Bmatrix} = \sum_{k=1}^{N} \int_{z_{k-1}}^{z_k} \begin{Bmatrix} \sigma_x \\ \sigma_y \\ \tau_{xy} \end{Bmatrix} z dz \ . \tag{3.21}$$

The limits of integration in Equations (3.20) and 3.21 are from z_{k-1} to z_k. This represents the thickness of the k^{th} ply. The convention used in defining positive stress and moment resultants are

shown in Figures 3.3 and 3.4.

The stresses, σ_x, σ_y, and τ_{xy}, can then be expressed in terms of the midplane strains and curvatures of the laminate and the transformed reduced stiffness matrix, $\overline{Q}$. The stiffness terms may be taken outside of the integral in Equations (3.20) and (3.21) since the stiffness of a single ply will not vary through its thickness. The stress and moment resultants can now be expressed as

$$\begin{Bmatrix} N_x \\ N_y \\ N_{xy} \end{Bmatrix} = \sum_{k=1}^{N} \left[\overline{Q}\right]_k \left\{ \int_{z_{k-1}}^{z_k} \begin{Bmatrix} \epsilon_x^0 \\ \epsilon_y^0 \\ \gamma_{xy}^0 \end{Bmatrix} dz + \int_{z_{k-1}}^{z_k} \begin{Bmatrix} \kappa_x \\ \kappa_y \\ \kappa_{xy} \end{Bmatrix} z dz \right\}, \tag{3.22}$$

$$\begin{Bmatrix} M_x \\ M_y \\ M_{xy} \end{Bmatrix} = \sum_{k=1}^{N} \left[\overline{Q}\right]_k \left\{ \int_{z_{k-1}}^{z_k} \begin{Bmatrix} \epsilon_x^0 \\ \epsilon_y^0 \\ \gamma_{xy}^0 \end{Bmatrix} z dz + \int_{z_{k-1}}^{z_k} \begin{Bmatrix} \kappa_x \\ \kappa_y \\ \kappa_{xy} \end{Bmatrix} z^2 dz \right\}. \tag{3.23}$$

By utilizing the stress-strain relations, the stress and moment resultants are now expressed in terms of the midplane values of strain and curvature, ϵ_x^0, ϵ_y^0, ϵ_{xy}^0, κ_x, κ_y, and κ_{xy}. This allows the integral expressions to be replaced with summations in a manner similar to what was done with the stiffness properties. The stress and moment resultants can therefore be defined by the midplane strains and curvatures, the extensional stiffness matrix, A, the coupling stiffness matrix, B, and the bending stiffness matrix, D, as follows:

$$\begin{Bmatrix} N_x \\ N_y \\ N_{xy} \end{Bmatrix} = \begin{bmatrix} A_{11} & A_{12} & A_{16} \\ A_{12} & A_{22} & A_{26} \\ A_{16} & A_{26} & A_{66} \end{bmatrix} \begin{Bmatrix} \epsilon_x^0 \\ \epsilon_y^0 \\ \gamma_{xy}^0 \end{Bmatrix} + \begin{bmatrix} B_{11} & B_{12} & B_{16} \\ B_{12} & B_{22} & B_{26} \\ B_{16} & B_{26} & B_{66} \end{bmatrix} \begin{Bmatrix} \kappa_x \\ \kappa_y \\ \kappa_{xy} \end{Bmatrix}, \tag{3.24}$$

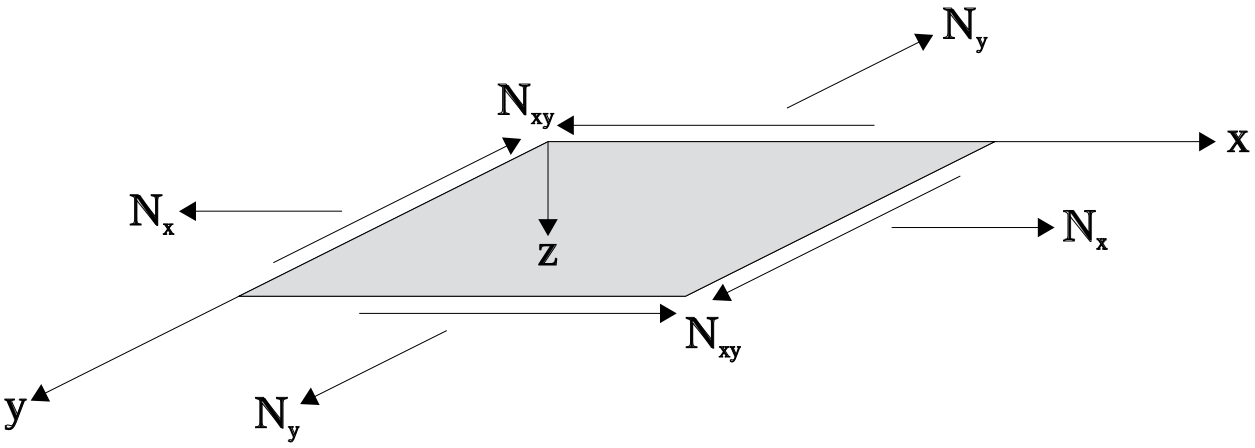

Figure 3.3: Direction of positive stress resultants.

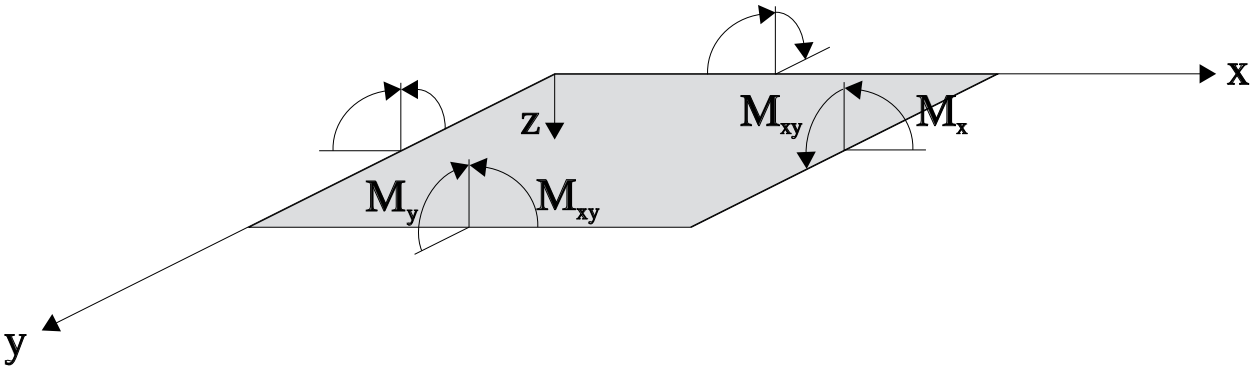

Figure 3.4: Direction of positive moment resultants.

$$\left\{ \begin{array}{c} M_x \\ M_y \\ M_{xy} \end{array} \right\} = \left[\begin{array}{ccc} B_{11} & B_{12} & B_{16} \\ B_{12} & B_{22} & B_{26} \\ B_{16} & B_{26} & B_{66} \end{array} \right] \left\{ \begin{array}{c} \epsilon_x^0 \\ \epsilon_y^0 \\ \gamma_{xy}^0 \end{array} \right\} + \left[\begin{array}{ccc} D_{11} & D_{12} & D_{16} \\ D_{12} & D_{22} & D_{26} \\ D_{16} & D_{26} & D_{66} \end{array} \right] \left\{ \begin{array}{c} \kappa_x \\ \kappa_y \\ \kappa_{xy} \end{array} \right\}, \quad (3.25)$$

$$\begin{aligned} \text{where} \quad A_{ij} &= \sum_{k=1}^{N} (\overline{Q}_{ij})_k \, (z_k - z_{k-1}), \\ B_{ij} &= \sum_{k=1}^{N} (\overline{Q}_{ij})_k \, (z_k^2 - z_{k-1}^2), \\ D_{ij} &= \sum_{k=1}^{N} (\overline{Q}_{ij})_k \, (z_k^3 - z_{k-1}^3). \end{aligned} \quad (3.26)$$

3.5 In-plane Response of Variable-Stiffness Laminated Plates

The differential equations of equilibrium for laminated plates expressed in terms of the stress and moment resultants are:

$$N_{x,x} + N_{xy,y} = 0 \, , \quad (3.27)$$

$$N_{y,y} + N_{xy,x} = 0 \, , \text{ and} \quad (3.28)$$

$$M_{x,xx} + 2M_{xy,xy} + M_{y,yy} = -p \, . \quad (3.29)$$

where a comma denotes a derivative with respect to the subscript.

Several simplifications accompany the analysis that will be performed. First, the laminates will be symmetric about the midplane so the contribution from the coupling stiffness matrix can be neglected since it is identically zero, $B = 0$. Also, there will be no applied transverse loading, $p = 0$, or moments, $M_x = M_y = M_{xy} = 0$, to the laminate. These conditions allow Equation (3.29) to be neglected. The resulting governing equations, Equations (3.27) and (3.28), after these simplifications can be expressed in terms of only the midplane strains, ϵ_x^0, ϵ_y^0, and γ_{xy}^0, and the A matrix.

In order to apply these governing equations to variable-stiffness laminates, it must be recognized that the A matrix is no longer constant because of the variation in orientation angle as a function of panel location. This means that the stiffness matrix terms and, hence, displacements can vary in both the x and y directions. Keeping this in mind while substituting Equation (3.24) into the governing equations, Equations (3.27) and (3.28), and grouping the u and v displacements terms yields:

$$\begin{aligned} A_{11}u_{,xx} + 2A_{16}u_{,xy} + A_{66}u_{,yy} + (A_{11,x} + A_{16,y})u_{,x} + (A_{16,x} + A_{66})u_{,y} \\ = -\{A_{16}v_{,xx} + (A_{12} + A_{66})v_{,xy} + A_{26}v_{,yy} \\ + (A_{16,x} + A_{26,y})v_{,x} + (A_{12,x} + A_{26,y})v_{,y}\}\,, \end{aligned} \tag{3.30}$$

$$\begin{aligned} A_{66}v_{,xx} + 2A_{26}v_{,xy} + A_{22}v_{,yy} + (A_{26,y} + A_{66,x})v_{,x} + (A_{22,y} + A_{26,x})v_{,y} \\ = -\{A_{16}u_{,xx} + (A_{12} + A_{66})u_{,xy} + A_{26}u_{,yy} \\ + (A_{12,y} + A_{16,x})u_{,x} + (A_{26,y} + A_{66,x})u_{,y}\}\,. \end{aligned} \tag{3.31}$$

These equilibrium equations form a set of coupled, elliptical, partial differential equations with variable coefficients. Their solution along with the boundary conditions around the panel edges gives both the u and v displacement fields from which the strains and stress resultants can then be found.

3.6 Numerical Solution of the In-plane Governing Equations

ELLPACK [14], a software package designed to solve elliptic, partial differential equations, was used to find the approximate solution to Equations (3.30) and (3.31) in terms of the u and v displacements. The numerical approximation scheme uses collocation with Hermite bicubic basis

functions, and a direct linear system solve. Since it is not possible to decouple the displacements, an iterative approach was used. This iterative process consisted of substituting an initial estimate for the v displacement in Equation (3.30) and then solving for u. Next, the solution found for u is input into Equation (3.31) and the v displacement is evaluated. This process continues until a convergence criteria has been met for both the u and v displacements. To obtain the coefficients, A_{ij} and their derivatives with respect to the x and y directions, used in Equations (3.30) and (3.31), ELLPACK needs to evaluate the orientation angles and the derivatives of the orientation angles with respect to x and y. Computation of the stiffness terms in terms of the fiber orientation angles variation is discussed in the next two sections for shifted and parallel fiber paths.

3.7 Fiber Orientation Angle and Derivatives for Shifted Fiber Laminae

This class of laminae has its fiber orientation varying only along the x' axis. For this case the determination of the orientation angle and its derivatives can be found analytically as a function of x and y. The fiber orientation only depends upon x' and is given in Equation (2.2). Substituting Equation (2.3) into Equation (2.2), it is possible to obtain the derivatives of the orientation angle with respect to x and y, Equations (3.32) and (3.33), respectively.

$$\frac{\partial\theta(x,y)}{\partial x} = \begin{cases} \frac{2}{a}(T_1 - T_0)\cos\phi, & -a \le x' \le -\frac{a}{2} \\ \frac{2}{a}(T_0 - T_1)\cos\phi, & -\frac{a}{2} \le x' \le 0 \\ \frac{2}{a}(T_1 - T_0)\cos\phi, & 0 \le x' \le \frac{a}{2} \\ \frac{2}{a}(T_0 - T_1)\cos\phi, & \frac{a}{2} \le x' \le a \end{cases} \tag{3.32}$$

$$\frac{\partial\theta(x,y)}{\partial y} = \begin{cases} \frac{2}{a}(T_1 - T_0)\sin\phi, & -a \le x' \le -\frac{a}{2} \\ \frac{2}{a}(T_0 - T_1)\sin\phi, & -\frac{a}{2} \le x' \le 0 \\ \frac{2}{a}(T_1 - T_0)\sin\phi, & 0 \le x' \le \frac{a}{2} \\ \frac{2}{a}(T_0 - T_1)\sin\phi, & \frac{a}{2} \le x' \le a \end{cases} \tag{3.33}$$

3.8 Fiber Orientation Angle and Derivatives for Parallel Fiber Laminae

The fiber paths are not used in the analysis by ELLPACK. The only information required by the program is the fiber orientation and its derivatives at a finite number of collocation points. The procedure for finding the orientation, and hence its derivatives, for laminae created by the parallel fiber method is essentially the reverse process of finding one curve that is parallel to another. Instead of finding a set of points that lie a constant distance along the normal direction from the reference curve, a normal is found from the collocation point to the curve. The fiber orientation at a point $P(x, y)$ is then set equal to the fiber orientation at the point along the reference curve obtained from forming a perpendicular line from point P to the reference curve. Since the normal direction is the shortest distance between a point and a curve, the problem lends itself to an optimization problem in terms of the distance between the point and the reference path.

Using the following definitions (see Figure 3.5)

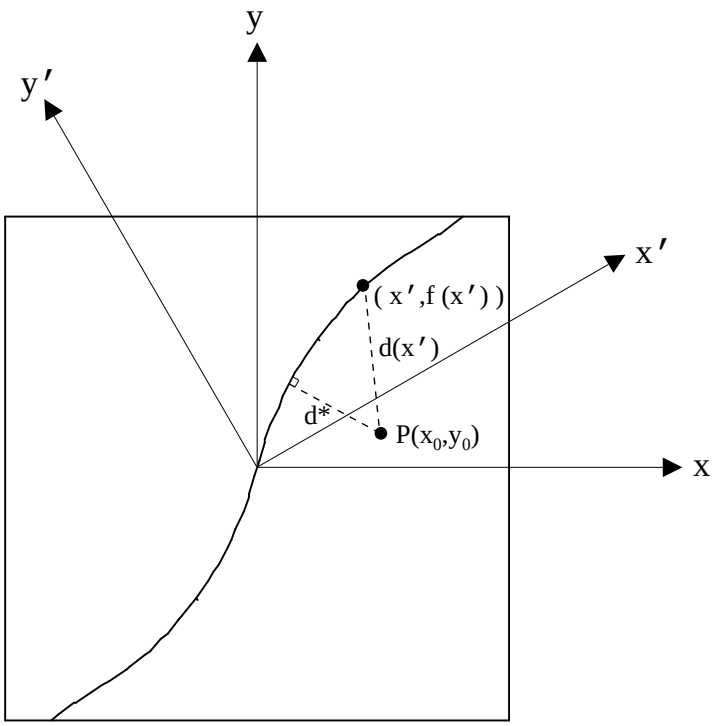

Figure 3.5: Definition of parameters used in the creation of parallel fiber paths.

$P(x_0, y_0)$	an arbitrary point at which the orientation is needed
x'	first coordinate of a point on the reference fiber path
$f(x')$	second coordinate location of a point on the fiber path corresponding to x'
$d(x')$	distance between $P(x, y)$ and $(x', f(x'))$
d^*	minimum distance between $P(x, y)$ and the reference path

where $f(x')$ is the function that describes the reference fiber path, Equation (2.1), the unconstrained, one-dimensional minimization problem can be stated as:

$$\text{Minimize} \quad d(x') = [(x - x')^2 + (y - f(x'))^2]^{1/2}. \tag{3.34}$$

Due to the complexity of the fiber path equation, an analytical expression for $d(x')$ could not be found. Therefore, a numerical method is required to solve the minimization problem.

The golden search method [15] was used to perform the minimization of the distance between a point on the panel and the reference fiber path. This is a variable interval search method that converges quite rapidly for unimodal functions, such as the distance in this case. The golden search method is composed of two parts. The first is bracketing the minimum. The second reduces the interval of uncertainty until a minimum interval is reached.

The first step is to determine the general interval in which the local minimum appears. A possible distance curve, $d(x')$, is shown in Figure 3.6. The search begins, for this case, with a function evaluation at $x' = 0$. Subsequent function values are evaluated for

$$x'_q = \sum_{j=0}^{q} \delta(1.618)^j \tag{3.35}$$

where δ is a small, positive number. The resulting initial step size in x' is relatively small. However, it becomes progressively larger for subsequent evaluations of the distance function. The bracketing

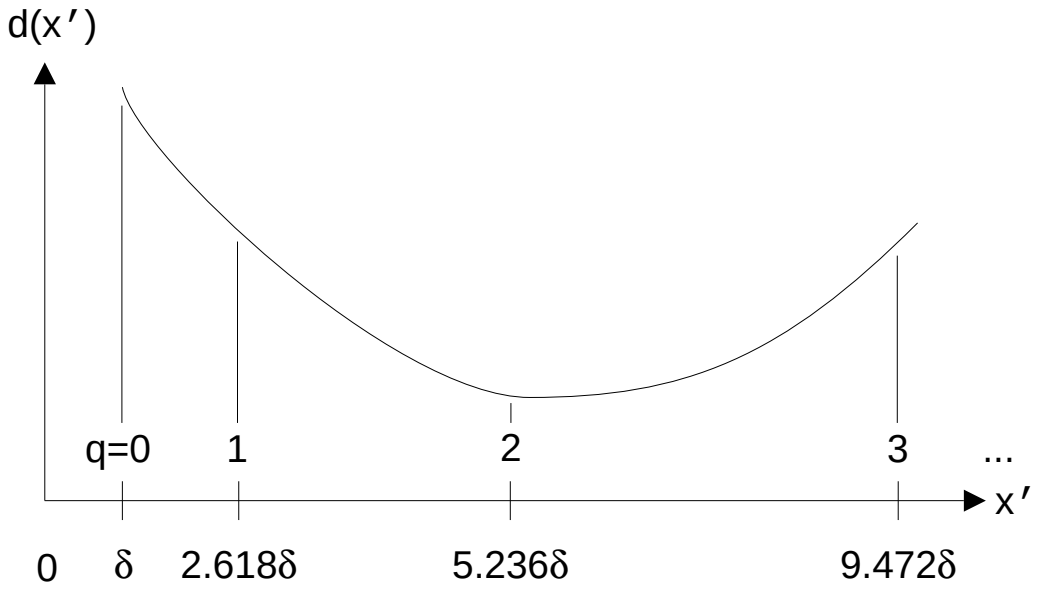

Figure 3.6: Sample distance curve.

of the minimum is completed after a sufficient number of iterations on x', q, result in satisfying the following criteria

$$d(x'_{q-2}) < d(x'_{q-1}) < d(x'_q). \tag{3.36}$$

At this point, the local minimum is known to be within the interval of uncertainty, I, between x'_{q-2} and x'_q.

After bracketing the local minimum, the second portion of the golden search method is performed. This portion will reduce the interval of uncertainty until a convergence criteria is met. The reduction of the interval requires two interior points in addition to the two end points. The points are chosen so that the function values at three of the points are already known, the two end points and one internal point. Therefore, the search requires only one additional function evaluation per iteration to conduct the golden search method.

Assuming that the minimum has been bracketed in q iterations, the end points of this interval are

$$x'_l = x'_{q-2} \, , \tag{3.37}$$

$$x'_u = x'_q \, . \tag{3.38}$$

These end points define an interval length, I, of

$$I = x'_q - x'_{q-2} \, . \tag{3.39}$$

One point obtained by the bracketing procedure, x'_{q-1}, is used as one of the interior points for the golden search method,

$$x'_a = x'_{q-1} \, . \tag{3.40}$$

The final point needed to reduce the interval of uncertainty is then given by

$$x'_b = x'_l + 0.618I \; . \tag{3.41}$$

The initial interval of uncertainty with the internal points marked and the process of reducing the interval through the second iteration is illustrated in Figure 3.7. For this case assume that x'_a has the lowest function evaluation of the four points. Therefore, the points used for the second iteration, denoted with a $*$, are

$$x'^{*}_l = x'_l \tag{3.42}$$

$$x'^{*}_b = x'_a \tag{3.43}$$

$$x'^{*}_u = x'_b \tag{3.44}$$

$$I^* = x'^{*}_u - x'^{*}_l \tag{3.45}$$

$$x'^{*}_a = x'^{*}_u + 0.328I^* \tag{3.46}$$

The major advantage of the golden search method over other search methods, as shown by Equations (3.42)–(3.46), is that it requires only a single function evaluation to reduce the interval of uncertainty.

This process will continue until the interval, I, is less than a given convergence criteria, at which point, the optimal point is set to be the midpoint of the interval defined by the final two end points, x'_u and x'_l. This optimal point will return the smallest distance between a given point and the reference curve. The given point, $P(x, y)$, is then assigned the same fiber orientation as the corresponding point on the reference curve. This is essentially the same as setting the tangent for the fiber path passing through the collocation point to be parallel to the tangent for the reference fiber path at the optimal point.

The solution for the in-plane response of a variable-stiffness composite panel using ELLPACK requires the use of not only the fiber orientation at the collocation points, but also the corresponding derivatives in the x and y directions. As with the fiber orientation, the procedure to find the orientation derivatives for parallel fiber paths was more complicated compared to the shifted fiber method.

A finite difference approximation was used to determine the derivatives of the fiber orientation with respect to the panel axes. A finite difference perturbs one of the variables by a known increment. A derivative is then calculated as a change in the function value over the change in the variable. For the fiber orientation derivatives, a central difference was used, yielding

$$\frac{\partial \theta(x,y)}{\partial x} = \frac{\theta(x+\Delta x, y) - \theta(x-\Delta x, y)}{2\Delta x}\,, \tag{3.47}$$

$$\frac{\partial \theta(x,y)}{\partial y} = \frac{\theta(x, y+\Delta y) - \theta(x, y-\Delta y)}{2\Delta y}\,. \tag{3.48}$$

A lower order finite difference did not offer the accuracy necessary for the program to converge and a higher order expression would be computationally expensive. Therefore, the central difference offered a good combination of accuracy and computational ease.

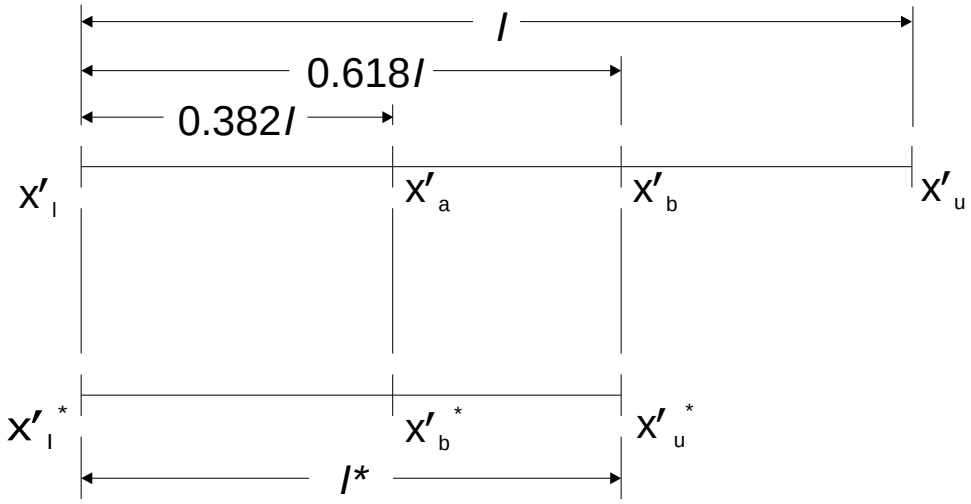

Figure 3.7: Reduction of the interval of uncertainty.

Chapter 4

Constraints on Variable-Stiffness Laminates

Variable-stiffness laminates in this investigation have to meet two criteria for minimal acceptable performance. These criteria are that the laminate does not fail under the applied loading and that the fiber paths do not form kinks due to excessive curvature.

4.1 Panel Failure

Strength failure of a laminate is determined using a first ply failure based on the Tsai-Hill criterion,

$$\frac{\sigma_1^2}{X_c^2} + \frac{\sigma_2^2}{Y_c^2} - \frac{\sigma_1\sigma_2}{X_c^2} + \frac{\tau_{12}^2}{S^2} < 1 \; . \tag{4.1}$$

As long as the relationship in Equation (4.1) is satisfied for every ply, no failure of the laminate occurs. However, if one ply fails then the entire laminate is said to fail regardless of the laminate's residual strength. The in-plane stress values in the principal material directions 1 and 2 are derived from the laminate midplane strains in the x and y directions, the fiber orientation angle θ, and the

reduced stiffness matrix, Q_{ij}. The procedure to convert strains in the x and y directions to the stresses in the principal material directions is given by

$$\begin{Bmatrix} \epsilon_1 \\ \epsilon_2 \\ \gamma_{12}/2 \end{Bmatrix} = \begin{bmatrix} \cos^2\theta & \sin^2\theta & 2\sin\theta\cos\theta \\ \sin^2\theta & \cos^2\theta & -2\sin\theta\cos\theta \\ -\sin\theta\cos\theta & \sin\theta\cos\theta & \cos^2\theta - \sin^2\theta \end{bmatrix} \begin{Bmatrix} \epsilon_x \\ \epsilon_y \\ \gamma_{xy}/2 \end{Bmatrix}, \text{ and} \tag{4.2}$$

$$\begin{Bmatrix} \sigma_1 \\ \sigma_2 \\ \tau_{12} \end{Bmatrix} = \begin{bmatrix} Q_{11} & Q_{12} & 0 \\ Q_{12} & Q_{22} & 0 \\ 0 & 0 & Q_{66} \end{bmatrix} \begin{Bmatrix} \epsilon_1 \\ \epsilon_2 \\ \gamma_{12} \end{Bmatrix}. \tag{4.3}$$

Recall that the subscripts 1 and 2 refer to the principal material directions which correspond to the fiber direction and the direction transverse to the fiber, respectively. In order to apply the Tsai-Hill criteria to variable-stiffness laminates, it must be recognized that strains, fiber orientation angles, and reduced stiffnesses will vary as a function of panel location. This requires that Equation (4.1) be satisfied at every point of every ply.

The use of the Tsai-Hill criteria was chosen over other failure prediction methods, such as the maximum stress and maximum strain theories, for several reasons. One is that it offers a more continuous strength variation that accompanies changes in orientation angle. Also, it incorporates interactions between the failure strengths that some other theories neglect completely. The draw back to using the Tsai-Hill method is that it does not tell how the laminate fails, only that it does.

4.2 Fiber Curvature Constraint

In order to create these variable-stiffness laminates, it is necessary to actually curve the tow paths. If a tow is curved too much, then it is quite possible that a kink in the fiber will develop. In an

effort to limit the degree of this kinking, the laminates are required to have the fiber paths be such that the largest curvature for any ply be less than a prescribed maximum curvature. The curvature constraint gives a measure of the change in orientation angle relative to the panel length. Since the panel dimensions, 20 $in \times 20$ in, are fixed in this study, the only values that will affect the curvature are the changes in orientation angles T_0 and T_1. If this change is too large, then a given fiber path will develop kinks which are undesirable. The implementation of this constraint depends upon whether the laminate is made using the shifted or parallel fiber method.

The fiber paths of a shifted fiber ply are identical to the reference fiber path. Therefore, it is sufficient to apply the fiber curvature constraint only to the reference fiber path. The definition of curvature, K, for a function of a single variable, $f(x)$, is given by

$$K = \frac{f''(x)}{(1 + (f'(x))^2)^{3/2}} \, . \tag{4.4}$$

Recognizing that the reference fiber path of a given ply is defined by the single variable x', its curvature, K, can be found by substituting the fiber path equation for $f(x)$ in Equation (4.4). Only the curvature of this path in the positive x' portion of the panel needs to be calculated since the reference fiber path is antisymmetric about the y' axis. At each location along the reference fiber path, the curvature, K, is required to be less than the maximum allowable curvature of $1/12in$ to insure that the laminate could be made. This critical value was determined from the use of the tow placement machine used by the Boeing Defense and Space Group in Philadelphia, Pa. If the curvature is less than this critical value, the analysis is performed. However, if the curvature exceeded the maximum allowable curvature, no further analysis was performed since the laminate can not be manufactured.

An interesting aspect of the procedure used to create parallel fiber paths is in the restriction

that must be placed on the radius of curvature of the reference path. If the radius of curvature is small, it is possible that a given point on the panel, $P(x, y)$, can become equidistant from two or more (possibly infinitely many) locations on the reference curve. In that situation, the search method will select only one of these points as having the minimum distance to $P(x, y)$. In Figure 4.1, the point P that we want to calculate the fiber orientation for is at the center of curvature of the reference fiber path. Therefore, the fiber orientation angle may be assigned to that of point 1, point 2, or any point between points 1 and 2 depending on which was initially bracketed in the golden search method. If approaching the point P from point B, for a small change in location of the point, it is possible to have a very large change in fiber orientation, almost 90^o if the angle at point P was obtained from point 1 on the reference curve. If this were to occur, a kink would appear in the fiber path in the vicinity of point P.

While this may seem like a serious disadvantage, it actually reflects a realistic manufacturing constraint which disqualifies laminates with large changes in fiber orientation angles (due to the tendency of the fibers to kink). This manufacturing constraint requires the radius of curvature to be large enough so as to essentially put the center of curvature outside of the bounds of the panel. This generally eliminates the possibility of having a problem associated with being near the center of curvature for laminae utilized in this analysis.

The analysis for the parallel fiber laminates uses an approach for determining laminates with acceptable curvature that is similar to the method for shifted fiber laminates. The modified procedure reflects the fact that the curvature of fibers that are parallel to the reference fiber path may be different from that of the reference path since they are no longer the same curves. That is, it is entirely possible that a lamina with an acceptable reference fiber path will have other fiber paths that violate the curvature constraint. Therefore, it is necessary to modify the curvature check of

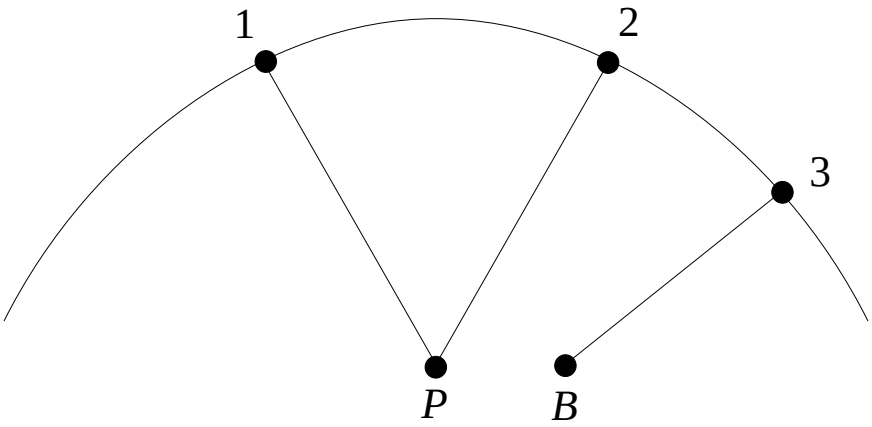

Figure 4.1: Problem of minimum distance for a point at the center of curvature.

the parallel fiber laminates to take into account the variation of curvature as a function of position.

As with the shifted fiber laminae, we first ensure that the reference fiber path does not violate the curvature constraint. Assuming that the reference path satisfies the curvature constraint, next step involves the determination of the curvature of the fiber paths that are parallel to the reference fiber path. Reviewing the way parallel paths are created will help demonstrate how the curvature of these paths is determined. The necessary information is provided in Figure 2.5. The reference fiber path in this case is defined by an infinite number of points, A_i. The path parallel to it B is defined by a set of points, B_i, which lay at a fixed distance from the reference fiber path, measured along the normal to the reference path, $\hat{n}_{A_i}$. The centers of curvature, O_i, corresponding to different points on the reference path can also be seen in Figure 2.5. (Note that the radius of curvature for the reference path, $R_{A_i} = |\overline{A_i O_i}|$, changes as a function of location along the reference fiber path.) Since the paths A and B are parallel, they must have the same centers of curvature. As such, it is possible to define the radius of curvature of a point B_i, $R_{B_i} = |\overline{B_i O_i}|$, in terms of two values that can be calculated - the normal distance between the two paths $|\overline{A_i B_i}|$ and the radius of curvature for the reference path R_{A_i}:

$$R_{B_i} = R_{A_i} - |\overline{A_i B_i}|. \tag{4.5}$$

For parallel fiber variable-stiffness laminates, the radius of curvature for a fiber path passing through point B_i will be less than the curvature of the reference fiber path at A_i provided that B_i lies between A_i and O_i. Since the curvature is defined to be the reciprocal of the radius of curvature, this will create larger curvature for the fiber path passing through point B_i compared to the reference fiber path at A_i. Thus, a lamina with a reference fiber path that meets the curvature constraint may still exceed the maximum allowable curvature for another path in the panel if the path passes through a point at less than 12.0 in from the center of curvature. Therefore, by marking 12.0 in from the

center of curvature O_i of each point along the reference path A we can create a set of points that we refer to as critical points. A path passing closer to the center of curvature than the critical points will violate the radius of curvature constraint. That is, if the critical point remains inside the boundaries of the panel, then all of the fiber paths passing between the critical point and the panel boundary will violate the constraint.

An example of this is $0\langle 0|30\rangle$ reference fiber path for a $20\ in \times 20\ in$ ply. The reference fiber path for this laminate is shown in Figure 4.2. The reference fiber path does meet the curvature constraint since its maximum curvature is approximately $1/19.1in$. However, as subsequent paths are created towards the edge at $y = b/2$, the curvature increases. The points shown by an open symbol and marked as critical points in Figure 4.2 indicate where a fiber path will have a curvature equal to the critical curvature. Any path closer to the center of curvature than these critical points will violate the constraint since its curvature will be slightly larger than that of a path passing through a critical point.

The design space for square $20\ in \times 20\ in$ variable-stiffness laminae having reference fiber paths varying either along or transverse to the loading axis, $\phi = 0^o$ or 90^o, respectively, can be seen in Figure 4.3. The black region represents laminae that can not be manufactured by either method because the reference fiber path violates the curvature constraint. Laminae shown in grey can be made using the shifted fiber method since the reference fiber path does not violate the curvature constraint. However if fiber paths parallel to the reference fiber path are created, the curvature constraint will be violated. The white region is where both the parallel and shifted fiber formats are valid designs. Allowing the curvature to vary as a function of position significantly reduces the number of valid variable-stiffness parallel fiber laminae. This will most likely reduce the degree to which the parallel fiber format can improve upon traditional straight fiber laminates.

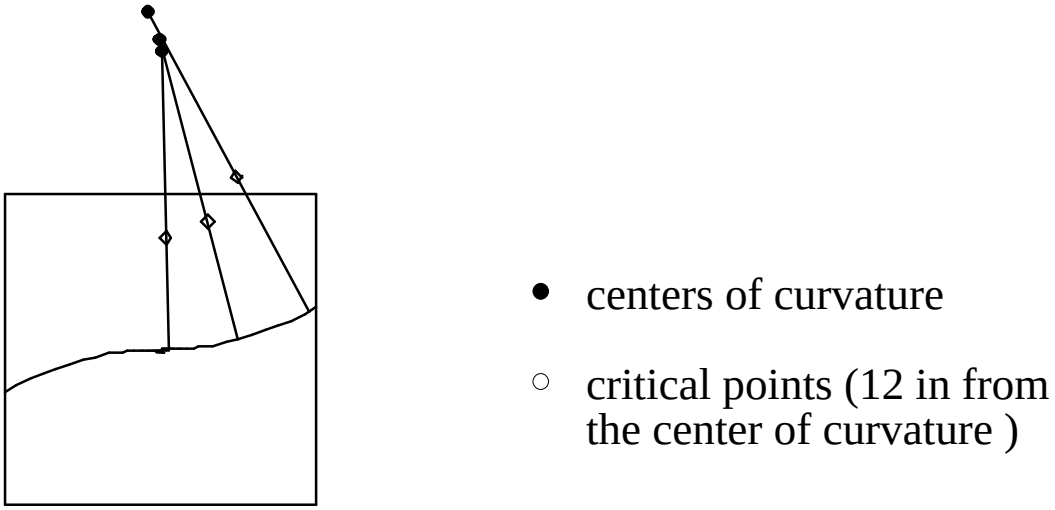

Figure 4.2: Violation of the curvature constraint by a $0\langle 0|30\rangle$ ply.

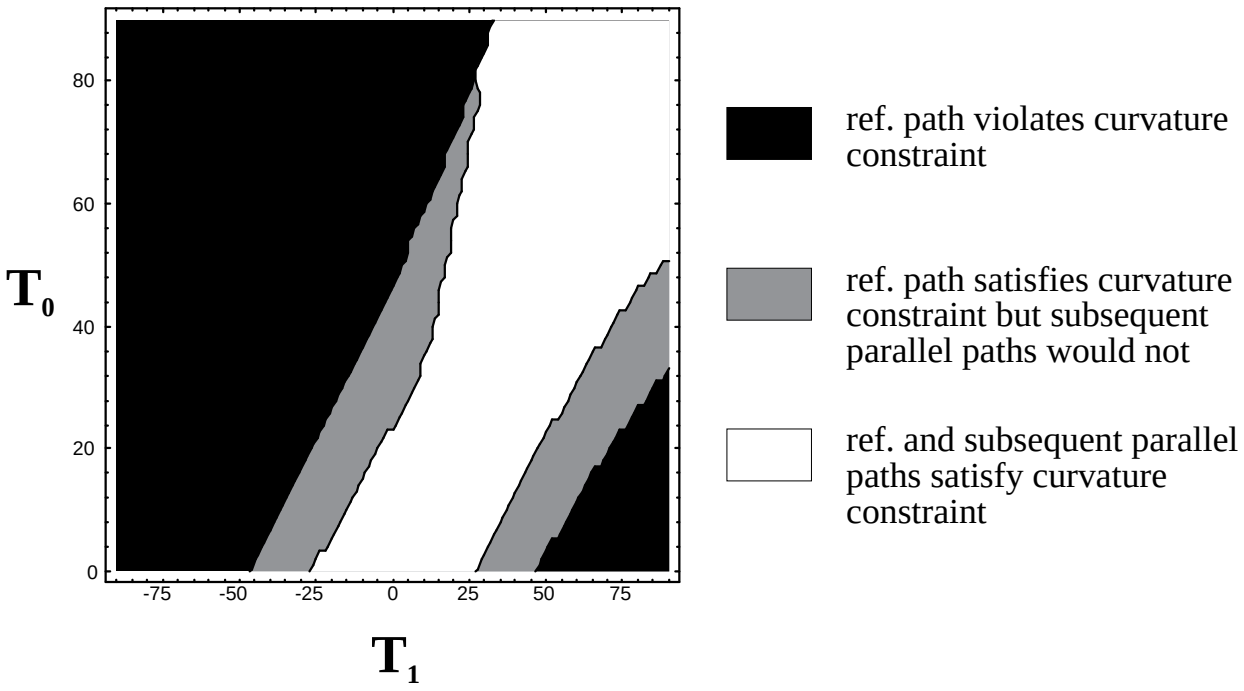

Figure 4.3: Effect of including the curvature constraint on variable-stiffness laminae with $\phi = 0^o$ or 90^o.

Chapter 5

Analysis of Laminates Subjected to Uniaxial Compression

The first loading condition to be examined is the case of a panel under a uniform end-shortening in one direction with the transverse edges free to expand. First the model used to find the in-plane results will be defined. Next, the in-plane results will be explored in order to give an insight into the mechanisms involved in the uniaxial loading of variable-stiffness laminates. And finally, the critical buckling loads and equivalent axial stiffnesses of shifted and parallel fiber laminates will be examined.

5.1 Model Definition for Uniaxial Compression

The boundary conditions for this report correspond to a panel under uniform end shortening, u_0, with the transverse edges free to expand. The model created to simulate this loading condition can be seen in Figure 5.1. The in-plane boundary conditions are as follows:

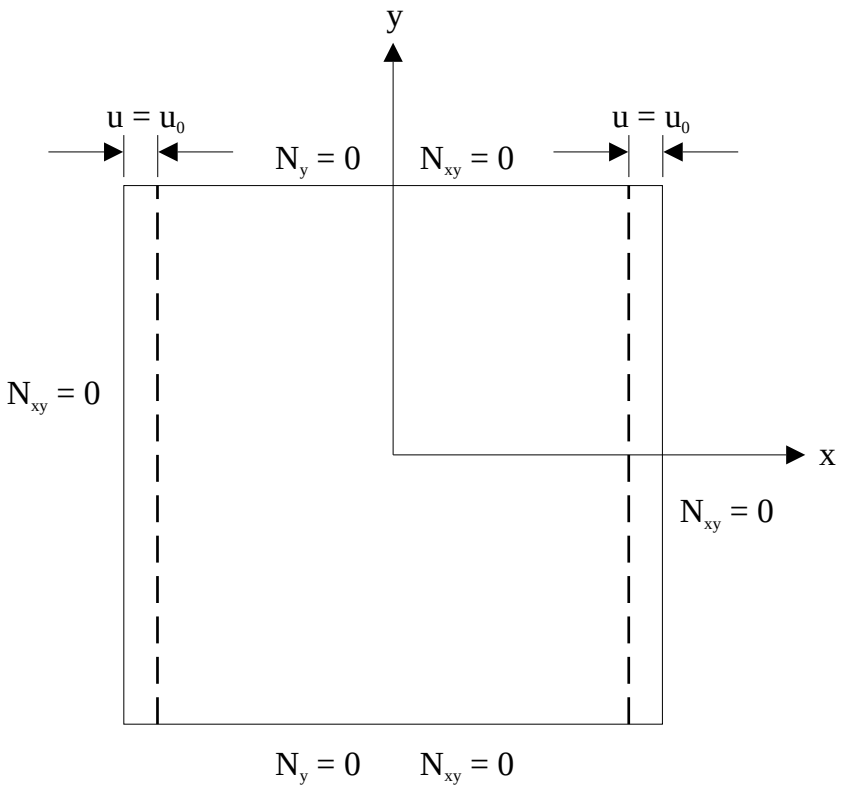

Figure 5.1: Model with boundary conditions for uniaxial compression.

$$\begin{aligned} \text{along} \quad & x = \pm\tfrac{a}{2} \quad u = \mp u_0 \quad N_{xy} = 0 \ , \\ & y = \pm\tfrac{b}{2} \quad N_y = 0 \quad N_{xy} = 0 \ . \end{aligned} \tag{5.1}$$

The only applied loading is that created by the uniform end shortening in the x direction. The N_y and N_{xy} stress resultants are set equal to zero along the edges of the panel since there is no applied loading along these directions. Due to the fact that only derivative conditions exist on the v displacements along the boundaries, it is necessary to enforce an additional constraint, $v(-a/2, -b/2) = 0$, to prevent the translation of the model in the y direction. The material properties used in this analysis are as follows:

$$\begin{aligned} E_1 &= 21.0\, Msi, \qquad E_2 = 1.40\, Msi, \qquad G_{12} = 0.80\, Msi, \\ \nu_{12} &= 0.34, \qquad\qquad t = 0.0055\, in. \end{aligned}$$

5.2 In-plane Analysis for Uniaxial Compression of Variable-Stiffness Laminates

To gain a better understanding of the behavior of variable-stiffness laminates, the in-plane response for two different laminates will be explored. These are balanced, symmetric laminates of the form $[\phi \pm \langle T_0|T_1\rangle]_{9s}$. The first will have its reference fiber orientation change transverse to the loading axis, $\phi = 90^o$. The other laminate will have its reference fiber orientation vary along the loading axis, $\phi = 0^o$. Since there are two methods to define the fiber paths of these laminates, a comparison of the shifted and parallel fiber laminates will also be made.

5.2.1 In-plane Response of Shifted Fiber $[90 \pm \langle 45|75\rangle]_{9s}$ Variable-Stiffness Laminate to Uniaxial Compression

The fiber paths for a $[90 \pm \langle 45|75\rangle]_{9s}$ laminate created by the shifted fiber method can be seen in Figure 5.2. This laminate is composed of thirty six layers, each with properties varying transverse to the applied loading, $\phi = 90^o$. The normalized stress resultant in the x direction is expressed as

$$\overline{N}_x = \frac{a}{|u_0 A_{11}(0,0)|} N_x \tag{5.2}$$

with N_y and N_{xy} also normalized in the same way. The normalized stress resultants are shown in Figures 5.3–5.5. Because the fiber orientation changes as a function of panel location, the stress resultants for this laminate, unlike a straight fiber laminate, are no longer be constant. $\overline{N}_x$ is not constant throughout the laminate, Figure 5.3, but it is constant for each y coordinate. The largest values of $\overline{N}_x$ are along the transverse edges. The fibers in vicinity of these edges are oriented closer to the loading axis thus creating regions with relatively large stiffness values. By requiring uniform end displacements along $x = \pm a/2$, the larger portion of the load is carried in the region along the edges at $y = \pm b/2$.

The equilibrium shear stress resultant distribution depends upon both N_x and N_y as given in Equations (3.27) and (3.28). Since N_x does not vary in the x direction, Equation (3.27) requires that the distribution of N_{xy} can not vary in the y direction. The boundary conditions defined in the model require N_{xy} to be zero along the top and bottom of the panel. Therefore, $\overline{N}_{xy}$ is identically equal to zero everywhere as shown in Figure 5.5.

The N_y is then found using Equation (3.28). Since N_{xy} is zero everywhere, the change of N_y with respect to the y direction must also equal zero. The value at the top and bottom of N_y is required to be zero along these boundaries. Again as with the shear stress resultant, $\overline{N}_y$ is also

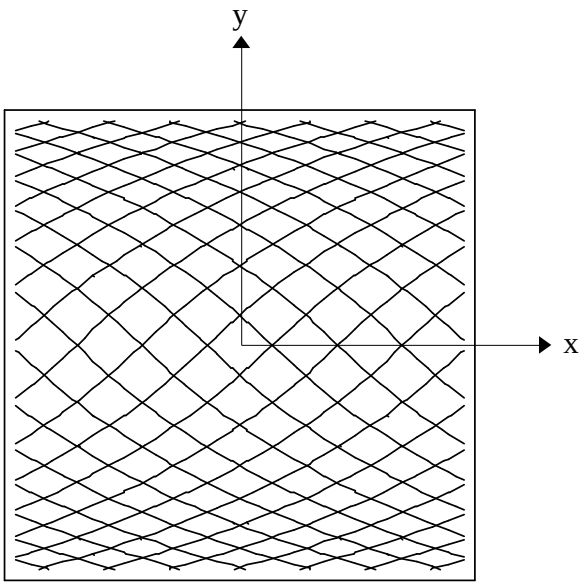

Figure 5.2: Fiber paths for $[90 \pm \langle 45|75\rangle]_{9s}$ made by the shifted fiber method.

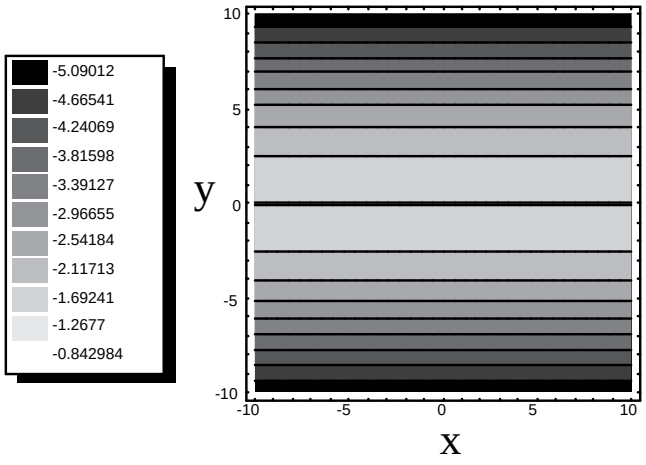

Figure 5.3: $\overline{N}_x$ as a function of panel location for $[90 \pm \langle 45|75\rangle]_{9s}$ made by the shifted fiber method.

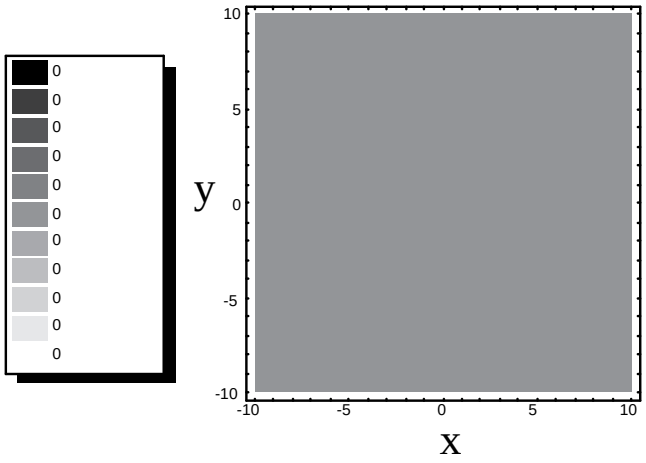

Figure 5.4: $\overline{N}_y$ as a function of panel location for $[90 \pm \langle 45|75 \rangle]_{9s}$ made by the shifted fiber method.

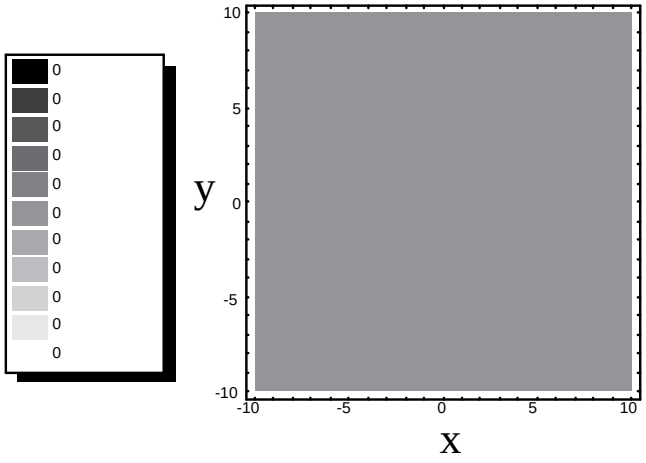

Figure 5.5: $\overline{N}_{xy}$ as a function of panel location for $[90 \pm \langle 45|75 \rangle]_{9s}$ made by the shifted fiber method.

identically zero, Figure 5.4.

5.2.2 In-plane Response of Shifted Fiber $[0 \pm \langle 45|75\rangle]_{9s}$ Variable-Stiffness Laminate to Uniaxial Compression

The fiber paths for a $[0 \pm \langle 45|75\rangle]_{9s}$ laminate are shown in Figure 5.6. Unlike the previous laminate, this one has its fiber orientation changing along the loading axis. The normalized stress resultants corresponding to the uniform end shortening of the shifted fiber $[0 \pm \langle 45|75\rangle]_{9s}$ laminate are shown in Figures 5.7–5.9.

The fiber orientation varies from 45^o at $x = 0$ to 75^o along $x = \pm a/2$. As such, the edges where the uniform end shortening takes place are more pliant to compression compared to the center. Therefore, the largest strains in the x direction occur in the regions $x = \pm a/2$. These strains are significantly reduced towards the center of the panel where the laminate is stiffer. This increase in stiffness and decrease in strains tend to create a fairly uniform distribution of the $\overline{N}_x$ over the central portion of the panel, Figure 5.7.

The distribution of the normalized shear stress resultant for the panel can be seen in Figure 5.9. When this laminate is subjected to the uniform end shortening, the amount of transverse expansion varies in the x direction from the center of the panel to the edges. At $x = 0$ where the fiber orientation angle is 45^o, the panel wants to expand more than at the edges $x = \pm a/2$ that have a 75^o orientation. This change in Poisson's ratio will tend to create shear stress resultants that vary both in both the x and y directions.

The values of $\overline{N}_y$ are shown in Figure 5.8. As with $\overline{N}_x$ and $\overline{N}_{xy}$, $\overline{N}_y$ also varies in both the x and y directions so as to satisfy Equation (3.28). As such, fairly large, tensile stress resultants appear near $x = \pm a/2$. Significant compressive $\overline{N}_y$ appear in the center portion of the panel and

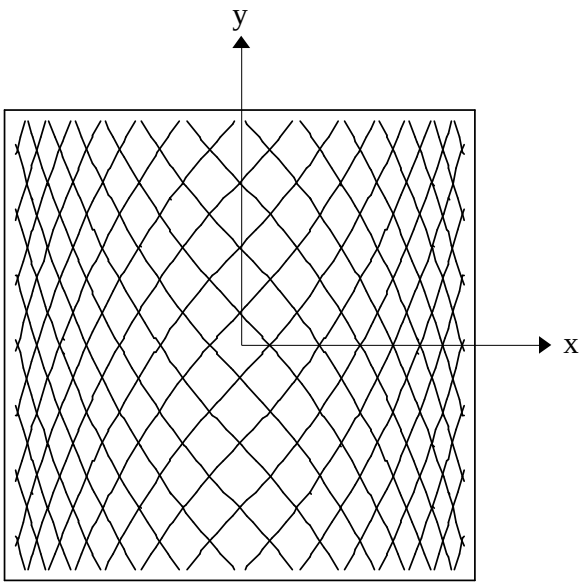

Figure 5.6: Fiber paths for $[0 \pm \langle 45|75 \rangle]_{9s}$ made by the shifted fiber method.

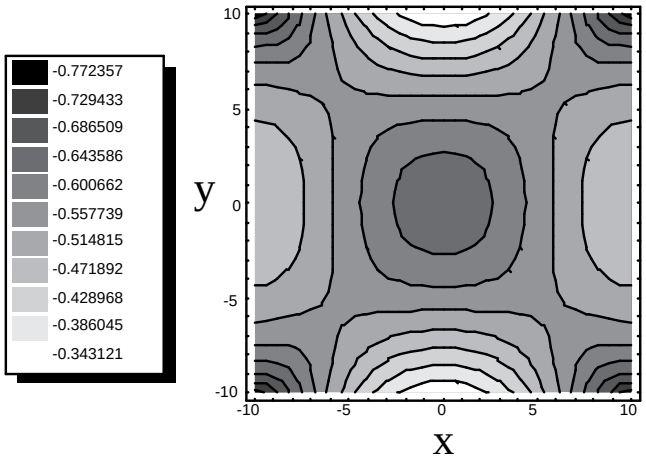

Figure 5.7: $\overline{N}_x$ as a function of panel location for $[0 \pm \langle 45|75 \rangle]_{9s}$ made by the shifted fiber method.

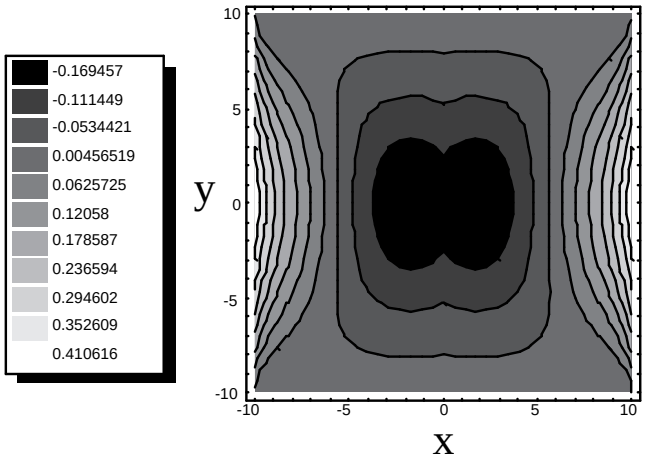

Figure 5.8: $\overline{N}_y$ as a function of panel location for $[0 \pm \langle 45|75 \rangle]_{9s}$ made by the shifted fiber method.

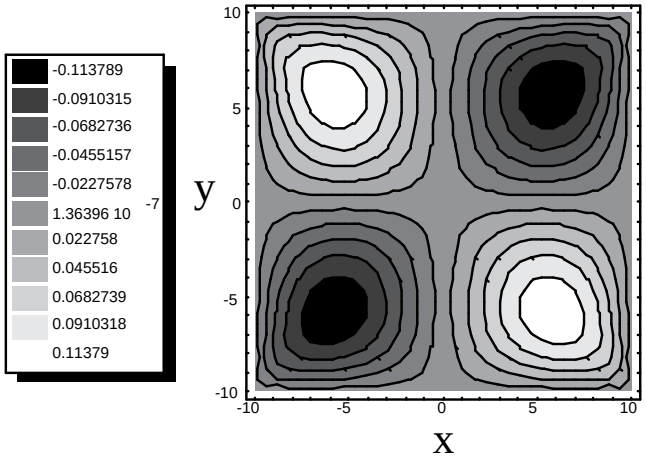

Figure 5.9: $\overline{N}_{xy}$ as a function of panel location for $[0 \pm \langle 45|75 \rangle]_{9s}$ made by the shifted fiber method.

remain fairly uniform over the region defined by $-a/4 \leq x \leq a/4$ and $-b/4 \leq y \leq b/4$.

5.2.3 In-plane Response of Parallel Fiber $[90 \pm \langle 45|75 \rangle]_{9s}$ Variable-Stiffness Laminate to Uniaxial Compression

The first laminate made by the parallel fiber method that will be investigated is the $[90 \pm \langle 45|75 \rangle]_{9s}$ laminate. The fiber paths for this laminate can be seen in Figure 5.10. Unlike the same laminate made by the shifted fiber, this has fiber orientation and stiffness properties varying in both the x and y directions.

The normalized stress resultants can be seen in Figures 5.11–5.13. The $\overline{N}_x$, Figure 5.11, for this laminate is similar to that of the shifted fiber laminate in that the largest stress resultants are concentrated along the transverse edges, $y = \pm b/2$. However, this distribution is no longer constant for a given y coordinate as was the case in the shifted fiber laminate. The parallel fiber method has its N_x distribution varying in both the x and y directions. The largest magnitudes of $\overline{N}_x$ for the parallel fiber case are significantly smaller than with the shifted fiber case. However, the parallel fiber $[90 \pm \langle 45|75 \rangle]_{9s}$ laminate experiences larger compressive stresses along $y = 0$ when compared to the shifted fiber panel.

An interesting feature of the parallel fiber laminates is shown in Figure 5.13 which demonstrates that the parallel fiber laminate has non-zero distribution of shear stress resultants. This is in stark contrast to the shifted fiber laminate that had the $\overline{N}_{xy}$ for a $[90 \pm \langle 45|75 \rangle]_{9s}$ laminate equal to zero throughout the panel. Two different mechanisms contribute to the nonzero shear stress resultants for the parallel fiber laminate. One of these relates to the shear created by the manner in which the panel wants to deform and the other is material coupling caused by locally unbalanced fiber orientations. The shifted fiber laminates with $\phi = 90^o$ will want to expand uniformly in the y

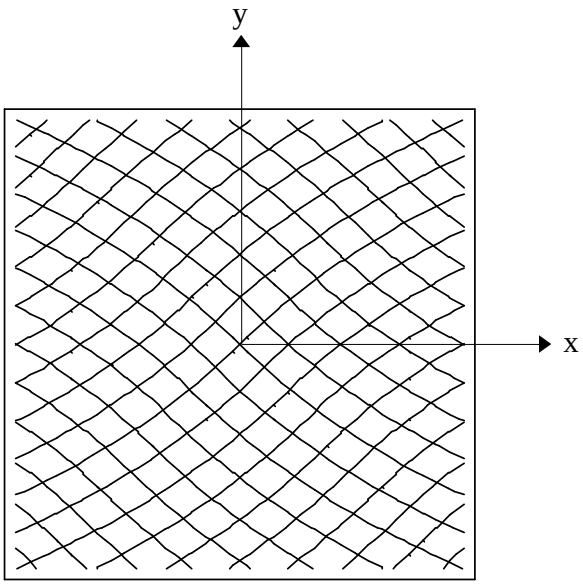

Figure 5.10: Fiber paths for $[90 \pm \langle 45|75\rangle]_{9s}$ made by the parallel fiber method.

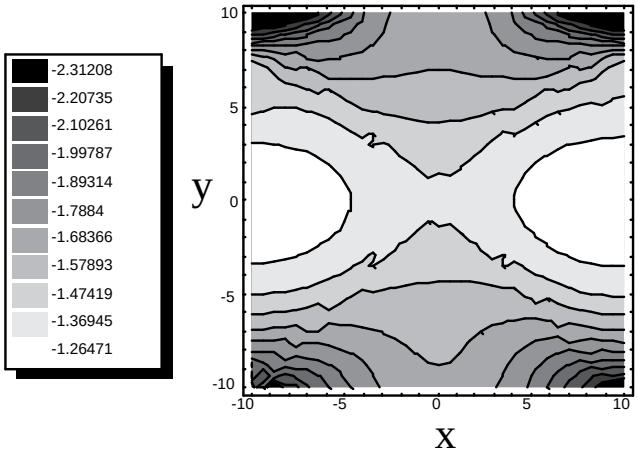

Figure 5.11: $\overline{N}_x$ as a function of panel location for $[90 \pm \langle 45|75\rangle]_{9s}$ created by the parallel fiber method.

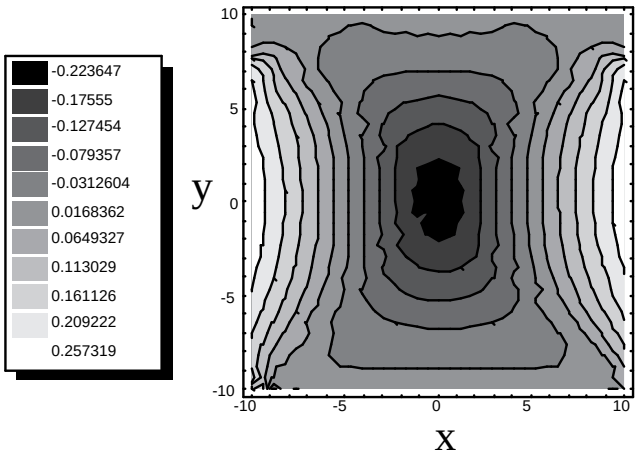

Figure 5.12: $\overline{N}_y$ as a function of panel location for $[90 \pm \langle 45|75\rangle]_{9s}$ created by the parallel fiber method.

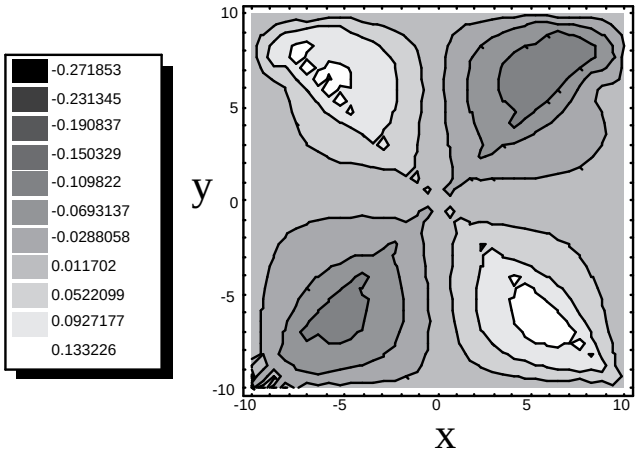

Figure 5.13: $\overline{N}_{xy}$ as a function of panel location for $[90 \pm \langle 45|75\rangle]_{9s}$ created by the parallel fiber method.

direction. However, the stiffness variation for a parallel fiber laminate in both the x and y directions will tend to cause shear deformation when the laminate is subjected to a uniform end shortening. This response is similar to that of a shifted fiber laminate with $\phi = 0^o$. The material coupling that arises from locally unbalanced fiber orientation only occurs in the parallel fiber formulation. The reason for this can be seen by examining the difference between the calculation of fiber orientation angle for a given point $P(x, y)$ by the shifted and parallel fiber methods as shown in Figure 5.14. The reference paths for a $[0 \pm \langle 45|0\rangle]_s$ laminate are shown, Reference fiber path 1 corresponds to a $0 + \langle 45|0\rangle$ fiber path while reference fiber path 2 is a $0 - \langle 45|0\rangle$ fiber path. The shifted fiber format assigns point P the orientation at points x'_{1_s} and x'_{2_s} for layers 1 and 2 respectively. These orientations are approximately $\pm 20^o$ which makes the laminate balanced. The parallel fiber method finds normal lines between point P and the reference curves. The points on the reference curves that create these normal lines are denoted by x'_{2_p} and x'_{2_p}. This method gives the point the orientations of approximately 45^o and -15^o for the two layers which are clearly not balanced. It is possible, however, for other points on the laminate to be positioned such that its fiber orientations are balanced. Hence, the use of the parallel fiber method tends to create local regions of unbalanced fiber orientations.

The $\overline{N}_y$ for the parallel fiber $[90 \pm \langle 45|75\rangle]_{9s}$ laminate is shown in Figure 5.12. It is no longer essentially zero as it was for the shifted fiber laminate. To satisfy the prescribed boundary conditions, the values of $\overline{N}_y$ are close to zero near the transverse edges, $y = \pm b/2$. There are significant tensile N_y along the edges at $x = \pm a/2$. The center of the panel experiences compressive stress resultants in the y direction. Relatively large tensile $\overline{N}_y$ occur along $x = \pm a/2$.

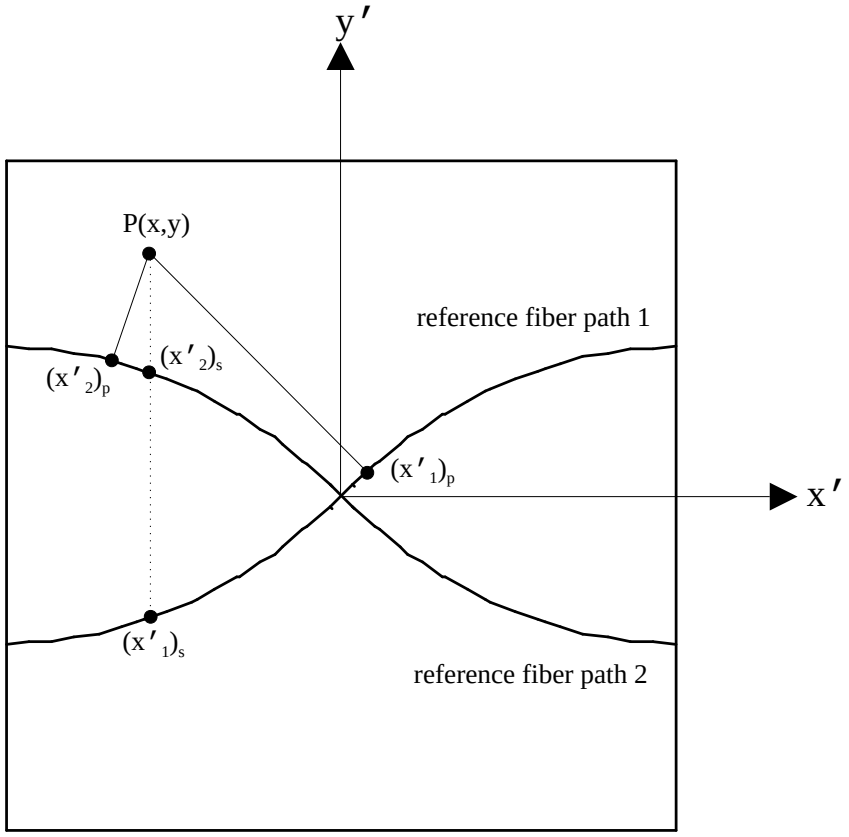

Figure 5.14: Formation of unbalanced laminates by parallel fiber configuration.

5.2.4 In-plane Response of Parallel Fiber $[0 \pm \langle 45|75 \rangle]_{9s}$ Variable-Stiffness Laminate to Uniaxial Compression

The fiber paths for the parallel fiber $[0 \pm \langle 45|75 \rangle]_{9s}$ laminate are provided in Figure 5.15, with the normalized stress resultants shown in Figures 5.16–5.18.

The $\overline{N}_x$ distribution for the parallel fiber laminate can be seen in Figure 5.16. As with the parallel fiber $[90 \pm \langle 45|75 \rangle]_{9s}$ and shifted fiber $[0 \pm \langle 45|75 \rangle]_{9s}$ laminates, this also has $\overline{N}_x$ varying in both the x and y directions. The largest compressive $\overline{N}_x$ are located primarily along $y = 0$. The compressive $\overline{N}_x$ along $y = 0$ are not as large as those carried in the center of the panel. The smallest compressive $\overline{N}_x$ occur in the vicinity of the transverse edges, $y = \pm b/2$.

The shear stress resultants for the parallel fiber $[0 \pm \langle 45|75 \rangle]_{9s}$ laminate are given in Figure 5.18. The shearing that is present is smaller than that of the shifted fiber $[0 \pm \langle 45|75 \rangle]_{9s}$. There are two distinct mechanisms which tend to couple shear and extension for variable-stiffness laminates: material coupling and locally unbalanced fiber orientations. The degree of material coupling is dependent upon the variation of the fiber orientation with position. Since the fiber variation over the panel for the parallel fiber method is more gradual than the shifted fiber, the material coupling of shifted fiber laminate will tend to be larger than a parallel fiber laminate with the same reference fiber path. While the parallel fiber method does create locally unbalanced fiber orientations which will also couple shear and extension, it is still not able to create the magnitudes of the shear stresses present in the shifted fiber laminate.

The values of $\overline{N}_y$ for the panel can be seen in Figure 5.17. Unlike the shifted fiber $[0 \pm \langle 45|75 \rangle]_{9s}$ and parallel fiber $[90 \pm \langle 45|75 \rangle]_{9s}$, tensile $\overline{N}_y$ are present in the central portion of the panel. Along $x = \pm a/2$, however, compressive $\overline{N}_y$ exist.

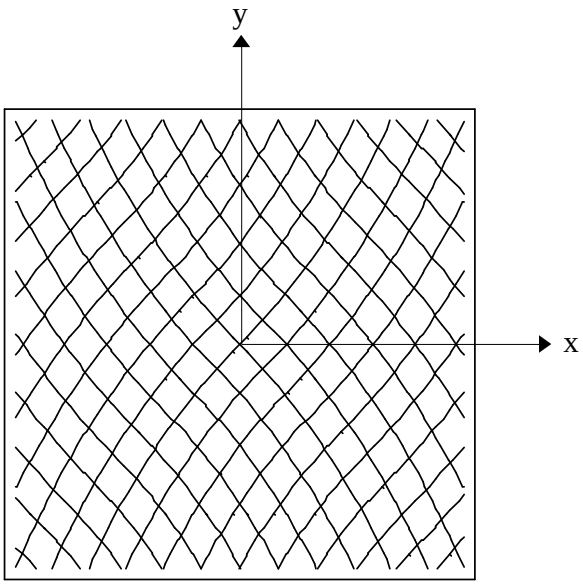

Figure 5.15: Fiber paths for $[0 \pm \langle 45|75\rangle]_{9s}$ made by the parallel fiber method.

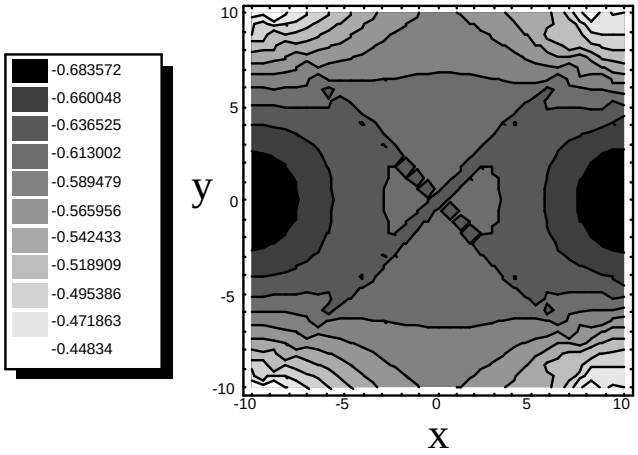

Figure 5.16: $\overline{N}_x$ as a function of panel location for $[0 \pm \langle 45|75\rangle]_{9s}$ created by the parallel fiber method.

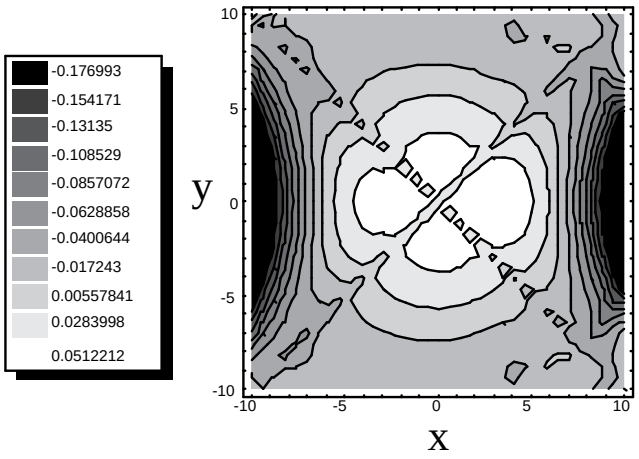

Figure 5.17: $\overline{N}_y$ as a function of panel location for $[0 \pm \langle 45|75\rangle]_{9s}$ created by the parallel fiber method.

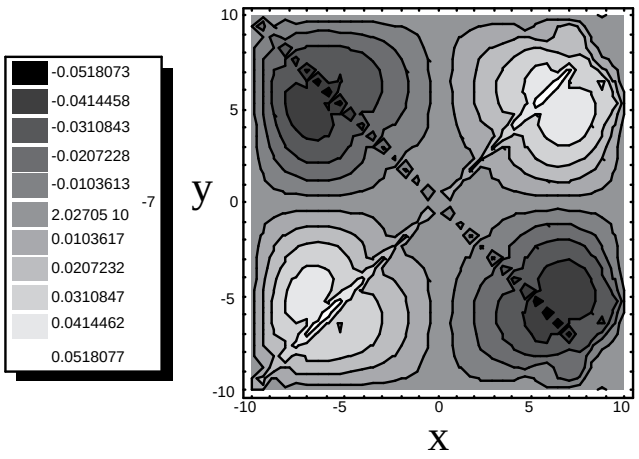

Figure 5.18: $\overline{N}_{xy}$ as a function of panel location for $[0 \pm \langle 45|75\rangle]_{9s}$ created by the parallel fiber method.

5.3 Buckling Response of Variable-Stiffness Laminates Subjected to Uniform End Shortening

The buckling response of laminates having variable-stiffness plies will be examined. These laminates will be compared to the straight fiber laminate with the largest buckling load, $[\pm 45]_{9s}$. Various types of laminates will be explored. Initially, only laminates composed of layers having the reference fiber path either along or transverse to the loading axis are examined. Next, straight fiber plies are added to the first case resulting in hybrid laminates. The buckling loads of laminates created by combining variable-stiffness plies with reference fibers varying both along and transverse to the loading axis will be examined.

5.3.1 Formulation of the Buckling Analysis for Uniform End Shortening of Variable-Stiffness Laminates

The procedure for determining the critical buckling load of a variable-stiffness composite panel is the same regardless of the prescribed in-plane loading conditions. However, it is helpful to define several quantities that describe the panel loading conditions. In this case, the primary quantity of interest relates to the force necessary to create the uniform end displacement. This quantity can then be used to aid in the buckling load representation of the panel as well as defining an equivalent axial stiffness.

When the panel is loaded by uniform end shortening, the total force induced on the panel is given by

$$F_x = \int_{-b/2}^{b/2} N_x(\frac{a}{2}, y)\, dy \tag{5.3}$$

with a and b representing the total length and width of the panel, respectively. The average value

of N_x is simply the total force acting on the panel per unit width,

$$N_x^{av} = \frac{F_x}{b} \, . \tag{5.4}$$

Another quantity of interest is the equivalent axial stiffness of the panel, E_x^{eq}. Using Hooke's law, $\sigma = E\epsilon$, E_x^{eq} can be expressed as

$$E_x^{eq} = \frac{F_x a}{h b u_0} \tag{5.5}$$

where h is the total thickness of the panel and u_0 is the uniform end shortening. The normalized equivalent axial stiffness, $\overline{E}_x^{eq} = E_x^{eq}/E_1$, is created such that a value of 0.8 represents a laminate that is effectively 80% as stiff as that of an all 0^o laminate.

The buckling analysis was performed using subroutines from LAPACK to solve the eigenvalue problem formulated from the Ritz method,

$$\delta U + \delta V = 0 \tag{5.6}$$

where U is the strain energy due to bending and V is the potential energy of the in-plane loads. The strain energy of an elastic body is given by

$$U = \frac{1}{2} \iiint \left(\sigma_x \epsilon_x + \sigma_y \epsilon_y + \sigma_z \epsilon_z + \sigma_{xy} \epsilon_{xy} + \sigma_{zx} \epsilon_{zx} + \sigma_{zy} \epsilon_{zy} \right) dx \, dy \, dz \, . \tag{5.7}$$

This expression can be simplified by using the Kirchhoff assumptions, i.e. $\epsilon_z = \epsilon_{xz} = \epsilon_{yz} = 0$, explained in Section 3.3. If integration is performed with respect to the z direction, it can be shown that the strain energy is given by

$$U = \frac{1}{2} \iint \left[D_{11} \left(\frac{\partial^2 w}{\partial x^2} \right)^2 + D_{12} \frac{\partial^2 w}{\partial x^2} \frac{\partial^2 w}{\partial y^2} + D_{22} \left(\frac{\partial^2 w}{\partial y^2} \right)^2 + D_{66} \left(\frac{\partial^2 w}{\partial x \partial y} \right)^2 \right] dx \, dy \, . \tag{5.8}$$

Note that the current analysis neglects the contribution of the twist coupling stiffnesses, $D_{16} = 0$ and $D_{26} = 0$. The potential energy, V, of the in-plane loads created from an out of plane displacement,

w, is

$$V = \lambda \iint \left(N_x \epsilon'_x + N_y \epsilon'_y + N_{xy} \epsilon'_{xy} \right) \, dx \, dy \tag{5.9}$$

where λ is an arbitrary multiplier used to determine the buckling load, N_x, N_y, and N_{xy} are the stress resultants associated with the prebuckled configuration, and ϵ'_x, ϵ'_y, and ϵ'_{xy} are the midplane strains that result from the w displacement. These strains are defined as the nonlinear terms in the Green strain tensor involving w:

$$\epsilon'_x = \frac{1}{2} \left(\frac{\partial w}{\partial x} \right)^2 , \tag{5.10}$$

$$\epsilon'_y = \frac{1}{2} \left(\frac{\partial w}{\partial y} \right)^2 , \tag{5.11}$$

$$\epsilon'_{xy} = \frac{\partial w}{\partial x} \frac{\partial w}{\partial y} . \tag{5.12}$$

Substituting the definitions in Equations (5.10)-(5.12) into the expression for the potential energy results in the following

$$V = \frac{1}{2} \lambda \iint \left[N_x \left(\frac{\partial w}{\partial x} \right)^2 + N_y \left(\frac{\partial w}{\partial y} \right)^2 + 2 N_{xy} \frac{\partial w}{\partial x} \frac{\partial w}{\partial y} \right] dx \, dy . \tag{5.13}$$

A double sine series approximation of the w displacement can be used and is given by

$$w(x, y) = \sum_{m=1}^{M} \sum_{n=1}^{N} A_{mn} \sin \frac{m \pi x}{a} \sin \frac{n \pi y}{b} . \tag{5.14}$$

When this series approximation for w is substituted into Equations 5.8 and 5.13, the Ritz method can be reduced to an eigenvalue problem of the form

$$[K]\{A\} - \lambda [M]\{A\} = 0 \tag{5.15}$$

where the stiffness matrix, $[K]$, is the sums of the integrals containing terms involving D_{ij}, and the geometric stiffness matrix, $[M]$, is the summation of integrals involving the stress resultants. The critical eigenvalue for the solution is designated by λ_{cr} and can be used to find the critical buckling

load. The manner that λ_{cr} is defined depends upon the applied loading condition. For uniform end shortening, λ_{cr} is taken to be the smallest positive eigenvalue.

The average N_x acting on the panel, Equation (5.5), and the critical eigenvalue determined by Equation (5.15) are used to determine an average critical buckling load,

$$N_{xcr}^{av} = \lambda_{cr} N_x^{av} \ . \tag{5.16}$$

A normalized critical buckling load will be used to present the results. To do this, N_{xcr}^{av} is multiplied by a normalization term,

$$\overline{N}_{xcr}^{av} = \frac{a^2 N_{xcr}^{av}}{E_1 h^3} \ . \tag{5.17}$$

In each case, the laminate must satisfy both the strength and curvature constraints. The failure constraint placed on the laminate due to strength considerations does not impact the selection of acceptable variable-stiffness laminates under the uniform end-shortening. In the cases examined so far, the panel will buckle before it fails under uniaxial loading. The failure and buckling loads of several laminates are provided in Table 5.1. On the other hand, Figure 4.3 shows that the curvature constraint disqualifies many laminates that might otherwise produce excellent results. The critical buckling load of a laminate that fails either the strength or curvature constraint is assigned $\overline{N}_{xcr}^{av} = 0$.

5.3.2 Critical Buckling Load for Laminates with $\phi = 90^o$

The critical buckling load for both the shifted and parallel fiber variable-stiffness laminates with $\phi = 90^o$ can be seen in Figures 5.19 and 5.20, respectively. The white regions in the upper left and lower right corners of Figures 5.19 and 5.20 indicate that the laminates have failed the curvature constraint. Certain laminates with fiber orientation varying transverse to the loading axis offer

Table 5.1: Failure and buckling loads for various laminates under uniaxial loading.

Laminate	Failure N_x (lbs/in)	Buckling N_x (lbs/in)
$[0]_{18s}$	-61,380	-426.7
$[\pm 45]_{9s}$	-5,917	-720.6
$[90]_{18s}$	-33,660	-240.9
$[0 \pm \langle 15 \vert 60 \rangle]_{9s}$	-13,690	-692.2
$[90 \pm \langle 30 \vert 75 \rangle]_{9s}$	-14,343	-1,043

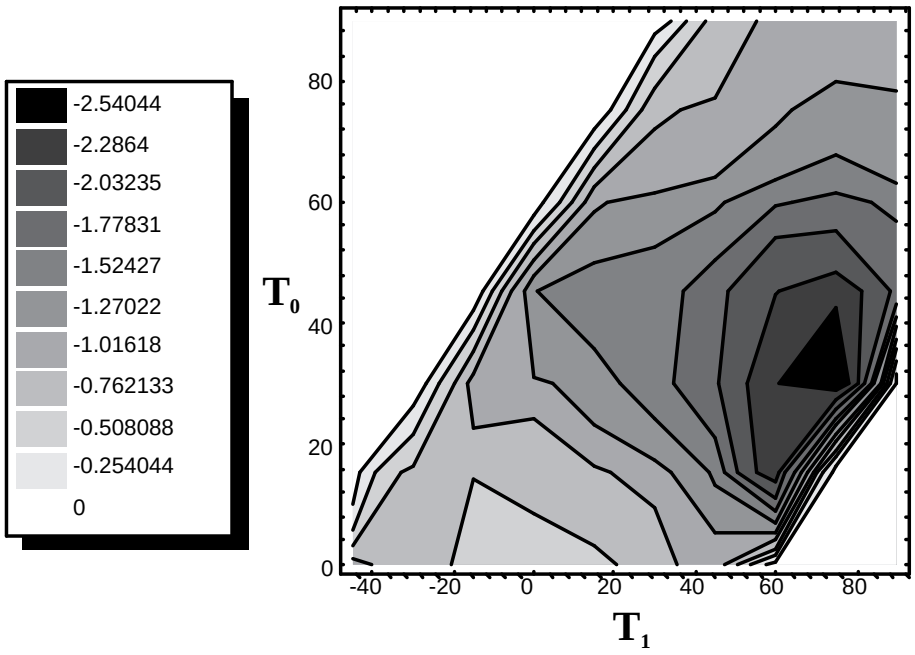

Figure 5.19: $\overline{N}_{xcr}^{av}$ for shifted fiber laminates with $\phi = 90^o$ and various combinations of T_0 and T_1.

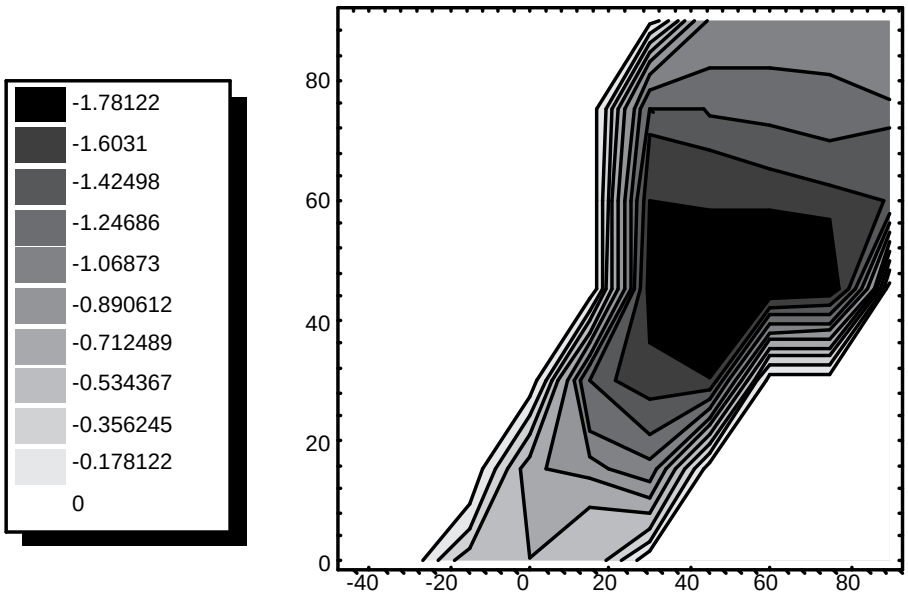

Figure 5.20: $\overline{N}_{xcr}^{av}$ for parallel fiber laminates with $\phi = 90^o$ and various combinations of T_0 and T_1.

increases in buckling load over that of the optimal straight fiber laminate, $[\pm 45]_{9s}$. For example, the shifted fiber $[90 \pm \langle 30|75 \rangle]_{9s}$ has the largest normalized critical buckling load of -2.540. This is an increase of 44% compared to the $[\pm 45]_{9s}$ laminate's normalized critical buckling load of -1.768. The best parallel fiber laminate was $[90 \pm \langle 45|60 \rangle]_{9s}$ which has a normalized critical buckling load of only -1.781. This is only slightly larger, 0.74%, than $[\pm 45]_{9s}$ and considerably less than the shifted fiber $[90 \pm \langle 30|75 \rangle]_{9s}$.

These two classes of laminates, as shown by the in-plane response for both the shifted and parallel fiber $[90 \pm \langle 45|75 \rangle]_{9s}$, can redistribute a large portion of the loading induced by the uniform end shortening towards the transverse edges at $y = \pm b/2$. The panel, however, can not buckle near the edges because it is restrained from out-of-plane displacements along all of the edges. At the same time, the center portion of the panel will experience a lower N_x compared to the transverse edges and will not buckle until a higher loading level is encountered. The region that typically wants to buckle first for a square panel under uniform end shortening is near the center. By reducing the stresses in this region, some variable-stiffness laminates with $\phi = 90^o$ can increase the critical buckling load over traditional straight fiber laminates.

The major reason for the differences between the critical buckling loads for the laminates made by the two different methods lies with the redistribution of the applied loading. The shifted fibers redistribute the loading towards the edges to a greater degree compared to the parallel fiber laminates do. When this is added to the fact that the parallel fiber laminates can have compressive N_y and nonzero N_{xy} in center of the panel, as shown by the parallel fiber $[90 \pm \langle 45|75 \rangle]_{9s}$ laminate, it is clear why the parallel fiber laminates are not able to achieve as high a critical buckling load as for the shifted fiber laminates.

5.3.3 Critical Buckling Load for Laminates with $\phi = 0^o$

The normalized critical buckling load for laminates with $\phi = 0^o$ created by the shifted and parallel fiber methods are shown in Figures 5.21 and 5.22, respectively. Both fiber formats were able to slightly increase upon the critical buckling load of $[\pm 45]_{9s}$. The largest $\overline{N}^{av}_{xcr}$ for the shifted fiber laminate with $\phi = 0^o$ was -1.843 for $[0 \pm \langle 60|30 \rangle]_{9s}$. This is a 4.2% improvement over $[\pm 45]_{9s}$. The parallel fiber $[0 \pm \langle 45|30 \rangle]_{9s}$ laminate had a $\overline{N}^{av}_{xcr}$ of -1.792, a 1.4% improvement.

Two different mechanisms were used by these laminates to improve upon the critical buckling load of $[\pm 45]_{9s}$. For the shifted fiber laminate, beneficial transverse stresses were created in the center of the panel. For a shifted fiber $[0 \pm \langle 60|30 \rangle]_{9s}$ laminate, the fiber orientation is such that the panel will expand less along $x = 0$ than at $x = \pm a/2$. This will tend to create tensile loadings in the y direction along $x = 0$. The $[0 \pm \langle 45|30 \rangle]_{9s}$ parallel fiber laminate is such that the reference fiber paths, and hence fiber paths in general, are quite similar to the parallel fiber $[90 \pm \langle 45|60 \rangle]_{9s}$, Figure 5.23. As such, this laminate was also able to redistribute the loading towards the transverse edges. The responses of these two parallel fiber laminates to uniform end shortening are quite similar, as shown by the $[0 \pm \langle 45|30 \rangle]_{9s}$ laminate buckling load being only 0.62% higher than that of $[90 \pm \langle 45|60 \rangle]_{9s}$.

5.4 Equivalent Axial Stiffness of Shifted and Parallel Fiber Laminates With $\phi = 0^o$ and $\phi = 90^o$

The equivalent axial stiffness of shifted and parallel fiber variable-stiffness laminates with $\phi = 90^o$ is shown in Figures 5.24 and 5.25, respectively. As with the critical buckling loads, laminates violating either the strength or curvature constraint are assigned $\overline{E}^{eq}_{x} = 0$ and are located in the

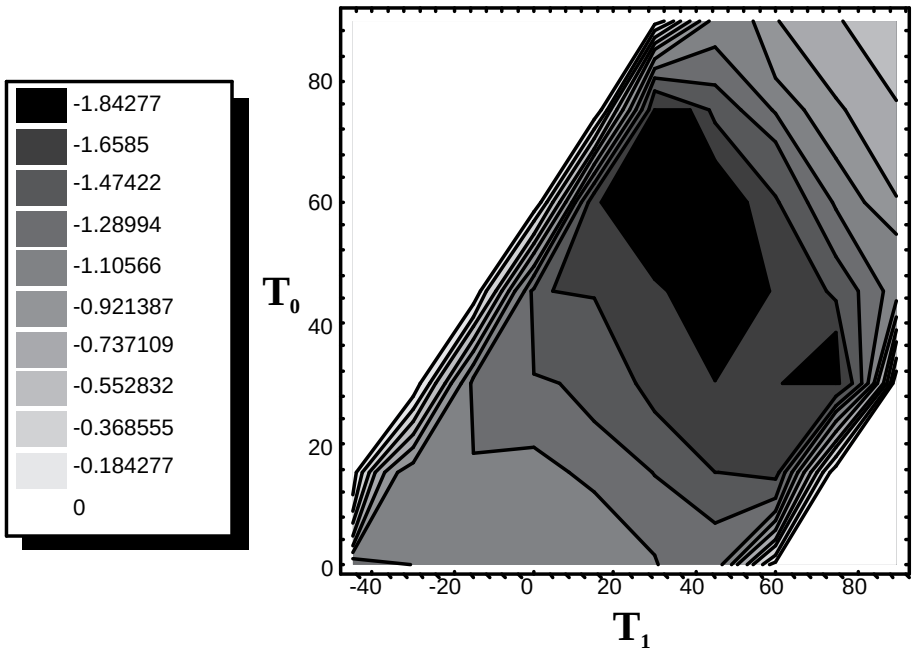

Figure 5.21: $\overline{N}_{xcr}^{av}$ for shifted fiber laminates with $\phi = 0^o$ and various combinations of T_0 and T_1.

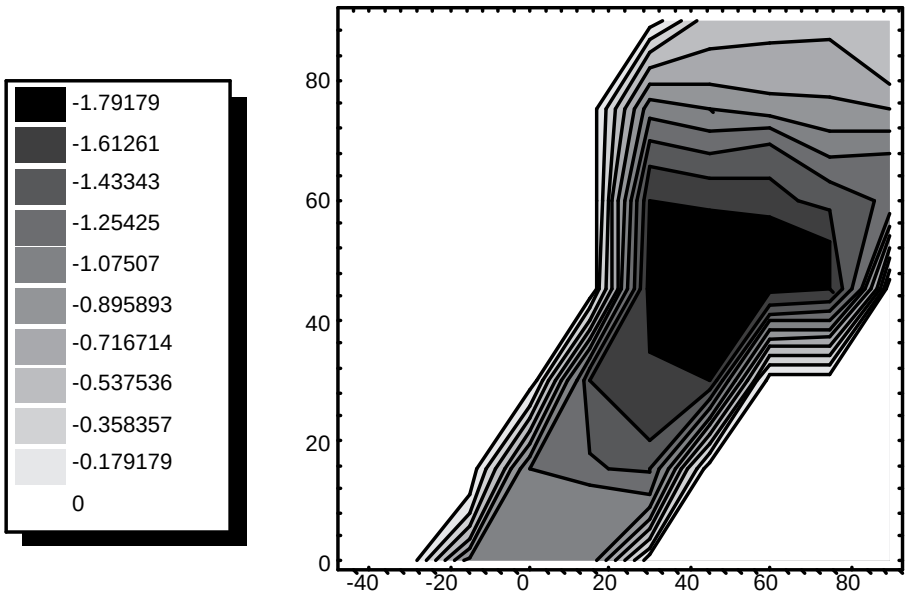

Figure 5.22: $\overline{N}_{xcr}^{av}$ for parallel fiber laminates with $\phi = 0^o$ and various combinations of T_0 and T_1.

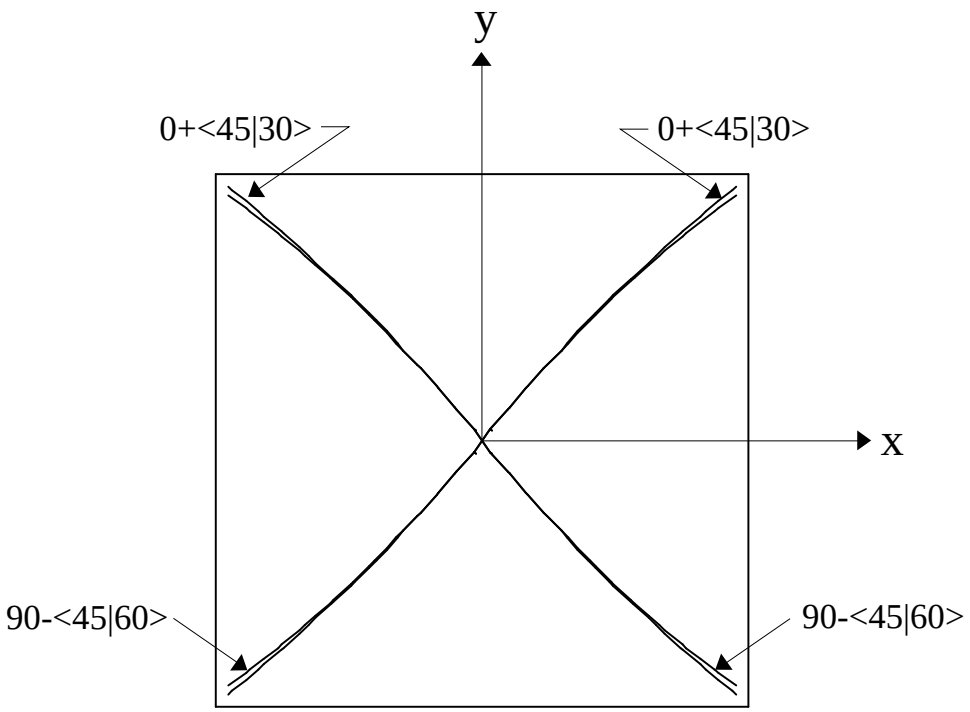

Figure 5.23: Similarity between the reference paths for $[0 \pm \langle 45|30 \rangle]_{9s}$ and $[90 \pm \langle 45|60 \rangle]_{9s}$ laminates.

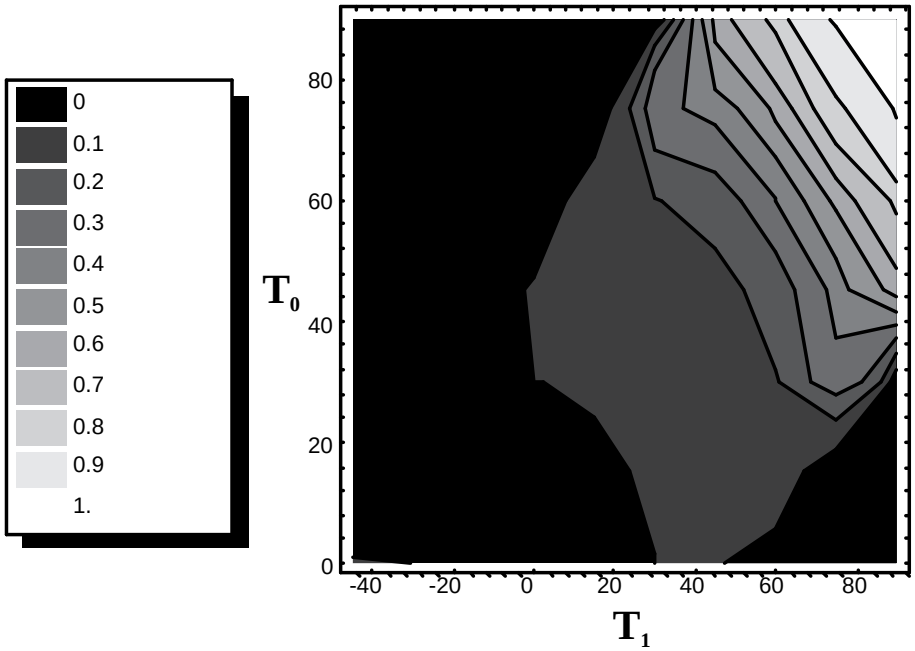

Figure 5.24: $\overline{E}_x^{eq}$ for shifted fiber laminates with $\phi = 90^o$ and various combinations of T_0 and T_1.

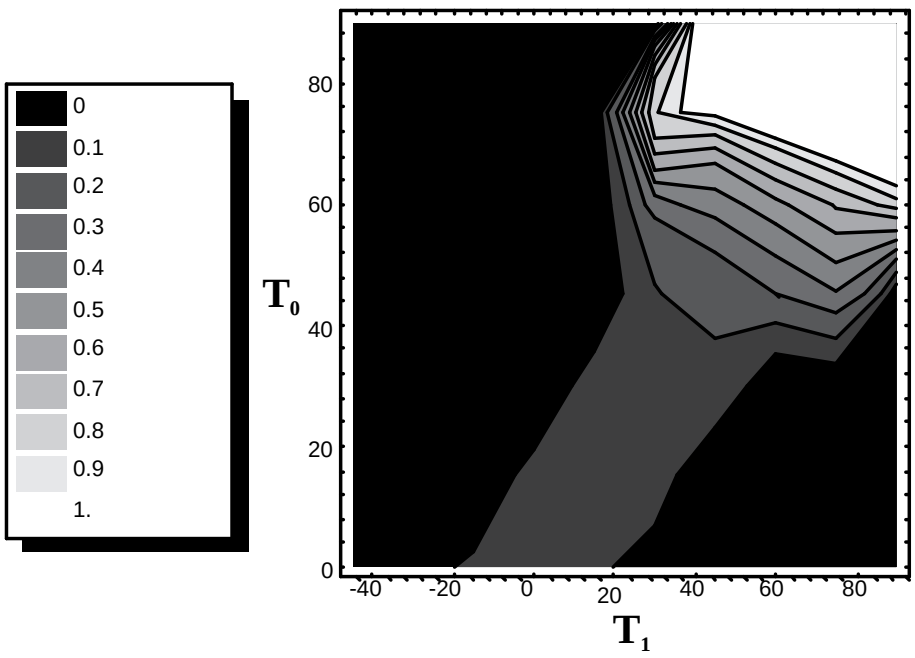

Figure 5.25: $\overline{E}_x^{eq}$ for parallel fiber laminates with $\phi = 90^o$ and various combinations of T_0 and T_1.

upper left and lower right corners of Figures 5.24 and 5.25. As expected, the largest stiffnesses occur for laminates with T_0 and T_1 close to 90^o since this will align a larger portion of the fibers with the loading axis. The equivalent axial stiffness of shifted and parallel fiber variable-stiffness laminates with $\phi = 0^o$ is shown in Figures 5.26 and 5.27, respectively. Similar to the laminates with $\phi = 90^o$, the largest stiffnesses appear when the fibers are closely aligned with the loading axis, $T_0 \approx T_1 \approx 0^o$.

By comparing the equivalent axial stiffnesses of the shifted and parallel fiber laminates with $\phi = 0^o$ and $\phi = 90^o$, an important design consideration can be found relating the stiffness of a shifted fiber laminate to a parallel fiber laminate having the same reference path. As explained before, the variation of the fiber orientation for parallel fiber laminates is not as dramatic as for shifted fiber ones. This results in the parallel fiber laminate tending to have a large portion of the panel with fiber orientation closer to T_0 than T_1. Therefore, if T_0 is aligned closer to the loading axis than T_1, the parallel fiber laminate will have a higher equivalent axial stiffness. However, if T_1 is closer to the loading axis than T_0, the shifted fiber laminates will have the larger equivalent axial stiffness. Two examples of this generalization are provided in Table 5.4. The first two laminates in Table 5.4 are shifted and parallel fiber $[90 \pm \langle 45|30 \rangle]_{9s}$. In this case, T_0 is 45^o off of the loading axis while T_1 is 60^o. Since T_0 is closer to the loading axis than T_1, it follows from the generalization stated earlier that the equivalent axial stiffness of the parallel fiber laminate will be higher than that of the shift fiber. The generalization is validated since $\overline{E}_x^{eq}$ for the parallel fiber laminate is almost 6% larger than the shifted fiber. The other laminates in Table 5.4 have a 0^o rotation angle from the loading axis. Since T_0 is further from the loading axis than T_1, the shifted fiber $[0 \pm \langle 75|60 \rangle]_{9s}$ laminate should, and does, have a larger equivalent axial stiffness than the parallel fiber laminate, 0.073 and 0.070, respectively.

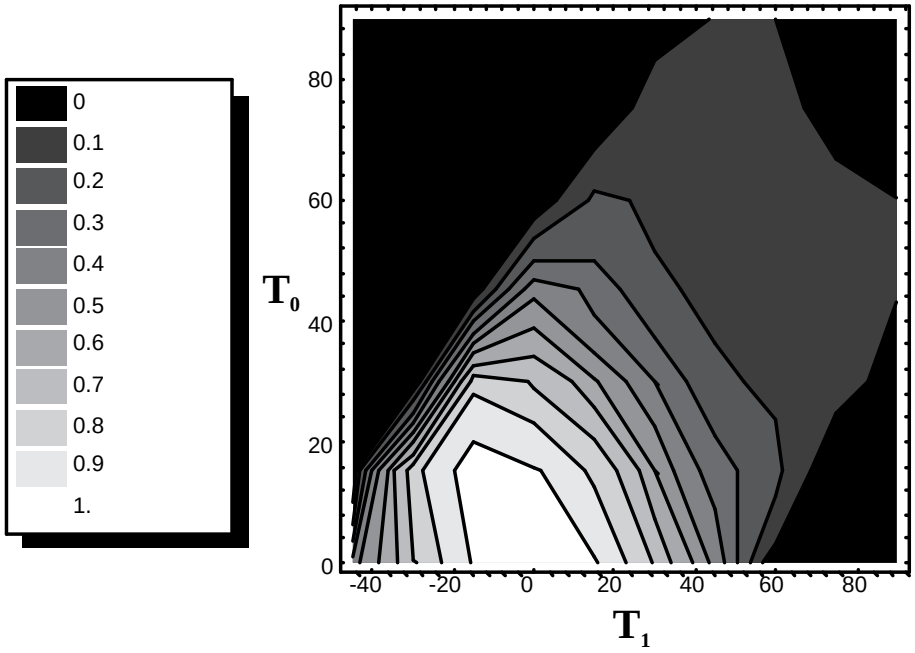

Figure 5.26: $\overline{E}_x^{eq}$ for shifted fiber laminates with $\phi = 0^o$ and various combinations of T_0 and T_1.

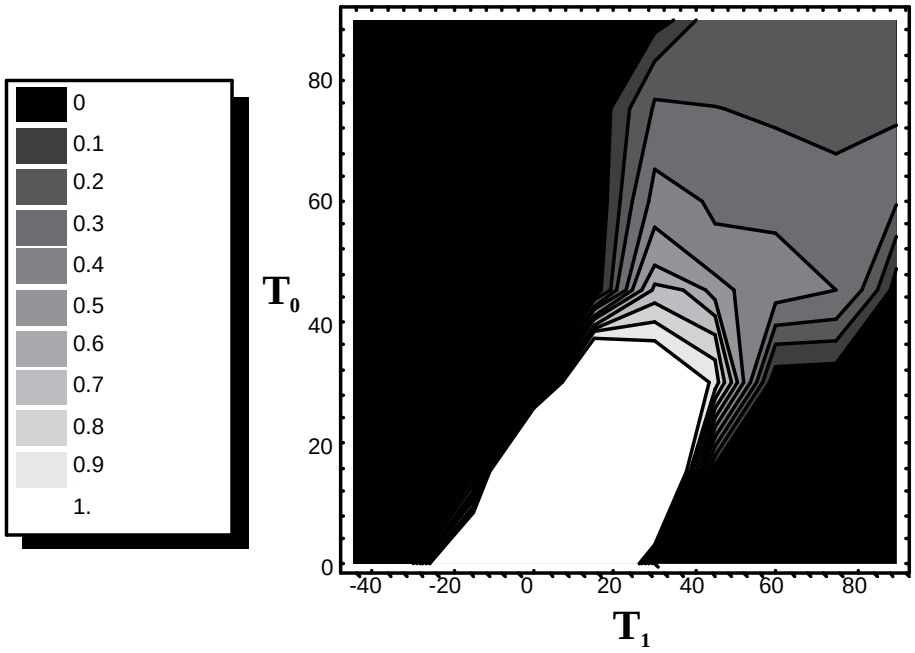

Figure 5.27: $\overline{E}_x^{eq}$ for parallel fiber laminates with $\phi = 0^o$ and various combinations of T_0 and T_1.

Table 5.2: Examples of how $\overline{E}_x^{eq}$ varies between the shifted and parallel fiber laminates with the same reference fiber path.

Laminate	Fiber Type	$\overline{E}_x^{eq}$
$[90 \pm \langle 45 \vert 30 \rangle]_{9s}$	shifted	0.101
$[90 \pm \langle 45 \vert 30 \rangle]_{9s}$	parallel	0.107
$[0 \pm \langle 75 \vert 60 \rangle]_{9s}$	shifted	0.073
$[0 \pm \langle 75 \vert 60 \rangle]_{9s}$	parallel	0.070

A feature of interest is to see how the equivalent axial stiffness of the variable-stiffness laminates with the highest critical buckling load compares to that of the $[\pm 45]_{9s}$, Table 5.4. Both the shifted and parallel fiber laminates are able to simultaneously increase the critical buckling load and equivalent axial stiffness over $[\pm 45]_{9s}$. The shifted fiber $[90 \pm \langle 30|75 \rangle]_{9s}$ can increase the critical buckling load by over 40% while more than doubling the equivalent axial stiffness of the straight fiber $[\pm 45]_{9s}$. The parallel fiber laminates are only able to increase the critical buckling load slightly, 1.4%, with $[0 \pm \langle 45|30 \rangle]_{9s}$. However, the same laminate offers an axial stiffness that is 39% larger than $[\pm 45]_{9s}$.

5.5 Performance Enhancements for Variable-Stiffness Laminates under Uniaxial Loading

The laminates that have been examined so far were such that the reference fiber path either varied along the loading axis or transverse to it. This section will examine the changes in buckling load and equivalent axial stiffness for hybrid and combination variable-stiffness laminates. A hybrid laminate will be defined as one which has a mixture of straight fiber plies and variable-stiffness laminae with reference fiber varying along the same axis. A combination variable-stiffness laminate will combine variable-stiffness plies which vary along two different axes. The goal of this section is to further explore the possible increases in performance offered by using variable-stiffness laminates.

5.5.1 Hybrid Laminates under Uniaxial Loading

A hybrid laminate is created by combining straight fiber and variable-stiffness plies. The two quantities of interest for a panel under uniform end shortening in this research are the critical

Table 5.3: $\overline{E}_x^{eq}$ for shifted and parallel fiber $[\phi \pm \langle T_0|T_1\rangle]_{9s}$ variable-stiffness laminates with $\phi = 0^o$ or $\phi = 90^o$ having the largest critical buckling loads.

Laminate	Fiber Type	$\overline{N}_{xcr}^{av}$	% increase in $\overline{N}_{xcr}^{av}$	$\overline{E}_x^{eq}$	% increase in $\overline{E}_x^{eq}$
$[\pm 45]_{9s}$	straight	-1.768	—	0.134	—
$[90 \pm \langle 30\|75\rangle]_{9s}$	shifted	-2.540	+44	0.300	+124
$[0 \pm \langle 45\|30\rangle]_{9s}$	parallel	-1.792	+1.4	0.186	+39

buckling load and equivalent axial stiffness. Two different stacks of straight fiber plies will be added to the variable-stiffness laminae, 0_2 and ± 45. These two plies are selected for different reasons. The benefit of adding the ± 45 plies comes when considering the buckling of the panel since it will increase the D matrix terms. Plies with the largest in-plane axial stiffness, the 0_2 stack, will be used in an effort to increase the equivalent axial stiffness of the laminate. In either case, the two straight fiber plies will replace two of the variable-stiffness plies so as to keep the total number of plies fixed at thirty six. The variation in the critical buckling load and equivalent axial stiffness which accompany changes in location of the straight fiber plies in the stacking sequence will also be examined. This aspect will be examined by placing the straight fiber plies either at the surface or midplane of the laminate.

Hybrid Laminates with Shifted Fiber Variable-Stiffness Plies

The shifted fiber laminate initially having the largest $\overline{N}_{xcr}^{av}$, $[90 \pm \langle 30|75 \rangle]_{9s}$, will be the base laminate for comparing the effect of adding straight fiber plies to shifted fiber variable-stiffness laminates. The changes in the critical buckling loads and the resulting equivalent axial stiffness created by combining either 0_2 or ± 45 plies with the shifted fiber $[90 \pm \langle 30|75 \rangle]_{9s}$ are provided in Table 5.5.1. The critical buckling load for $[90 \pm \langle 30|75 \rangle]_{9s}$ was increased by the addition of ± 45 plies at the surface of the laminate, $[\pm 45/ (90 \pm \langle 30|75 \rangle)_8]_s$, but not at the midplane, $[(90 \pm \langle 30|75 \rangle)_8 / \pm 45]_s$. The reason for this is that even though the ± 45 plies will tend to increase the D matrix terms of the laminate, their presence will tend to reduce the laminate's ability to redistribute an applied loading. Since these symmetric laminates are only under in-plane loads, changes in stacking sequence will not affect the stress distributions. However, placing the ± 45 plies at the surface will create larger D matrix terms than if they were placed at the midplane. Since the $[\pm 45/ (90 \pm \langle 30|75 \rangle)_8]_s$

and $[(90 \pm \langle 30|75\rangle)_8 / \pm 45]_s$ have identical stress distributions and the $[\pm 45/ (90 \pm \langle 30|75\rangle)_8]_s$ has larger D matrix terms, it becomes evident that the normalized critical buckling load of the $[\pm 45/ (90 \pm \langle 30|75\rangle)_8]_s$ should be larger than the $[(90 \pm \langle 30|75\rangle)_8 / \pm 45]_s$. The placement of the ± 45 or 0_2 plies in the stacking sequence will have no affect on the equivalent axial stiffness of the laminate since the stress distributions will be identical. While adding 0_2 plies did improve the axial stiffness of the laminate, a significant reduction in critical buckling load for shifted fiber hybrid laminates is observed in Table 5.5.1. Since the 0^o plies have small D matrix terms, it follows that a larger buckling load is obtained by $[(90 \pm \langle 30|75\rangle)_8 /0_2]_s$ compared to $[0_2/ (90 \pm \langle 30|75\rangle)_8]_s$.

Hybrid Laminates with Parallel Fiber Variable-Stiffness Plies

The parallel fiber laminate with the largest critical buckling load, $[0 \pm \langle 45|30\rangle]_{9s}$, will be used for comparing the affect that adding straight fiber plies has on parallel fiber variable-stiffness laminates. The effect of adding either 0_2 or ± 45 plies to the parallel fiber $[0 \pm \langle 45|30\rangle]_{9s}$ are provided in Table 5.5. In this case, the addition of ± 45 plies did not significantly alter the buckling performance of the parallel fiber $[0 \pm \langle 45|30\rangle]_{9s}$ laminate. The primary reason is that the fiber orientation of the parallel fiber laminate is quite similar to the $[\pm 45]_{9s}$ to begin with so adding ± 45 plies will not significantly alter the D matrix terms or the stress distributions. Adding the 0_2 plies at the midplane of the laminate increased the axial stiffness by over 50% while only reducing the critical buckling load by less than 1%.

5.5.2 Combination Variable-Stiffness Laminates under Uniaxial Loading

By varying the fiber orientation along the loading axis, it is possible to create beneficial tensile stresses in the y direction. This is achieved by having the fiber orientation at $x = \pm a/2$ such

Table 5.4: $\overline{N}_{xcr}^{av}$ and $\overline{E}_{x}^{eq}$ for hybrid laminates with shifted fibers.

Laminate	$\overline{N}_{xcr}^{av}$	% increase in $\overline{N}_{xcr}^{av}$	$\overline{E}_{x}^{eq}$	% increase in $\overline{E}_{x}^{eq}$
$[90 \pm \langle 30\|75\rangle]_{9s}$	-2.540	—	0.300	—
$[\pm 45/\,(90 \pm \langle 30\|75\rangle)_8]_s$	-2.729	+7.4	0.287	-4.3
$[(90 \pm \langle 30\|75\rangle)_8\,/\,\pm 45]_s$	-2.473	-2.6	0.287	-4.3
$[0_2/\,(90 \pm \langle 30\|75\rangle)_8]_s$	-2.005	-21	0.381	+27
$[(90 \pm \langle 30\|75\rangle)_8\,/0_2]_s$	-2.225	-12	0.381	+27

Table 5.5: $\overline{N}_{xcr}^{av}$ and $\overline{E}_{x}^{eq}$ for hybrid laminates with parallel fibers.

Laminate	$\overline{N}_{xcr}^{av}$	% increase in $\overline{N}_{xcr}^{av}$	$\overline{E}_{x}^{eq}$	% increase in $\overline{E}_{x}^{eq}$
$[0 \pm \langle 45\|30\rangle]_{9s}$	-1.792	—	0.186	—
$[\pm 45/\,(0 \pm \langle 45\|30\rangle)_8]_s$	-1.792	+0	0.182	-2.2
$[(0 \pm \langle 45\|30\rangle)_8\,/\,\pm 45]_s$	-1.786	-0.3	0.182	-2.2
$[0_2/\,(0 \pm \langle 45\|30\rangle)_8]_s$	-1.571	-12	0.280	+51
$[(0 \pm \langle 45\|30\rangle)_8\,/0_2]_s$	-1.782	-0.6	0.280	+51

that the panel will want to expand more in these regions than at $x = 0$. An example of this is a $[0 \pm \langle 75|45\rangle]_{9s}$ laminate. This section examines the addition of two plies which can create these beneficial transverse stress resultants to the shifted fiber $[90 \pm \langle 30|75\rangle]_{9s}$ and parallel fiber $[0 \pm \langle 45|30\rangle]_{9s}$. The two plies for the shifted fiber laminate will be slightly different than the parallel fiber case, $0 \pm \langle 75|30\rangle$ and $0 \pm \langle 75|45\rangle$, respectively. The reason for using two different plies is that the parallel fiber $0 \pm \langle 75|30\rangle$ would not satisfy the curvature constraint.

The changes in critical buckling and axial stiffness when these plies are added to the shifted and parallel fiber laminates are provided in Table 5.6. The shifted fiber laminates responded quite favorably when to the addition of the $0 \pm \langle 75|45\rangle$ plies at the surface. The presence of plies with fiber orientation varying along the loading axis appears to have significantly delayed to onset of buckling without reducing the equivalent axial stiffness. However when the same plies were placed at the midplane, a drop in the buckling load was noticed. The parallel fiber $[0 \pm \langle 45|30\rangle]_{9s}$ laminate responded unfavorably to the addition of the $0 \pm \langle 75|45\rangle$ from a buckling standpoint. Regardless of where the plies were placed, the buckling load was reduced. This reduction could be minimized, however, by placing the $0 \pm \langle 75|45\rangle$ plies at the midplane. This helped keep the critical buckling within 1% from the $[0 \pm \langle 45|30\rangle]_{9s}$ case. While the addition of the variables stiffness plies did not improve the buckling load of the parallel fiber laminate, a drastic increase in the equivalent axial stiffness was noticed. The primary reason that the shifted fiber laminates were able to increase the critical buckling load and the parallel fiber ones could not has to do with the variation of stiffness properties in the laminates. The stiffness properties in the parallel fiber laminate are much more gradual compared to the shifted fiber case. This will tend to diminish the magnitude of the tensile stresses in the y direction which was the primary justification for adding the $0 \pm \langle 75|45\rangle$ plies.

Table 5.6: $\overline{N}_{xcr}^{av}$ and $\overline{E}_{x}^{eq}$ for shifted and parallel fiber combination laminates.

Laminate	Fiber Type	$\overline{N}_{xcr}^{av}$	% increase in $\overline{N}_{xcr}^{av}$	$\overline{E}_{x}^{eq}$	% increase in $\overline{E}_{x}^{eq}$
$[\pm 45]_{9s}$	straight	-1.768	—	0.134	—
$[90 \pm \langle 30 \vert 75 \rangle]_{9s}$	shifted	-2.540	+44	0.300	+124
$[0 \pm \langle 75 \vert 30 \rangle / 90 \pm \langle 30 \vert 75 \rangle_8]_s$	shifted	-2.782	+57	0.300	+124
$[90 \pm \langle 30 \vert 75 \rangle_8 / 0 \pm \langle 75 \vert 30 \rangle]_s$	shifted	-2.478	+40	0.300	124
$[0 \pm \langle 45 \vert 30 \rangle]_{9s}$	parallel	-1.792	+1.4	0.186	+39
$[0 \pm \langle 75 \vert 45 \rangle / 0 \pm \langle 45 \vert 30 \rangle_8]_s$	parallel	-1.616	-8.6	0.218	+63
$[0 \pm \langle 45 \vert 30 \rangle_8 / 0 \pm \langle 75 \vert 30 \rangle]_s$	parallel	-1.755	-0.7	0.218	+63

5.5.3 Largest Gains in Critical Buckling Load for Variable-Stiffness Laminates Over Traditional Straight Fiber Laminates

Sections 5.5.1 and 5.5.2 showed that it is possible to improve the design of a variable-stiffness laminate, either in terms of the critical buckling load or axial stiffness, by adding plies which have different characteristics from the initial laminate. Table 5.7 presents the results of the search for the shifted and parallel fiber laminates with the largest critical buckling loads by using ± 45, $0 \pm \langle 75|30 \rangle$, or $0 \pm \langle 75|45 \rangle$. The search for the largest critical buckling loads for the variable-stiffness laminates began with shifted and parallel fiber laminates which had the fiber orientation of the reference fiber paths only varying along a single axis. This search provided a starting point, the shifted fiber $[90 \pm \langle 30|75 \rangle]_{9s}$ and the parallel fiber $[0 \pm \langle 45|30 \rangle]_{9s}$. Next, stacks of two plies, Sections 5.5.1 and 5.5.2, were sequentially added until a drop in the buckling load was calculated. While no parallel fiber laminate laminate was found using this search method which improved on the buckling load of $[0 \pm \langle 45|30 \rangle]_{9s}$, the search proved more successful for the shifted fiber laminates. Adding either ± 45 or $0 \pm \langle 75|30 \rangle$ plies to the $[90 \pm \langle 30|75 \rangle]_{9s}$ resulted in increasing the critical buckling load of the panel. However, the largest increase was found for the laminate which employed plies that helped create tensile stresses in the y direction in the center of the panel, $[0 \pm \langle 75|30 \rangle_3 / 90 \pm \langle 30|75 \rangle_6]_s$.

Table 5.7: Summary of maximum gains in critical buckling loads of shifted and parallel fiber variable-stiffness laminates under uniaxial loading.

Laminate	Fiber Type	$\overline{N}_{xcr}^{av}$	% increase in $\overline{N}_{xcr}^{av}$	$\overline{E}_x^{eq}$	% increase in $\overline{E}_x^{eq}$
$[\pm 45]_{9s}$	straight	-1.768	—	0.134	—
$[90 \pm \langle 30 \vert 75 \rangle]_{9s}$	shifted	-2.540	+44	0.300	+124
$[0 \pm \langle 45 \vert 30 \rangle]_{9s}$	parallel	-1.792	+1.4	0.186	+39
$[0 \pm \langle 75 \vert 30 \rangle_3 / 90 \pm \langle 30 \vert 75 \rangle_6]_s$	shifted	-3.101	+75	0.273	+104
$[\pm 45_2 / 90 \pm \langle 30 \vert 75 \rangle_7]_s$	shifted	-2.774	+57	0.271	+102

Chapter 6

Response of Variable-Stiffness Laminates to Shear Deformation

This section will focus on the in-plane and buckling responses of square variable-stiffness laminates created by either the shifted or parallel fiber method subjected to applied shear deformation. First the shear load introduction and boundary conditions will be described. Next, the in-plane response of several variable-stiffness laminates to the prescribed loading conditions will be examined. Finally, the shear buckling load of various laminates will be determined in order to find the largest critical buckling load of a laminate subjected to shear deformation. As before for the uniform end shortening loading condition, all of the shifted and parallel fiber laminates will be subject to the failure and curvature constraints as before.

The applied shear deformation model is similar to a shear frame test of a square panel, Figure 6.1, except that the panel edges are simply supported rather than being clamped. Prescribed panel displacements are defined around the panel perimeter so that each edge remains straight and does

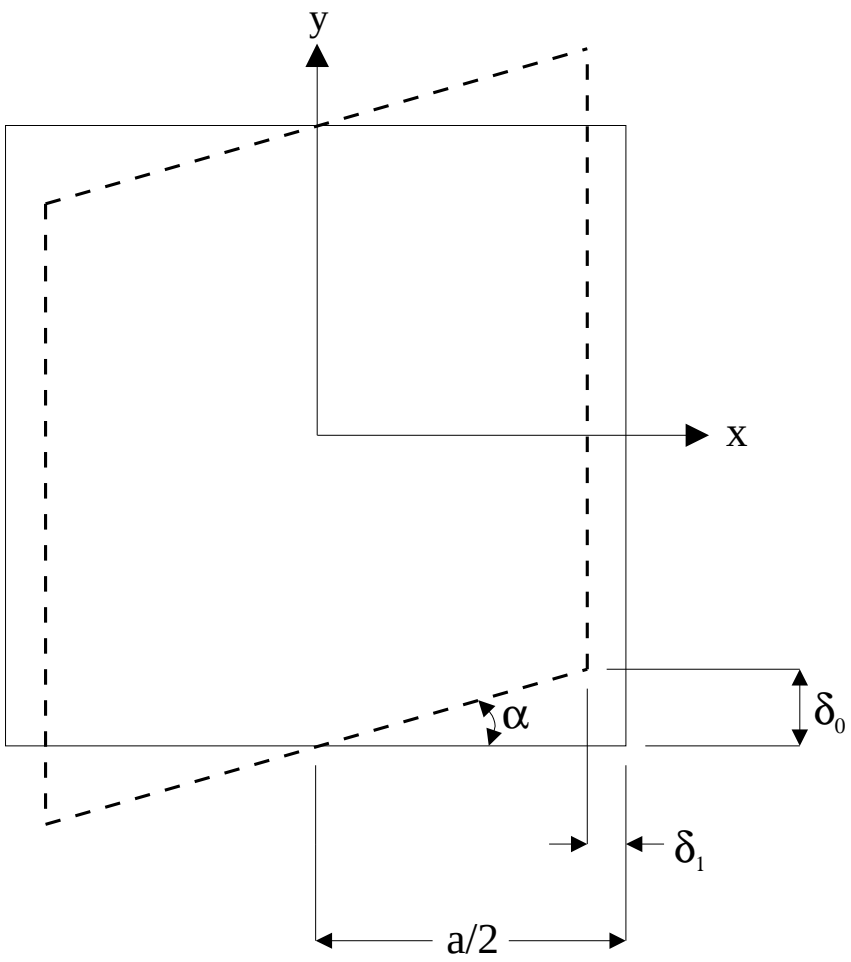

Figure 6.1: Shear deformation model geometry

not change in length. The in-plane shear deformation only depends upon a single parameter, δ_0, from which all of the displacements can be determined. The displacements are as follows:

$$\begin{aligned} u &= \begin{cases} \mp\delta_1, & \text{along } x = \pm\frac{a}{2} \\ -\frac{2\delta_1}{a}x, & \text{along } y = \pm\frac{b}{2} \end{cases} \\ v &= \begin{cases} \pm\delta_0, & \text{along } x = \pm\frac{a}{2} \\ \frac{2\delta_0}{a}x, & \text{along } y = \pm\frac{b}{2} \end{cases} \end{aligned} \tag{6.1}$$

$$\begin{aligned} \text{where} \quad \delta_0 &= \text{a constant,} \\ \delta_1 &= \tfrac{a}{2}(1-\cos\alpha)\ , \\ \alpha &= \sin^{-1}\left(\tfrac{2\delta_0}{a}\right)\ . \end{aligned}$$

The material properties, strengths, and minimum radius of curvature are the same as with the uniaxial compression.

6.1 In-plane Analysis of Variable-Stiffness Laminates under In-Plane Shear Deformations

The in-plane analysis of variable-stiffness laminates created by the shifted and parallel fiber methods are performed in order to better understand the mechanisms involved in their deformations. Since this is a more complicated loading than the uniaxial compression previously discussed, the responses of four different shifted and parallel fiber laminates to applied shear deformation will be examined. As before, two cases will involve laminates with reference fiber orientation varying along a geometric axis of the panel, $[0 \pm \langle 45|75\rangle]_{9s}$ and $[90 \pm \langle 45|75\rangle]_{9s}$. The two additional laminates discussed have fiber orientation varying along axes that are rotated 45^o from the geometric axis of the panel, $[45 \pm \langle 45|75\rangle]_{9s}$ and $[\pm(45\langle 45|75\rangle)]_{9s}$.

6.1.1 Shifted Fiber Laminates under In-Plane Shear Deformations

The first type of laminates to be examined are the shifted fiber laminates. The primary reason for this is that their behavior is simpler than that of variable-stiffness laminates with parallel fibers. As was the case for the uniaxial loading, the stress resultants will be expressed in terms of a normalized quantity, similar to Equation 5.2, defined as:

$$\overline{N}_x = \frac{a}{|\delta_0 A_{11}(0,0)|} N_x \tag{6.2}$$

where a is the panel width and δ_0 is defined in Figure 6.1.

Response of a $[\mathbf{0} \pm \langle \mathbf{45}|\mathbf{75} \rangle]_{\mathbf{9s}}$ Shifted Fiber Laminate

The fiber paths for a $[0 \pm \langle 45|75 \rangle]_{9s}$ shifted fiber laminate are shown in Figure 6.2. The distribution of the in-plane stress resultants, $\overline{N}_x$, $\overline{N}_y$, and $\overline{N}_{xy}$, for the laminate can be seen in Figures 6.3–6.5.

Unlike the $[\pm 45]_{9s}$, significant non-zero $\overline{N}_x$ and $\overline{N}_y$ values are present, Figures 6.3 and 6.4, respectively, and localized primarily in the vicinity of the edges, $x = \pm a/2$ and $y = \pm b/2$. The distributions over the panel are such that the $\overline{N}_x$ and $\overline{N}_y$ are both essentially zero in the center portion of the panel. Also, the distribution for both $\overline{N}_x$ and $\overline{N}_y$ are antisymmetric about the geometric axes of the panel. Unlike the stress resultants in the x and y directions, the shear stress resultant is largest in the center of the panel in a band parallel to the y axis, Figure 6.5. Since $\overline{N}_x$ and $\overline{N}_y$ are fairly constant in this region, the equilibrium equations for laminated plates require the shear stresses in the center of the planform to also be constant. Near the edges of the panel, there are also significant changes in $\overline{N}_{xy}$. The values of $\overline{N}_{xy}$ along $x = \pm a/2$ of approximately 0.45 are significantly lower than those near the center of the laminate which are close to 0.75.

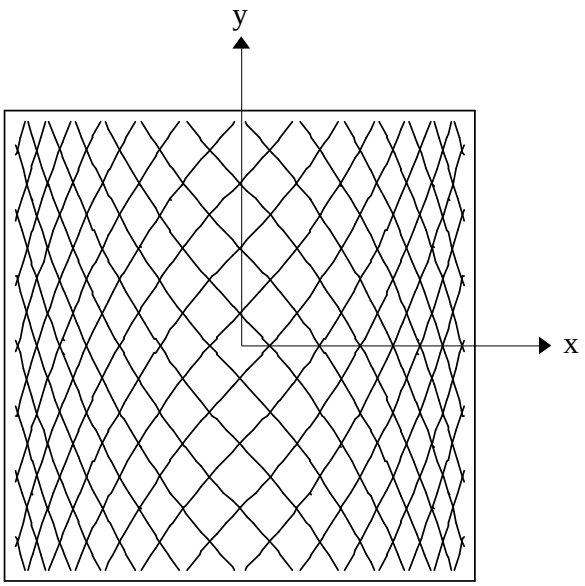

Figure 6.2: Fiber paths for a $[0 \pm \langle 45|75\rangle]_{9s}$ shifted fiber laminate

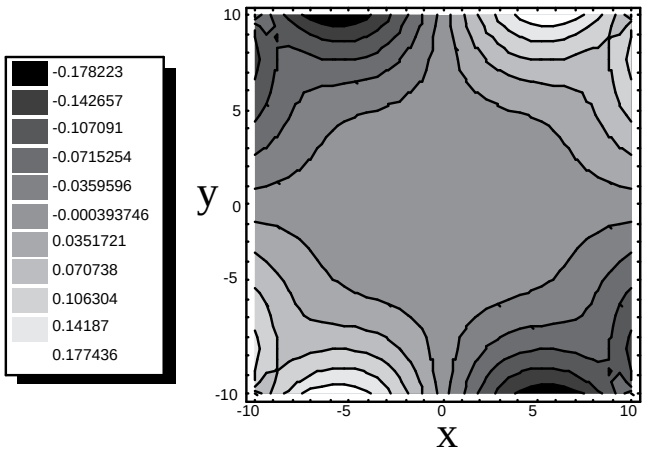

Figure 6.3: $\overline{N}_x$ as a function of panel location for $[0 \pm \langle 45|75\rangle]_{9s}$ made by the shifted fiber method

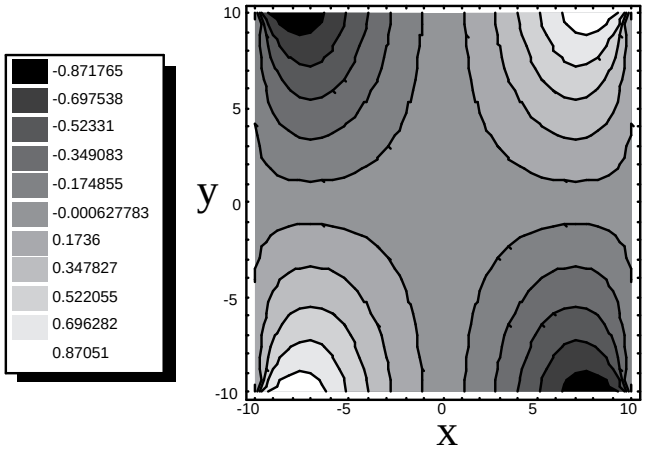

Figure 6.4: $\overline{N}_y$ as a function of panel location for $[0 \pm \langle 45|75 \rangle]_{9s}$ made by the shifted fiber method

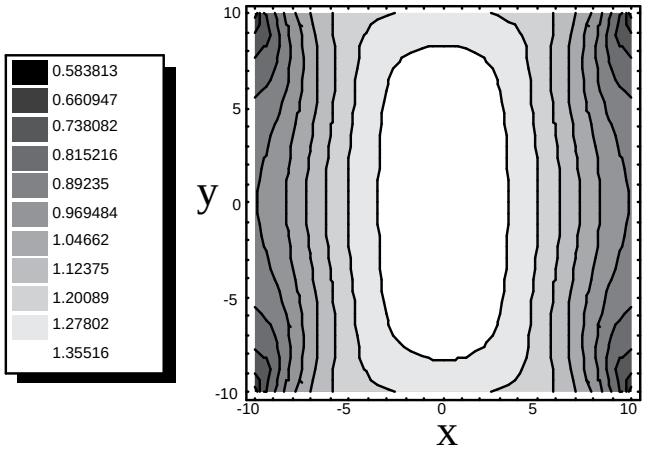

Figure 6.5: $\overline{N}_{xy}$ as a function of panel location for $[0 \pm \langle 45|75 \rangle]_{9s}$ made by the shifted fiber method

Response of a $[\mathbf{90 \pm \langle 45|75 \rangle}]_{\mathbf{9s}}$ Shifted Fiber Laminate

The fiber paths for a shifted fiber $[90 \pm \langle 45|75\rangle]_{9s}$ laminate are shown in Figure 6.6. Unlike the $[0\pm\langle 45|75\rangle]_{9s}$ laminate with its fiber orientation varying along the geometric x axis, this laminate has the fiber orientation vary along the y axis. The normalized stress resultants, $\overline{N}_x$, $\overline{N}_y$, and $\overline{N}_{xy}$, that are created by shear deforming the $[90 \pm \langle 45|75\rangle]_{9s}$ laminate are shown in Figures 6.7–6.9. When the stress resultants of the $[90\pm\langle 45|75\rangle]_{9s}$ laminate are compared to those of the $[0\pm\langle 45|75\rangle]_{9s}$, it is evident that the distribution of the stress resultants for the $[90\pm\langle 45|75\rangle]_{9s}$ laminate are essentially the same as those for $[0 \pm \langle 45|75\rangle]_{9s}$ rotated by 90^o. That is, if the distribution of the $\overline{N}_x$, $\overline{N}_y$, and $\overline{N}_{xy}$ for the $[0 \pm \langle 45|75\rangle]_{9s}$ laminate where rotated 90^o, then they would closely approximate the $\overline{N}_y$, $\overline{N}_x$, and $\overline{N}_{xy}$, respectively, of the $[90 \pm \langle 45|75\rangle]_{9s}$. The main difference between the two is that for the laminate with $\phi = 90^o$ has $\overline{N}_x$ and $\overline{N}_y$ that are opposite in sign to the corresponding stress resultants of the $[0 \pm \langle 45|75\rangle]_{9s}$ laminate. This is not the case for the shear stress resultant which has the same distribution and sign as the $[0 \pm \langle 45|75\rangle]_{9s}$.

The responses of these two laminates offer a valuable insight into the dependence upon the sign of the shear loading relative to the response. Positive shear loading for a $[0 \pm \langle 45|75\rangle]_{9s}$ and $[90 \pm \langle 45|75\rangle]_{9s}$ laminate can be seen in Figure 6.10. However if a negative shear load is applied to $[90\pm\langle 45|75\rangle]_{9s}$, Figure 6.11, then the loading is the same as that of a $[0\pm\langle 45|75\rangle]_{9s}$ laminate rotated by 90^o. Therefore to get the equivalent loading of a $[0 \pm \langle 45|75\rangle]_{9s}$ laminate under positive shear, negative shear needs to be applied to the $[90\pm\langle 45|75\rangle]_{9s}$ laminate. An important conclusion can be made by considering the fact that the responses of the $[0\pm\langle 45|75\rangle]_{9s}$ and $[90\pm\langle 45|75\rangle]_{9s}$ laminates subjected to positive shear deformation are such that the distributions of the stress resultants for the $\phi = 0^o$ laminate are essentially identical to that of the $\phi = 90^o$ laminate if they are rotated by

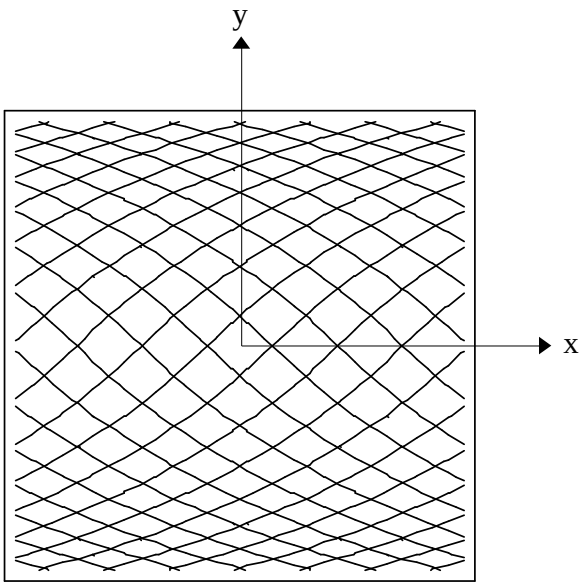

Figure 6.6: Fiber paths for a $[90 \pm \langle 45|75 \rangle]_{9s}$ shifted fiber laminate

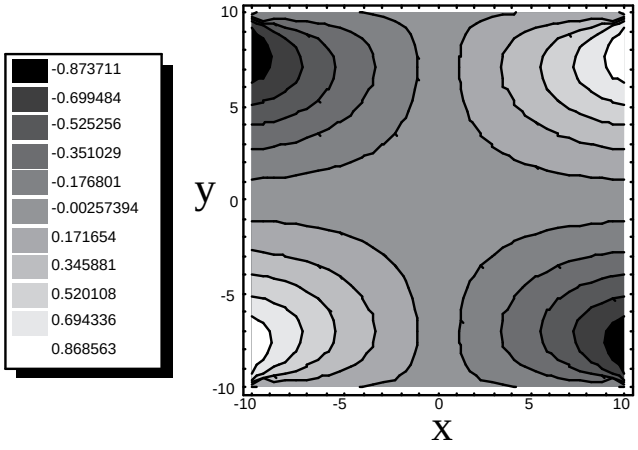

Figure 6.7: $\overline{N}_x$ as a function of panel location for $[90 \pm \langle 45|75 \rangle]_{9s}$ made by the shifted fiber method

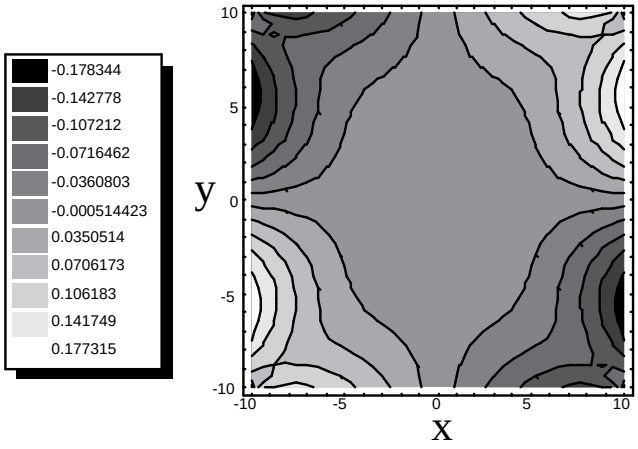

Figure 6.8: $\overline{N}_y$ as a function of panel location for $[90 \pm \langle 45|75 \rangle]_{9s}$ made by the shifted fiber method

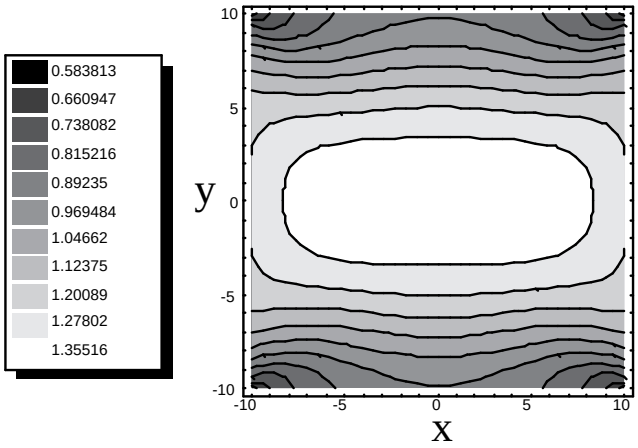

Figure 6.9: $\overline{N}_{xy}$ as a function of panel location for $[90 \pm \langle 45|75 \rangle]_{9s}$ made by the shifted fiber method

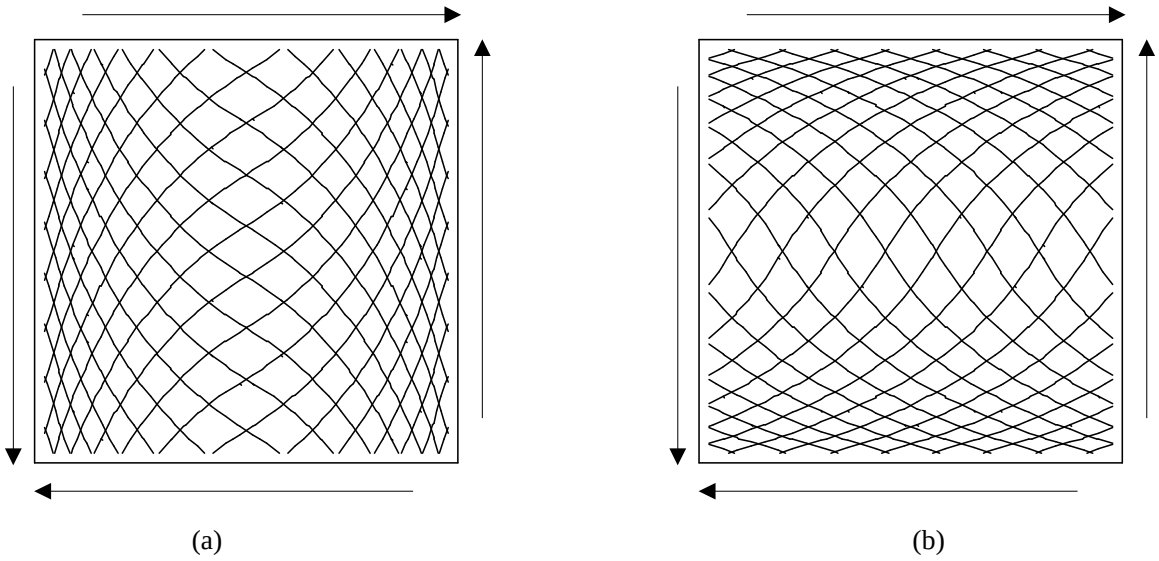

Figure 6.10: Positive shear loading of (a) $[0 \pm \langle 45|75\rangle]_{9s}$ and (b) $[90 \pm \langle 45|75\rangle]_{9s}$ shifted fiber laminates

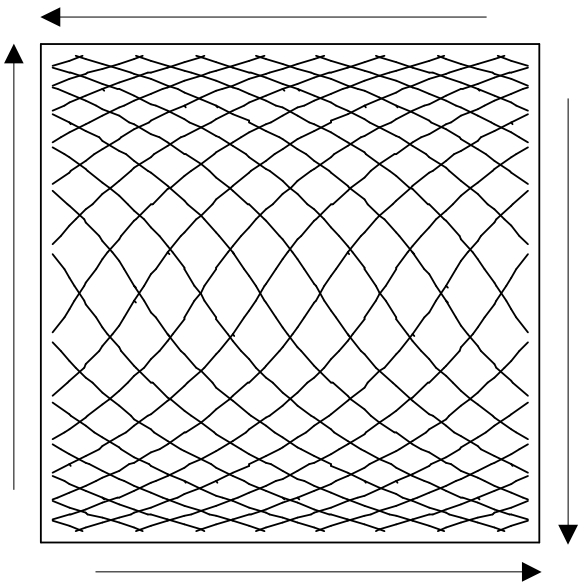

Figure 6.11: Negative shear loading of $[90 \pm \langle 45|75\rangle]_{9s}$ shifted fiber laminate

90^o. That conclusion is that the overall response of shifted fiber variable-stiffness laminates of the form $[\phi \pm \langle T_0|T_1\rangle]_{9s}$ will not depend upon whether the shear loading is positive or negative as long as ϕ is aligned with a geometric axis of the panel.

Response of a $[\mathbf{45 \pm \langle 45|75\rangle}]_{\mathbf{9s}}$ Shifted Fiber Laminate

The fiber paths for this laminate, Figure 6.12, are such that the orientation varies along an axis that is rotated 45^o from the geometric x axis. The $\overline{N}_x$, $\overline{N}_y$, and $\overline{N}_{xy}$ for this laminate under shear loading can be seen in Figures 6.13–6.15, respectively. Along the diagonal defined by $x' = 0$, the fiber paths are oriented primarily along the geometric axes of the panel. This creates a region which is relatively pliant under shear loading. However, the fiber orientation in the vicinity of the corners at $(a/2, b/2)$ and $(-a/2, -b/2)$ will offer greater resistance to the shearing force. As such, larger shear stresses will need to be applied in the upper right and lower left corners compared to the region near the $x' = 0$ diagonal, Figure 6.15. This shear stress resultant distribution creates large $\overline{N}_{xy}$ gradients in both the x and y directions in the vicinity of the corners at $(a/2, b/2)$ and $(-a/2, -b/2)$. However, the $\overline{N}_{xy}$ remains fairly constant near the $x' = 0$ diagonal. The $\overline{N}_x$ and $\overline{N}_y$ distributions, Figures 6.13 and 6.14, respectively, are such that they satisfy the equilibrium equations for laminate plates, Equations 3.27 and 3.28. Similar to the $\overline{N}_{xy}$ distribution, both $\overline{N}_x$ and $\overline{N}_y$ are relatively small and fairly uniform near the $x' = 0$ diagonal. However, $\overline{N}_x$ and $\overline{N}_y$ decrease as you proceed from the $x' = 0$ diagonal region towards the corners at $(a/2, b/2)$ and $(-a/2, -b/2)$ until maximum compressive $\overline{N}_x$ and $\overline{N}_y$ are achieved near $x' = \pm a/2$. An interesting feature of this laminate is that the $\overline{N}_y$ is almost identical, both in magnitude and sign, to the mirrored projection of $\overline{N}_x$ about the x' axis.

Overall, the shifted fiber $[45 \pm \langle 45|75\rangle]_{9s}$ laminate exhibits both beneficial and detrimental

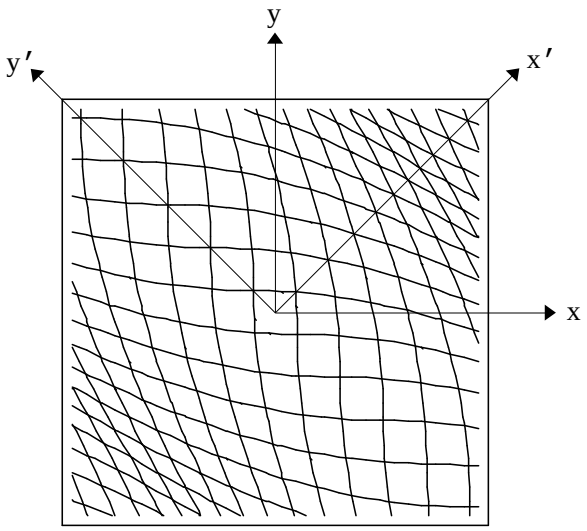

Figure 6.12: Fiber paths for a $[45 \pm \langle 45|75 \rangle]_{9s}$ shifted fiber laminate

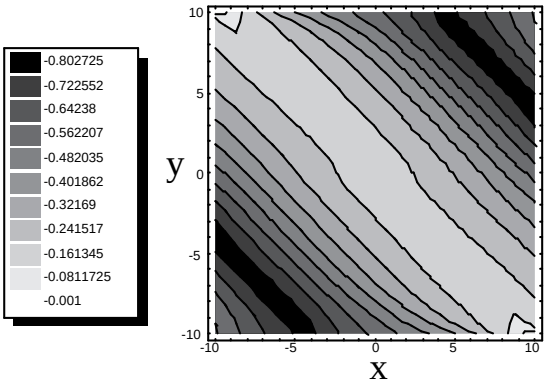

Figure 6.13: $\overline{N}_x$ as a function of panel location for $[45 \pm \langle 45|75 \rangle]_{9s}$ made by the shifted fiber method

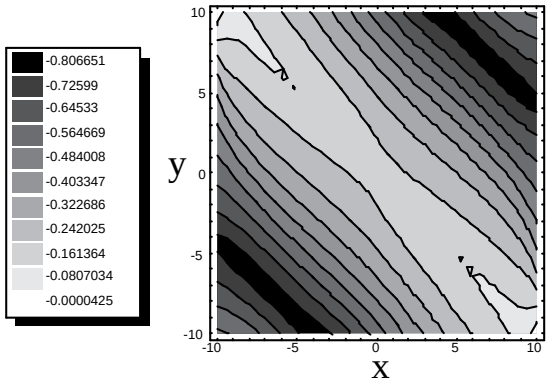

Figure 6.14: $\overline{N}_y$ as a function of panel location for $[45 \pm \langle 45|75\rangle]_{9s}$ made by the shifted fiber method

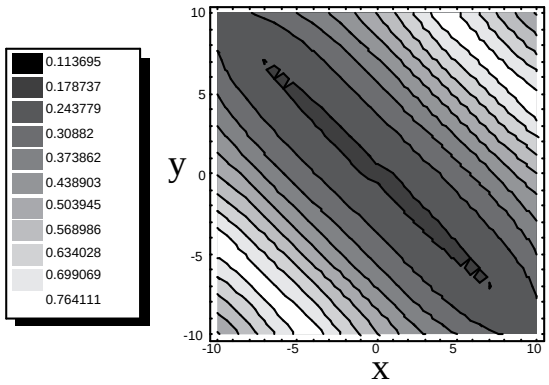

Figure 6.15: $\overline{N}_{xy}$ as a function of panel location for $[45 \pm \langle 45|75\rangle]_{9s}$ made by the shifted fiber method

effects of load redistribution. When viewed in terms of creating a larger critical buckling, it is advantageous to redistribute the load towards the edges where the supports will prevent out of plane displacements and delay the onset of buckling until a higher load is reached. While this laminate achieves this by creating a diagonal band along $x' = 0$ that experiences relatively small $\overline{N}_x$, $\overline{N}_y$, and $\overline{N}_{xy}$, it redistributes the loading to a small band in the vicinity of $x' = \pm a/2$. As such, these two corner regions will carry large compressive stress resultants in both the x and y directions in addition to the largest shear stress resultants. Therefore, to judge the effectiveness of this load redistribution, it is necessary to perform the buckling analysis since the benefit of having lower shear stresses in the center portion might be offset by the combination of large compressive and shear loads closer to the corners.

Response of a $[\pm(\mathbf{45}\langle\mathbf{45}|\mathbf{75}\rangle)]_{\mathbf{9s}}$ Shifted Fiber Laminate

The fiber paths corresponding to a $[\pm(45\langle 45|75\rangle)]_{9s}$ shifted fiber laminate are shown in Figure 6.16. This laminate is significantly different in its fiber path formation from the previous ones that were analyzed. The fiber orientation variation does not take place along a single rotated axis, but rather, the rotation angle changes from $\phi = +45^o$ on one ply to $\phi = -45^o$ on the next. The corresponding values of T_0 and T_1 are $\pm 45^o$ and $\pm 75^o$, respectively, where the signs are identical to ϕ for the given ply. The resulting laminate has regions with relatively high resistance to shear near each corner while the center is more pliant. This is in contrast to the $[45 \pm \langle 45|75\rangle]_{9s}$ laminate which had relatively stiff regions only near the two corners at $(a/2, b/2)$ and $(-a/2, -b/2)$.

The resulting $\overline{N}_x$, $\overline{N}_y$, and $\overline{N}_{xy}$ are given in Figures 6.17–6.19, respectively. Similar to the $\overline{N}_x$ and $\overline{N}_y$ for the $[45 \pm \langle 45|75\rangle]_{9s}$ laminate, this laminate has the largest magnitudes of $\overline{N}_x$ and $\overline{N}_y$ near the corners, Figures 6.17–6.18, respectively. The $[\pm(45\langle 45|75\rangle)]_{9s}$ laminate also offers the

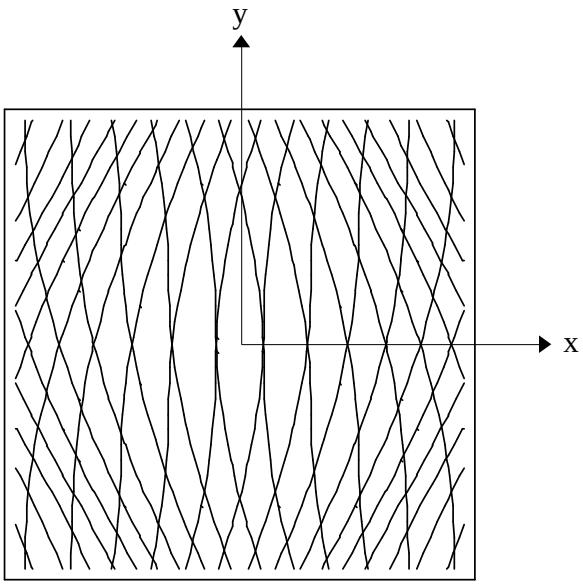

Figure 6.16: Fiber paths for a $[\pm(45\langle 45|75\rangle)]_{9s}$ shifted fiber laminate

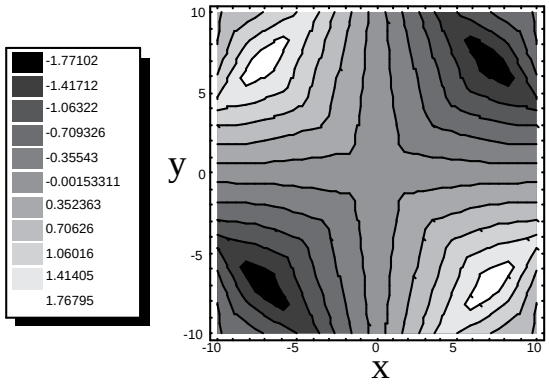

Figure 6.17: $\overline{N}_x$ as a function of panel location for $[\pm(45\langle 45|75\rangle)]_{9s}$ made by the shifted fiber method

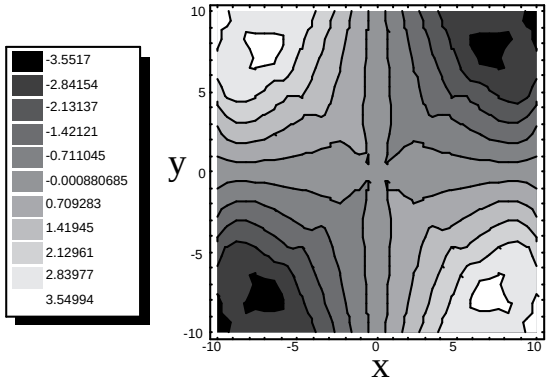

Figure 6.18: $\overline{N}_y$ as a function of panel location for $[\pm(45\langle 45|75\rangle)]_{9s}$ made by the shifted fiber method

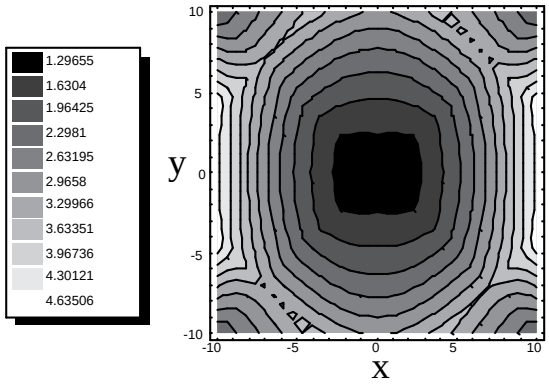

Figure 6.19: $\overline{N}_{xy}$ as a function of panel location for $[\pm(45\langle 45|75\rangle)]_{9s}$ made by the shifted fiber method

benefit of having extremely small $\overline{N}_x$ and $\overline{N}_y$ in the center portion of the panel. The $\overline{N}_{xy}$ for this laminate, Figure 6.19, is such that the largest larger shear stress resultants appear along the edges at $x = \pm a/2$ while smaller values appear in the center portion of the panel. It is important to note that, unlike the $[45 \pm \langle 45|75\rangle]_{9s}$ shifted fiber laminate, this laminate does not carry large $\overline{N}_{xy}$ in regions with significant $\overline{N}_x$ and $\overline{N}_y$.

This laminate appears to have the combination of properties that should help increase its critical shear buckling load. It is able to redistribute the largest loads towards regions that are simply supported, i.e. the corners or edges of the panel. The center portion of the panel, which would normally want to buckle first, carries the smallest $\overline{N}_x$, $\overline{N}_y$, and $\overline{N}_{xy}$ loads. Additionally, unlike the $[45 \pm \langle 45|75\rangle]_{9s}$ laminate that had relatively small regions where the the maximum compressive $\overline{N}_x$ and $\overline{N}_y$ and the largest $\overline{N}_{xy}$ occur simultaneously, there is no region that experiences the combined loadings in such a detrimental manner. As such, shifted fiber variable-stiffness laminates of the form $[\pm(45\langle 45|75\rangle)]_{9s}$ appear to offer the best opportunity for increasing the critical buckling load of this panel over that of a panel using only traditional straight fiber laminae.

6.1.2 Parallel Fiber Variable-Stiffness Laminates to Shear Deformation

The next group of variable-stiffness laminates will be created by the parallel fiber method. As was the case for the uniaxial loading, the same reference fiber paths used for the shifted fiber laminates will also be used for the parallel fiber.

Response of a $[\mathbf{0 \pm \langle 45|75\rangle]_{9s}}$ Parallel Fiber Laminate To Shear Deformation

This is the first of the parallel fiber laminates under shear loading to be examined. The fiber paths for the parallel fiber $[0 \pm \langle 45|75\rangle]_{9s}$ laminate are shown in Figure 6.20. The in-plane stress

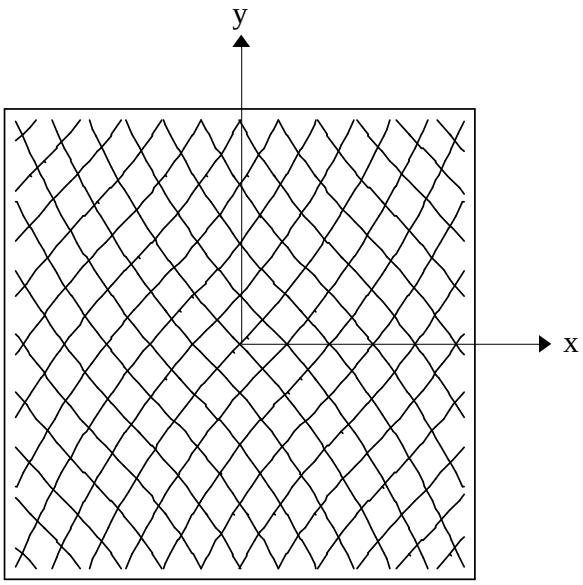

Figure 6.20: Fiber paths for a $[0 \pm \langle 45|75 \rangle]_{9s}$ parallel fiber laminate

resultants for the parallel fiber $[0 \pm \langle 45|75\rangle]_{9s}$ are shown in Figures 6.21–6.23, respectively. The largest $\overline{N}_x$ and $\overline{N}_y$ are experienced in the corners of the laminate while the center portion of the panel carries a relatively small portion of the normal loads, Figures 6.21 and 6.22. Also, regions with relatively high compressive $\overline{N}_x$ experience large tensile $\overline{N}_y$. The converse of this is also true, that large tensile $\overline{N}_x$ are present with large compressive $\overline{N}_x$. The $\overline{N}_{xy}$ distribution, Figure 6.23, is such that the largest portion of the load is carried along the center portion, $x = 0$. Within this region, the largest loads are along the transverse edges at $(0, \pm b/2)$. An advantage of this parallel fiber laminate over the shifted fiber $[0 \pm \langle 45|75\rangle]_{9s}$ is that the maximum shear stresses are not experienced over the central portion of the panel but rather in the vicinity of the edges at $(0, \pm b/2)$, Figures 6.23 and 6.5, respectively. Benefits shared by both shifted and parallel $[0 \pm \langle 45|75\rangle]_{9s}$ laminates is that the $\overline{N}_x$ and $\overline{N}_y$ are such that the maximum levels are close to the panel edges and the center of the panel carries small compressive loadings.

Response of a $[\mathbf{90 \pm \langle 45|75\rangle]_{9s}}$ Parallel Fiber Laminate To Shear Deformation

The fiber paths for the parallel fiber $[90 \pm \langle 45|75\rangle]_{9s}$ laminate are shown in Figure 6.24. The in-plane stress resultants for the parallel fiber $[90 \pm \langle 45|75\rangle]_{9s}$ are shown in Figures 6.25–6.27. The stress resultant distribution for the parallel fiber $[90 \pm \langle 45|75\rangle]_{9s}$ closely resembles that of the parallel fiber $[0 \pm \langle 45|75\rangle]_{9s}$. The difference is that the stress resultants for the $[90 \pm \langle 45|75\rangle]_{9s}$ are those of the $[0 \pm \langle 45|75\rangle]_{9s}$ rotated by ninety degrees. This is the same phenomena that appeared when considering the shifted fiber laminates with the same reference fiber paths. As a result, the in-plane response of some parallel fiber laminate with reference fiber paths varying along a geometric axis of the panel will not depend on the sign of the applied shear deformation. Therefore, extending the generalization made for shifted fiber laminates, the response of shifted and parallel fiber variable-

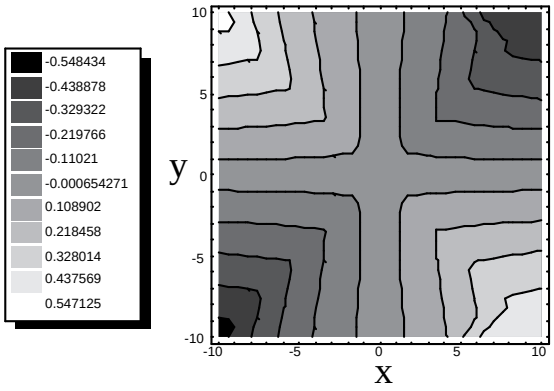

Figure 6.21: $\overline{N}_x$ as a function of panel location for $[0 \pm \langle 45|75 \rangle]_{9s}$ made by the parallel fiber method

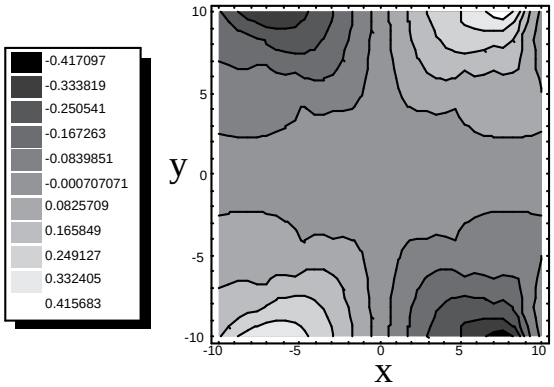

Figure 6.22: $\overline{N}_y$ as a function of panel location for $[0 \pm \langle 45|75 \rangle]_{9s}$ made by the parallel fiber method

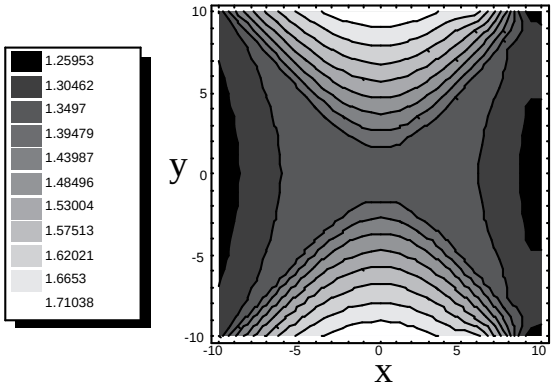

Figure 6.23: $\overline{N}_{xy}$ as a function of panel location for $[0 \pm \langle 45|75 \rangle]_{9s}$ made by the parallel fiber method

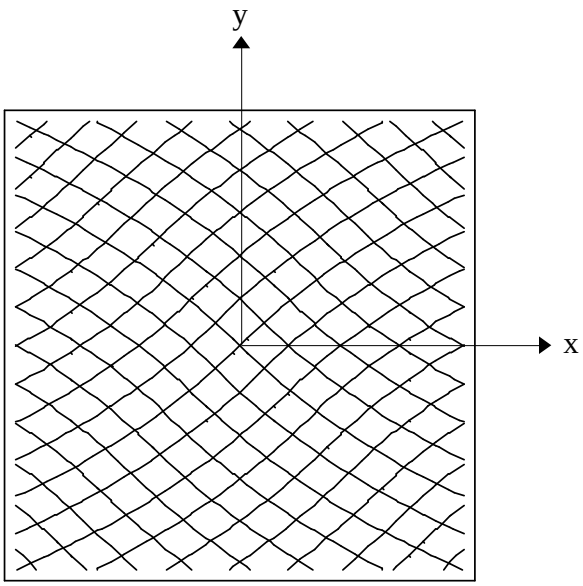

Figure 6.24: Fiber paths for a $[90 \pm \langle 45|75 \rangle]_{9s}$ parallel fiber laminate

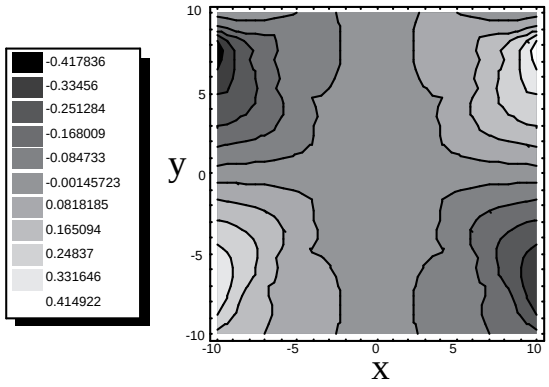

Figure 6.25: $\overline{N}_x$ as a function of panel location for $[90 \pm \langle 45|75 \rangle]_{9s}$ made by the parallel fiber method

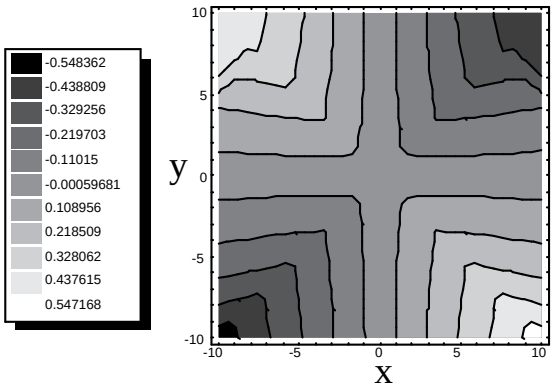

Figure 6.26: $\overline{N}_y$ as a function of panel location for $[90 \pm \langle 45|75 \rangle]_{9s}$ made by the parallel fiber method

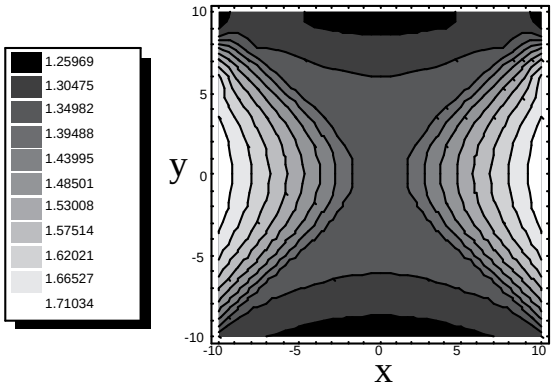

Figure 6.27: $\overline{N}_{xy}$ as a function of panel location for $[90 \pm \langle 45|75 \rangle]_{9s}$ made by the parallel fiber method

stiffness laminates of the form $[\phi \pm \langle T_0|T_1\rangle]_{9s}$ will not exhibit dependence upon the sign of the shear loading provided that ϕ is such that the fiber orientation varies along a geometric address.

Response of a $[\mathbf{45} \pm \langle \mathbf{45}|\mathbf{75}\rangle]_{\mathbf{9s}}$ Parallel Fiber Laminate To Shear Deformation

The reference fiber path for this laminate varies along an axis rotated by 45^o from the geometric x axis of the panel. The resulting parallel fiber paths for a $[45 \pm \langle 45|75\rangle]_{9s}$ laminate are shown in Figure 6.28. The in-plane stress resultants for the parallel fiber $[45 \pm \langle 45|75\rangle]_{9s}$ are shown in Figures 6.29–6.31, respectively. The resulting $\overline{N}_x$ and $\overline{N}_y$, Figures 6.29 and 6.30, are such that the largest magnitudes are carried in the vicinity of the simply supported edges while smaller stresses are carried in the central portion of the panel. Unlike the shifted fiber $[45 \pm \langle 45|75\rangle]_{9s}$ laminate, the parallel fiber $[45 \pm \langle 45|75\rangle]_{9s}$ does not have regions where large compressive $\overline{N}_x$ and $\overline{N}_y$ occur simultaneously. Similar to the $\overline{N}_x$ and $\overline{N}_y$ distributions, the center portion of the panel experiences small $\overline{N}_{xy}$, Figure 6.31, with the largest shear stresses appearing in the upper left and lower right corners, $(-a/2, b/2)$ and $(a/2, -b/2)$.

Response of a $[\pm(\mathbf{45}\langle \mathbf{45}|\mathbf{75}\rangle)]_{\mathbf{9s}}$ Parallel Fiber Laminate To Shear Deformation

The resulting parallel fiber paths for a $[\pm (45\langle 45|75\rangle)]_{9s}$ laminate are shown in Figure 6.32. The normalized stress resultants for this laminate under shear deformation are shown in Figures 6.33–6.35. The stress resultant distributions for this laminate have many advantageous features. The first is that the largest $\overline{N}_x$ and $\overline{N}_y$ are located close to the simply supported edges of the panel, Figures 6.33 and 6.34. Another advantage is that regions with relatively high compressive $\overline{N}_x$ also experience large tensile $\overline{N}_y$. The converse of this is also true, that large tensile $\overline{N}_x$ are present with large compressive $\overline{N}_y$. Both of these features should help delay the onset of buckling. The

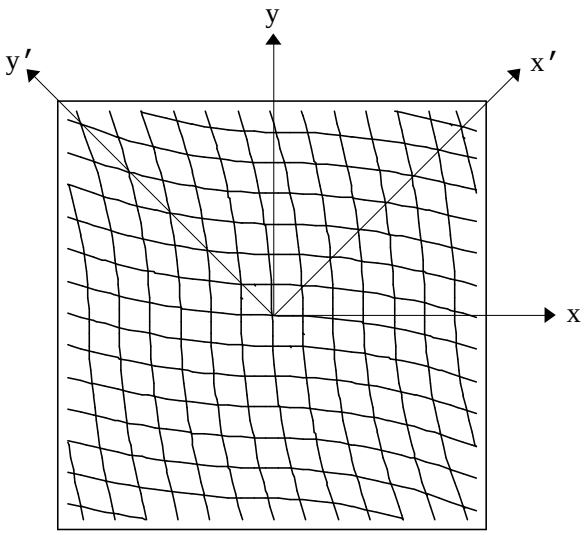

Figure 6.28: Fiber paths for a $[45 \pm \langle 45|75 \rangle]_{9s}$ parallel fiber laminate

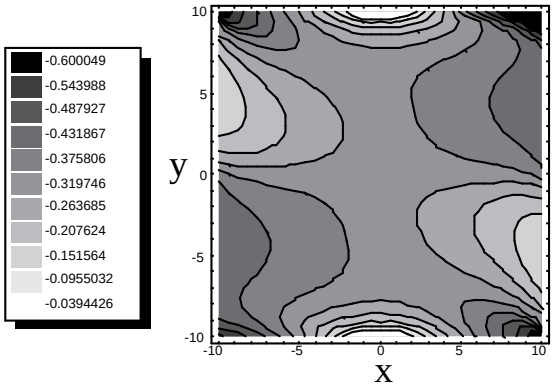

Figure 6.29: $\overline{N}_x$ as a function of panel location for $[45 \pm \langle 45|75 \rangle]_{9s}$ made by the parallel fiber method

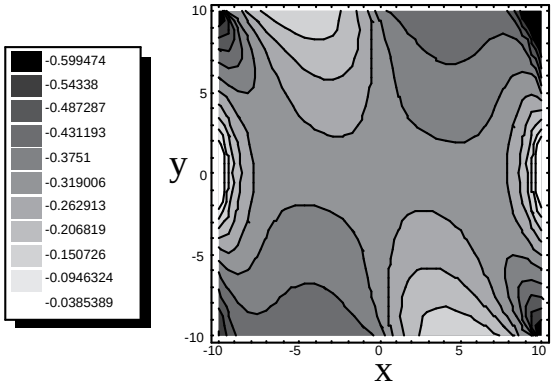

Figure 6.30: $\overline{N}_y$ as a function of panel location for $[45 \pm \langle 45|75 \rangle]_{9s}$ made by the parallel fiber method

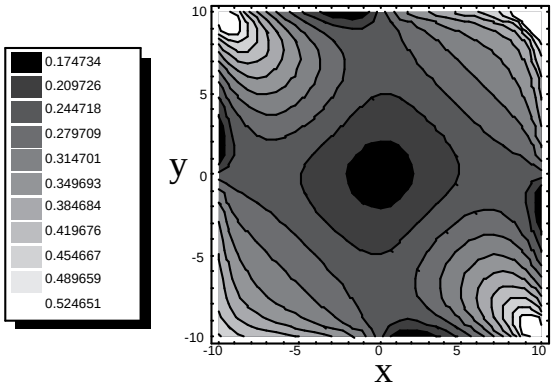

Figure 6.31: $\overline{N}_{xy}$ as a function of panel location for $[45 \pm \langle 45|75 \rangle]_{9s}$ made by the parallel fiber method

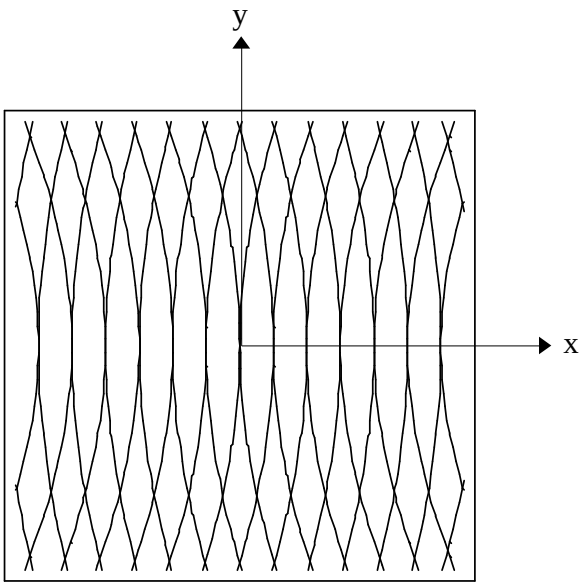

Figure 6.32: Fiber paths for a $[\pm(45\langle 45|75\rangle)]_{9s}$ parallel fiber laminate

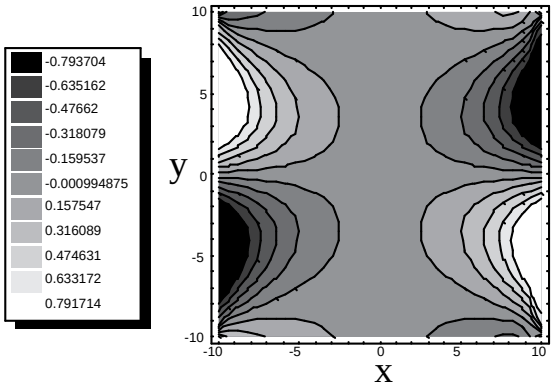

Figure 6.33: $\overline{N}_x$ as a function of panel location for $[\pm(45\langle 45|75\rangle)]_{9s}$ made by the parallel fiber method

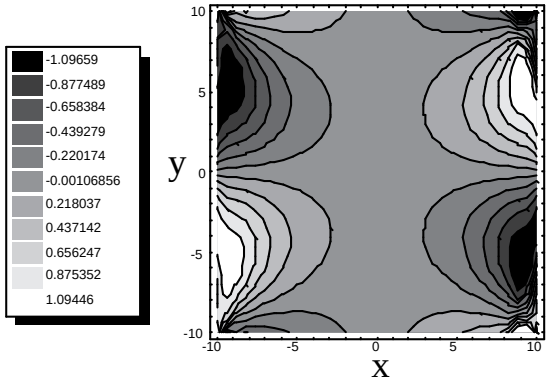

Figure 6.34: $\overline{N}_y$ as a function of panel location for $[\pm(45\langle 45|75\rangle)]_{9s}$ made by the parallel fiber method

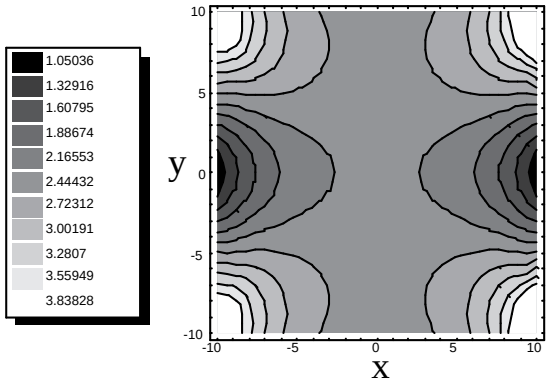

Figure 6.35: $\overline{N}_{xy}$ as a function of panel location for $[\pm(45\langle 45|75\rangle)]_{9s}$ made by the parallel fiber method

shear stress resultants, Figure 6.35, also have a beneficial distribution with the center portion of the panel not experiencing exceptionally high $\overline{N}_{xy}$.

6.2 Buckling Analysis of Shifted and Parallel Fiber, Variable-Stiffness Laminates Subjected to Shear Loading

The buckling response of shifted and parallel fiber, variable-stiffness laminates under applied shear deformation is examined next. The critical buckling loads for these laminates are determined using the Ritz method. The critical shear buckling loads of these laminates will be compared to the straight fiber $[\pm 45]_{9s}$ laminate. As with the uniform end shortening loading, several different types of variable-stiffness laminates are explored. Initially, these will consist of the four types used in the in-plane shear analysis. Finally, $\pm 45^o$ plies will be added to either the surface of midplane of the laminate to see how they affect the critical loading of the panel.

6.2.1 Formulation of the Buckling Analysis For Shear Loading of Variable-Stiffness Laminates

As with the case of laminates under uniform end shortening, it is desirable to determine a single quantity that describes the shear loading of variable-stiffness laminates. This will offer convenience in defining the critical buckling loads and equivalent shear stiffness for these laminates. Before this can be done, it is necessary to examine the loadings applied by creating in-plane shear deformation. These loadings will be determined by considering the stress resultants along the edges of the panel.

Determining the shear loading for a straight fiber $[\pm 45]_{9s}$ laminate is considered first since its stress resultants do not vary with position. A force normal and tangential to each edge can be

found if the stress resultants are integrated along each edge. These forces for the $[\pm 45]_{9s}$ laminate are shown in Figure 6.36. It is clear that the primary load is the shear force, $21,400 lbs$, while small compressive loads in the x and y directions of 13 and $10 lbs$, respectively, are present. Therefore, for this or any other straight fiber laminate under applied in-plane shear deformation, it is sufficient to consider the shearing force along a single edge when defining an average shear stress resultant.

Determining the shearing force acting on a variable-stiffness laminate is not as straight forward as for the straight fiber case. For example, consider the stress resultant distribution for a $[0 \pm \langle 45|75 \rangle]_{9s}$ laminate under in-plane shear deformation, Figures 6.3-6.5. From these stress resultant distributions, the total force applied to the edges of the panels can be found and are given in Figure 6.37. Similar to the case with $[\pm 45]_{9s}$, the net compressive loadings in the x and y directions are relatively small compared to the shearing forces. The shear forces acting along the top and bottom edges of the panel, $y = \pm b/2$, are greater than the shear force acting along the left and right edges, $x = \pm a/2$. When verifying that the panel is in equilibrium, the summation of forces in the x and y directions clearly equal zero. However, the moments created by the two shear force couples are not equal and opposite. This condition would seem to indicate that the panel is not in equilibrium. At this point, is convenient to consider the symmetric nature of the applied loading and only deal with the moments created by the loading along $x = a/2$ and $y = b/2$. If the N_x and N_y stress resultants are examined along $x = a/2$ and $y = b/2$, it becomes evident that they will contribute significant moments also about the z axis. An idealized model of this is created in Figure 6.38. This simplified model, which shows a linear variation in both N_x and N_y along the edges, shows that a moment will be created along each edge. This is in stark contrast to the $[\pm 45]_{9s}$ laminate with its constant values of N_x and N_y. Since there is no variation of N_x and N_y along an edge, there can not be a moment created by these stress resultants. The net moment found by summing the

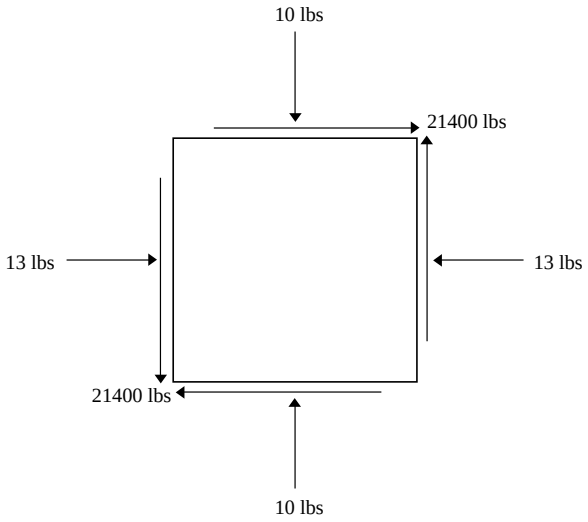

Figure 6.36: Normal and tangential forces for a $[\pm 45]_{9s}$ laminate under in-plane shear deformation.

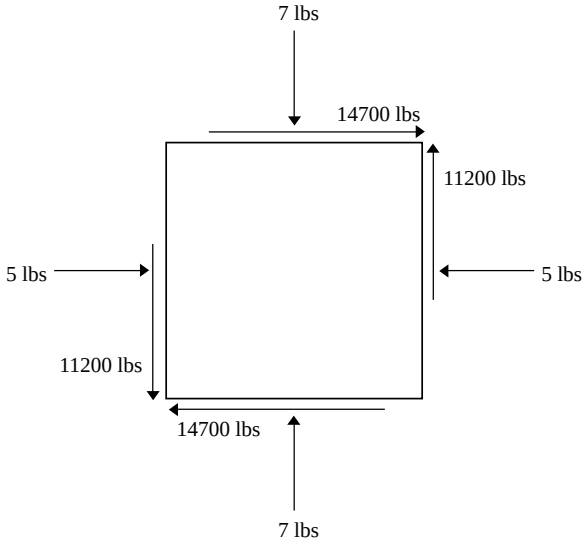

Figure 6.37: Normal and tangential forces for a $[0 \pm \langle 45|75\rangle]_{9s}$ laminate under in-plane shear deformation.

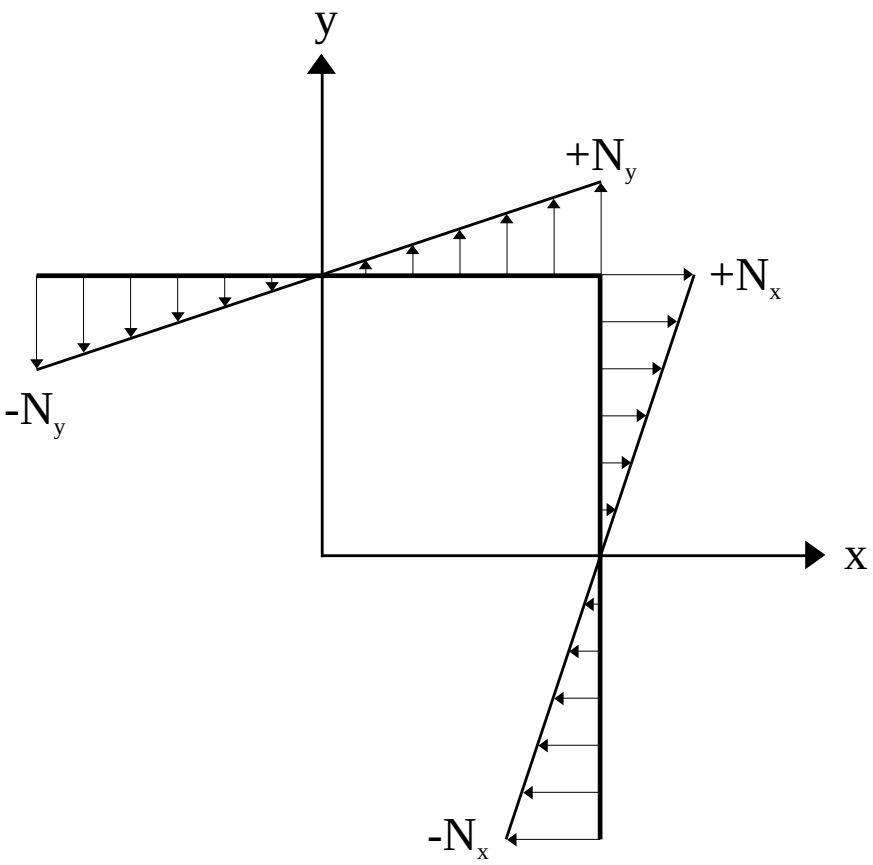

Figure 6.38: Idealized variation of $[0 \pm \langle 45|75\rangle]_{9s}$ N_y and N_x along the top and right edges of the panel.

moments created by the normal and tangential forces acting along the edges of the $[0 \pm \langle 45|75\rangle]_{9s}$ does equate to zero after the moments created by the N_x and N_y are take into account.

In order to determine an average shear load applied to a variable-stiffness panel, it is necessary to examine the effect that each stress resultant has in creating the desired shear deformation, Figure 6.1. Again, only the edges at $y = b/2$ and $x = a/2$ are considered in determining an average shear load due to the symmetry of the problem. The most obvious contribution is from N_{xy} along each edge. However, the N_x and N_y stress resultants also play a role in the applied shear deformation. The moment created by N_y along the edge at $y = b/2$ about the z axis will tend to rotate this edge of the panel in a counterclockwise direction. Similarly, the moment from the N_x distribution on the right edge of the panel will cause that edge to rotate in the clockwise direction. The effect that these moments have in creating the desired in-plane shear deformation need to be taken into consideration when determining an equivalent shear loading parameter. An average applied shear stress resultant, N_{xy}^{av}, can be found using the moments created by the N_y and N_{xy} along $y = b/2$ and N_x and N_{xy} along $x = a/2$. The moments due to each stress resultant are defined as follows:

$$M_z^i = \int_{-a/2}^{a/2} x N_y(x, b/2) dx \,, \tag{6.3}$$

$$M_z^{ii} = \int_{-b/2}^{b/2} y N_x(a/2, y) dy \,, \tag{6.4}$$

$$M_z^{iii} = -b/2 \int_{-a/2}^{a/2} N_{xy}(x, b/2) dx \,, \tag{6.5}$$

$$M_z^{iv} = a/2 \int_{-b/2}^{b/2} N_{xy}(a/2, y) dy \tag{6.6}$$

where M_z^i is the moment about the z axis by the N_y acting along the top of the panel, M_z^{ii} is the moment about the z axis by the N_x acting along the right edge of the panel, and M_{xy}^{iii} and M_{xy}^{iv} are

the moments created by N_{xy} acting along the top and right edges of the panel, respectively. In each case, the moments were calculated so that a counterclockwise moment is positive. For laminates under positive in-plane shear deformation, M_{xy}^{iii} will be negative and M_{xy}^{iv} positive. However, the signs on M_z^i and M_z^{ii} can not be predetermined. Therefore, the resulting negative and positive moments, M_{neg} and M_{pos}, respectively, can be expressed as:

$$M_{neg} = M_z^{iii} + \left\{ \begin{array}{ll} 0, & M_z^i \geq 0 \\ M_z^i, & M_z^i < 0 \end{array} \right\} + \left\{ \begin{array}{ll} 0, & M_z^{ii} \geq 0 \\ M_z^{ii}, & M_z^{ii} < 0 \end{array} \right\} , \tag{6.7}$$

$$M_{pos} = M_z^{iv} + \left\{ \begin{array}{ll} M_z^i, & M_z^i \geq 0 \\ 0, & M_z^i < 0 \end{array} \right\} + \left\{ \begin{array}{ll} M_z^{ii}, & M_z^{ii} \geq 0 \\ 0, & M_z^{ii} < 0 \end{array} \right\} . \tag{6.8}$$

These moments, M_{neg} and M_{pos}, should be exactly equal and opposite. However, due to to nature of the solution from ELLPACK and the use of numerical integration, there will be a slight deviation between the magnitudes of the two moments. In order to minimize the effect of this variation, an average of the two moments and the corresponding distance from the center of the panel to the edges are used to determine N_{xy}^{av} as follows:

$$N_{xy}^{av} = \frac{\frac{2}{b^2}\left|M_{neg}\right| + \frac{2}{a^2}M_{pos}}{2} . \tag{6.9}$$

The remaining quantities of interest can now be defined in terms of this average shear stress resultant. An equivalent shear stiffness is found using Hooke's law for shearing stress and strain with the prescribed shear displacements:

$$G_{xy}^{eq} = \frac{N_{xy}^{av}}{h \sin^{-1}(\frac{2\delta_0}{a})} \tag{6.10}$$

where δ_0 is the vertical component of the shear deformation. The normalized shear stiffness, $\overline{G}_{xy}^{av} = G_{xy}^{av}/G_{12}$, gives a relative indication of the shear stiffness of the laminate compared to that

of an all 0^o or 90^o laminate. A value of 2.0 represents a laminate that is twice as resistant to shear as a laminate composed entirely of 0^o or 90^o plies.

The Ritz method is used to determine the critical buckling load, as it was for the uniform end shortening load case. When considering shear loading, the eigenvalues of Equation 5.15 have both positive and negative signs. Analysis of the sign revealed than the negative eigenvalues correspond to negative shear loading of the panel. For many laminates, the sign of the shear load will be important. For example, a laminate such as $[45]_{18s}$ will have a large buckling load under positive shear but a relatively small one under negative shear loading. While other laminates, such as $[\pm 45]_{9s}$ and $[0 \pm \langle 45|75\rangle]_{9s}$, will have critical buckling loads that are identical under positive of negative shear. The analysis considers both positive and negative shears to be valid loading conditions. As such, the critical eigenvalue, λ_{cr}, is defined to be the eigenvalue with the smallest magnitude. Therefore, the average critical shear buckling load is defined as

$$N^{av}_{xycr} = \lambda_{cr} N^{av}_{xy} \ . \tag{6.11}$$

The normalized critical buckling load is then obtained using the same normalization term used with the uniaxial loading case

$$\overline{N}^{av}_{xycr} = \frac{a^2 N^{av}_{xycr}}{E_1 h^3} \ . \tag{6.12}$$

6.2.2 Critical Buckling Load of Shifted Fiber Laminates

The critical buckling loads for the shifted fiber laminates are examined first. Four different values of ϕ will be examined: $\phi = 0^o, 90^o, 45^o,$ and $\pm 45^o$. For each case, the values of T_0 will range from 0^o to 90^o and T_1 will be between -45^o and 90^o. Both T_0 and T_1 will be adjusted in 15^o increments so as to reduce the number of analyses to a more manageable number while still providing a fairly

continuous distribution of buckling loads for a given value of ϕ.

Critical Shear Buckling Load for Shifted Fiber $[\mathbf{0} \pm \langle \mathbf{T_0} | \mathbf{T_1} \rangle]_{\mathbf{9s}}$ Laminates

The normalized critical shear buckling load, $\overline{N}^{av}_{xycr}$, for $[0 \pm \langle T_0|T_1\rangle]_{9s}$ made by the shifted fiber method can be seen in Figure 6.39. The straight fiber laminate that these laminates are compared to is a $[\pm 45]_{9s}$ laminate which has a normalized critical buckling load of 3.988. Several of the variable-stiffness laminates with $\phi = 0^o$ are able to improve upon the critical buckling load of the straight fiber laminate. The largest critical buckling load for this class of laminates is a $[0 \pm \langle 0|45\rangle]_{9s}$ laminate with buckling load of 4.660. This is a 17% increase over the straight fiber laminate. As was the case with the in-plane response of the $[0 \pm \langle 45|75\rangle]_{9s}$ laminate, this laminate will tend to have the non-zero N_x and N_y confined near the edges of the panel which helps increase the buckling load. However, the N_{xy} for the $[0 \pm \langle 0|45\rangle]_{9s}$ laminate were also localized in the vicinity of the simply supported edges. As such, it was able to significantly increase the critical buckling load of the laminate.

Critical Shear Buckling Load for Shifted Fiber $[\mathbf{90} \pm \langle \mathbf{T_0} | \mathbf{T_1} \rangle]_{\mathbf{9s}}$ Laminates

The normalized critical shear buckling load, $\overline{N}^{av}_{xycr}$, for $[90 \pm \langle T_0|T_1\rangle]_{9s}$ made by the shifted fiber method is presented in Figure 6.40. As expected the critical shear buckling loads of shifted fiber laminates with $\phi = 90^o$ are similar to those of laminates having $\phi = 0^o$. The T_0 and T_1 values for the best laminate for this case is the same as that for $\phi = 0^o$, 0^o and 45^o, respectively. It turns out that the normalized critical shear buckling load for $[90 \pm \langle 0|45\rangle]_{9s}$ laminate is 4.666 which is also a 17% increase over the best straight fiber laminate. This is virtually identical to the buckling load for a $[0 \pm \langle 0|45\rangle]_{9s}$. The similarities in both the critical buckling loads and in-plane stress

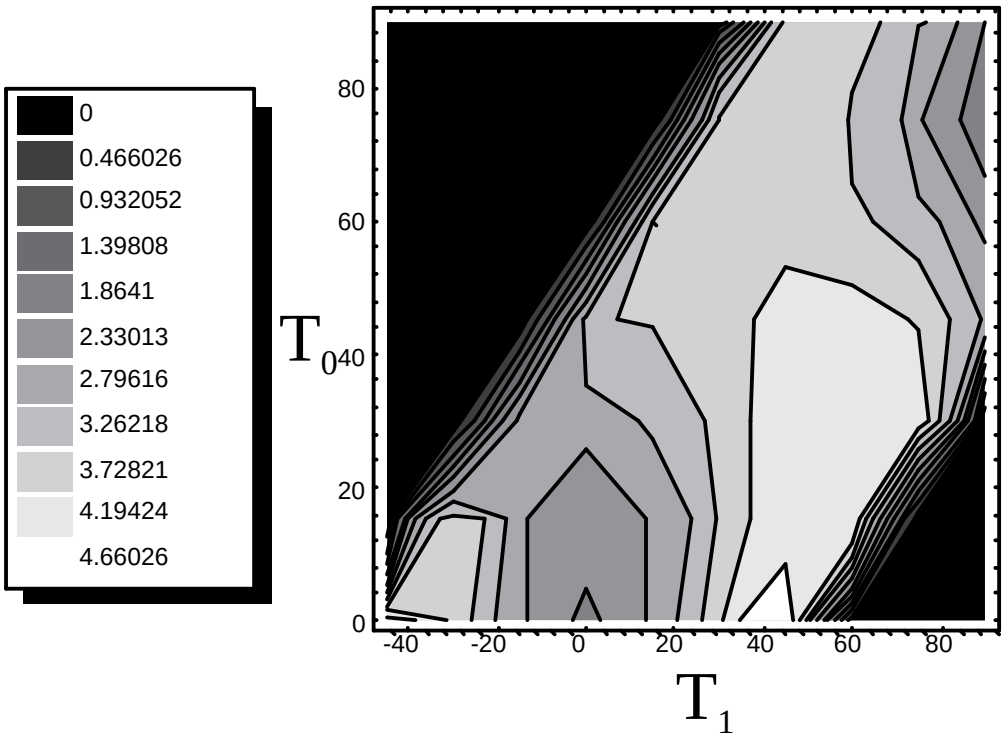

Figure 6.39: $\overline{N}^{av}_{xycr}$ for $[0 \pm \langle T_0|T_1\rangle]_{9s}$ made by the shifted fiber method

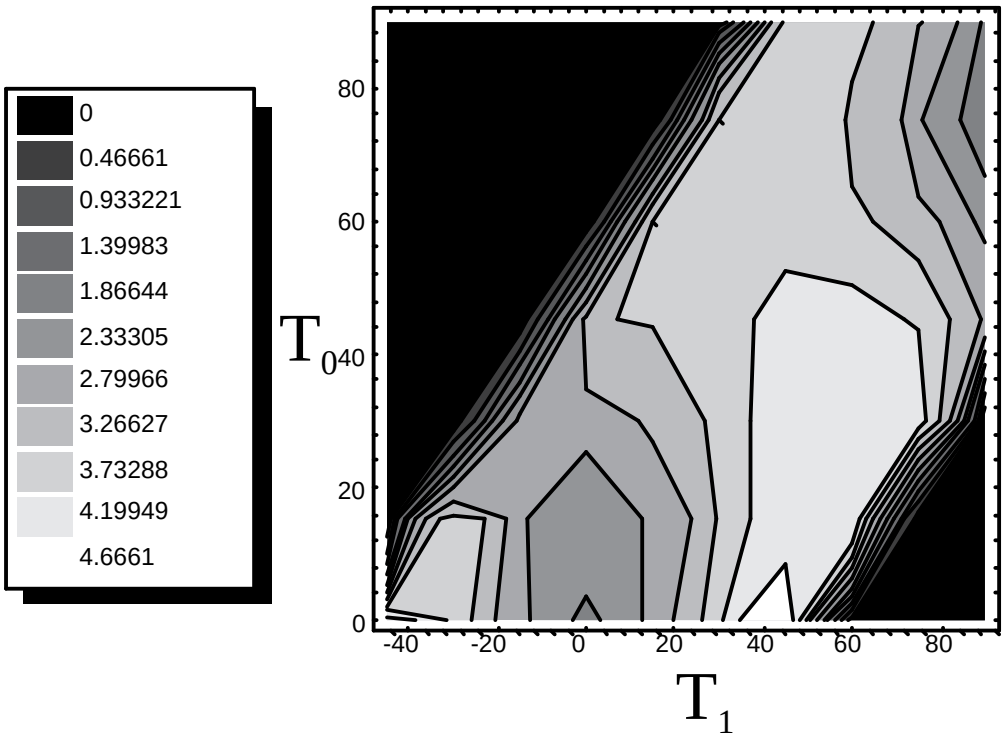

Figure 6.40: $\overline{N}^{av}_{xycr}$ for $[90 \pm \langle T_0|T_1\rangle]_{9s}$ made by the shifted fiber method

distributions for $[0 \pm \langle T_0|T_1\rangle]_{9s}$ and $[90 \pm \langle T_0|T_1\rangle]_{9s}$ laminates confirm that the response of these laminates has a minimal dependence on the sign of the applied shear.

Critical Shear Buckling Load for Shifted Fiber $[\mathbf{45 \pm \langle T_0|T_1\rangle]_{9s}}$ Laminates

The normalized critical shear buckling loads for the shifted fiber $[45 \pm \langle T_0|T_1\rangle]_{9s}$ are shown in Figure 6.41. The largest buckling load is obtained with a $[45 \pm \langle 30|60\rangle]_{9s}$ laminate that has a normalized critical buckling load of 3.026. Two other laminates also had buckling loads that were significantly larger than the typical shifted fiber laminate of the form $[45 \pm \langle T_0|T_1\rangle]_{9s}$. Those laminates were $[45 \pm \langle 45|45\rangle]_{9s}$ and $[45 \pm \langle 60|15\rangle]_{9s}$ with normalized shear buckling loads of 2.490 and 2.730, respectively. Overall, this group of laminates have very low critical buckling values. The primary reason for this is that most laminates with fiber orientation varying along a single axis not aligned with a geometric axes of the panel have critical buckling loads that are sensitive to the shear loading direction. The critical buckling loads for several variable-stiffness laminates with different values of ϕ are given in Table 6.1. (Note: $\left(\overline{N}^{av}_{xycr}\right)^{+}_{min}$ denotes the smallest critical buckling load under positive shear and $\left(\overline{N}^{av}_{xycr}\right)^{-}_{max}$ is the largest under negative shear.) The critical shear buckling loads for the laminate under positive and negative shear loading, respectively. It is clear from Table 6.1 that laminates with $\phi = 45^o$ can have extremely different buckling loads depending on the direction of the shear loading while having other laminates that do not exhibit a dependence on shear direction. This is in contrast to both the $\phi = 0^o$ and $\phi = 90^o$ shifted fiber laminates which tend to have critical shear buckling loads that are almost independent upon shear direction for every laminate. The critical eigenvalue and the prebuckled stress resultants combine to determine the critical buckling load for a given laminate. As such, the $[45 \pm \langle T_0|T_1\rangle]_{9s}$ class of laminates were not able to improve upon the straight fiber configuration.

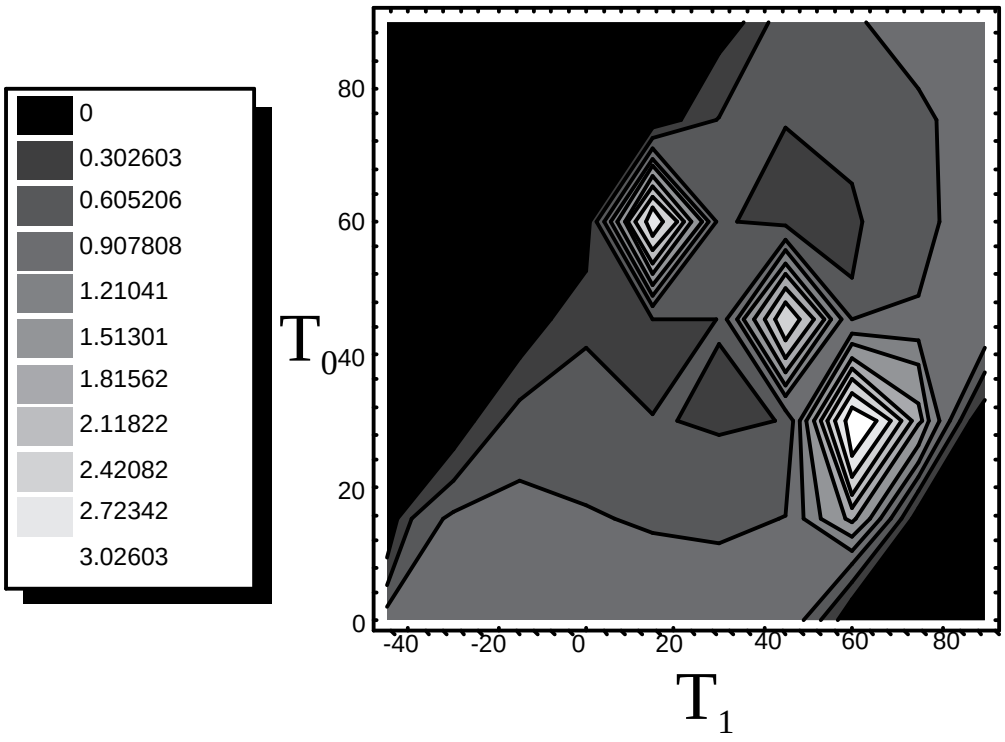

Figure 6.41: $\overline{N}^{av}_{xycr}$ for $[45 \pm \langle T_0|T_1\rangle]_{9s}$ made by the shifted fiber method

Table 6.1: Critical buckling loads for shifted fiber laminates under positive and negative shear, $\left(\overline{N}^{av}_{xycr}\right)^{+}_{min}$ and $\left(\overline{N}^{av}_{xycr}\right)^{-}_{max}$, respectively.

Laminate	$\left(\overline{N}^{av}_{xycr}\right)^{+}_{min}$	$\left(\overline{N}^{av}_{xycr}\right)^{-}_{max}$
$[0 \pm \langle 45 \vert 75 \rangle]_{9s}$	3.776	-3.784
$[90 \pm \langle 45 \vert 75 \rangle]_{9s}$	3.773	-3.784
$[45 \pm \langle 45 \vert 45 \rangle]_{9s}$	2.490	-2.536
$[45 \pm \langle 30 \vert 60 \rangle]_{9s}$	5.296	-3.026
$[45 \pm \langle 60 \vert 15 \rangle]_{9s}$	2.730	-2.812

Critical Shear Buckling Load for Shifted Fiber $[\pm(45\langle \mathbf{T_0}|\mathbf{T_1}\rangle)]_{9s}$ Laminates

The normalized critical shear buckling loads for the shifted fiber $[\pm(45\langle T_0|T_1\rangle)]_{9s}$ are shown in Figure 6.42. This fiber format shows the largest increase in critical shear buckling load compared to $[\pm 45]_{9s}$ among the laminates that have been examined. The largest normalized buckling load was that of a $[\pm(45\langle 15|60\rangle)]_{9s}$ with $\overline{N}^{av}_{xycr} = 5.817$ which is an improvement of 46% over $[\pm 45]_{9s}$. There are several explanations for the improvement over both $[\pm 45]_{9s}$ and the other shifted fiber, variable-stiffness laminates. The first is that, from the in-plane analysis, the laminates with $\phi = \pm 45^o$ redistribute the loading so that the largest stress resultants do not combine in a detrimental fashion within in a given region, as was the case for $[45 \pm \langle 45|75\rangle]_{9s}$. Another factor that helped these laminates improve the buckling load is that, unlike the $[0 \pm \langle 45|75\rangle]_{9s}$ and $[90 \pm \langle 45|75\rangle]_{9s}$ laminates, a large portion of the shear loading is transferred to regions close to the simply supported edges which will delay the onset of buckling.

6.2.3 Critical Buckling Load of Parallel Fiber Laminates

The same search performed with the shifted fiber laminates will be utilized to examine the critical shear buckling loads for parallel fiber laminates. As previously explained in Section 4.2, parallel fiber laminates experience a more restrictive curvature constraint which reduces the number of acceptable designs.

Critical Shear Buckling Load for Parallel Fiber $[\mathbf{0} \pm \langle \mathbf{T_0}|\mathbf{T_1}\rangle]_{\mathbf{9s}}$

The normalized critical shear buckling loads, $\overline{N}^{av}_{xycr}$, for parallel fiber $[0 \pm \langle T_0|T_1\rangle]_{9s}$ are shown in Figure 6.43. The $[0 \pm \langle 45|30\rangle]_{9s}$ laminate has the largest critical shear buckling load at 4.289. This is a 7.5% improvement over the critical shear buckling load of $[\pm 45]_{9s}$, 3.988. Despite having

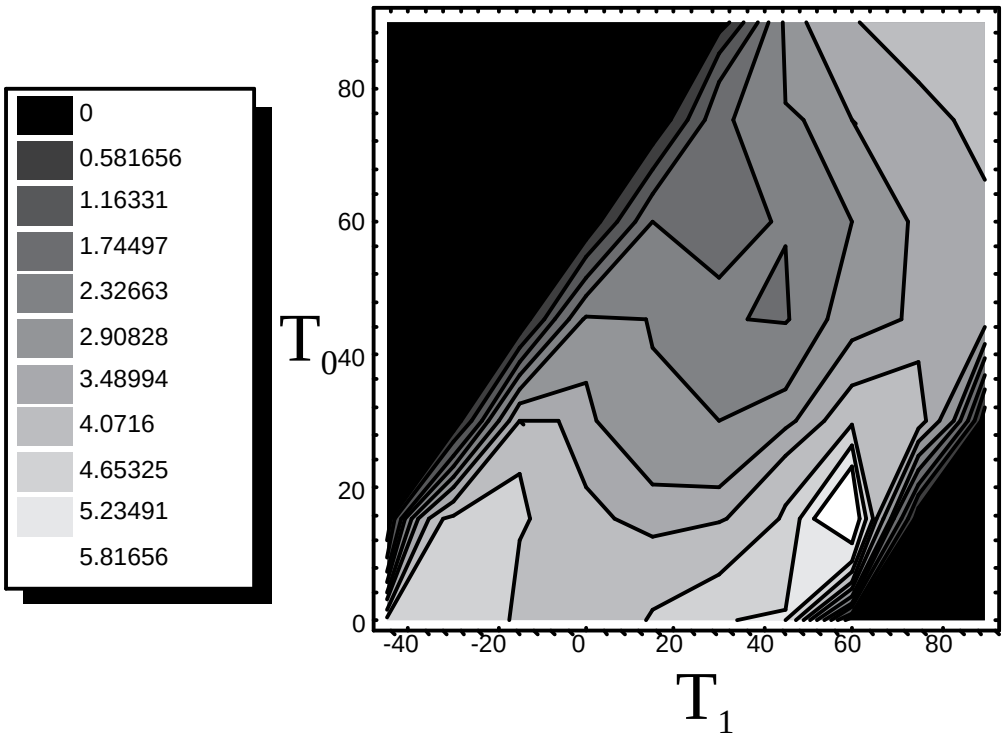

Figure 6.42: $\overline{N}^{av}_{xycr}$ for $[\pm(45\langle T_0|T_1\rangle)]_{9s}$ made by the shifted fiber method

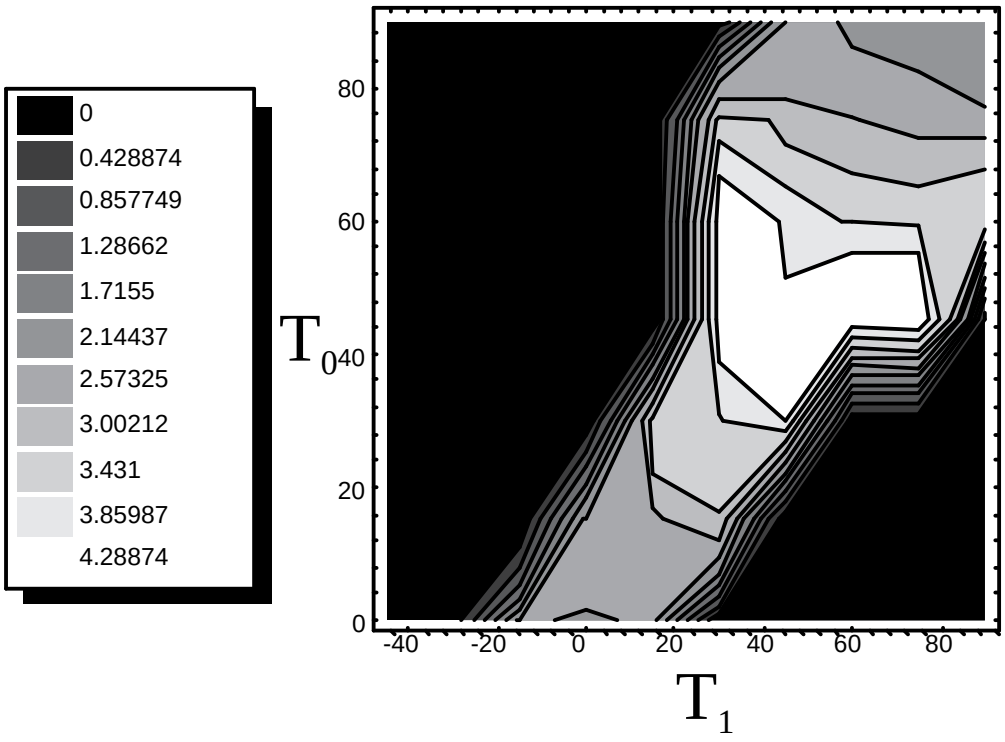

Figure 6.43: $\overline{N}^{av}_{xycr}$ for $[0 \pm \langle T_0|T_1\rangle]_{9s}$ made by the parallel fiber method

a more stringent constraint on fiber curvature than the shifted fiber laminates, the parallel fiber laminates with $\phi = 0^o$ still offered improved performance compared to the straight fiber $[\pm 45]_{9s}$. This is primarily due to the reduced shear stresses over the center portion of the panel for the parallel fiber. This slight reduction in shear stress delays the onset of buckling until a higher shear load is reached.

Critical Shear Buckling Load for Parallel Fiber $[\mathbf{90} \pm \langle \mathbf{T_0} | \mathbf{T_1} \rangle]_{\mathbf{9s}}$

$\overline{N}^{av}_{xycr}$ for parallel fiber $[90 \pm \langle T_0 | T_1 \rangle]_{9s}$ are shown in Figure 6.44. The largest $\overline{N}^{av}_{xycr}$ for laminates with $\phi = 90^o$ is a $[90 \pm \langle 45 | 75 \rangle]_{9s}$ laminate with a value of 4.301. This is an 7.8% increase over the best straight fiber laminate. The fiber paths of this laminate are similar to those of the parallel fiber $[0 \pm \langle 45 | 30 \rangle]_{9s}$. The only major difference is that there is a slightly greater curvature with the $\phi = 90^o$ laminate which allows for better load redistribution characteristics. This appears in the form of a 1.32% increase in critical buckling load of the $[90 \pm \langle 45 | 75 \rangle]_{9s}$ over $[0 \pm \langle 45 | 30 \rangle]_{9s}$. Overall, similar critical buckling loads can be obtained with either $\phi = 0^o$ or $\phi = 90^o$. The slight differences in buckling loads are a result of having truly parallel fiber paths.

Critical Shear Buckling Load for Parallel Fiber $[\mathbf{45} \pm \langle \mathbf{T_0} | \mathbf{T_1} \rangle]_{\mathbf{9s}}$

The normalized critical shear buckling loads, $\overline{N}^{av}_{xycr}$, for parallel fiber $[45 \pm \langle T_0 | T_1 \rangle]_{9s}$ are shown in Figure 6.45. Parallel fiber laminates with reference fiber orientation varying only along a single axis not aligned with a geometric axis of the panel, $\phi = 45^o$ in this case, have critical shear buckling loads that are strongly influenced by the sign of the applied shear deformation. This is identical to the shifted fiber $[45 \pm \langle T_0 | T_1 \rangle]_{9s}$ laminates. For the parallel fiber case the best $\overline{N}^{av}_{xycr}$ is for $[45 \pm \langle 45 | 45 \rangle]_{9s}$ with 2.490. (Note: this laminate, as with the shifted fiber one, is equivalent

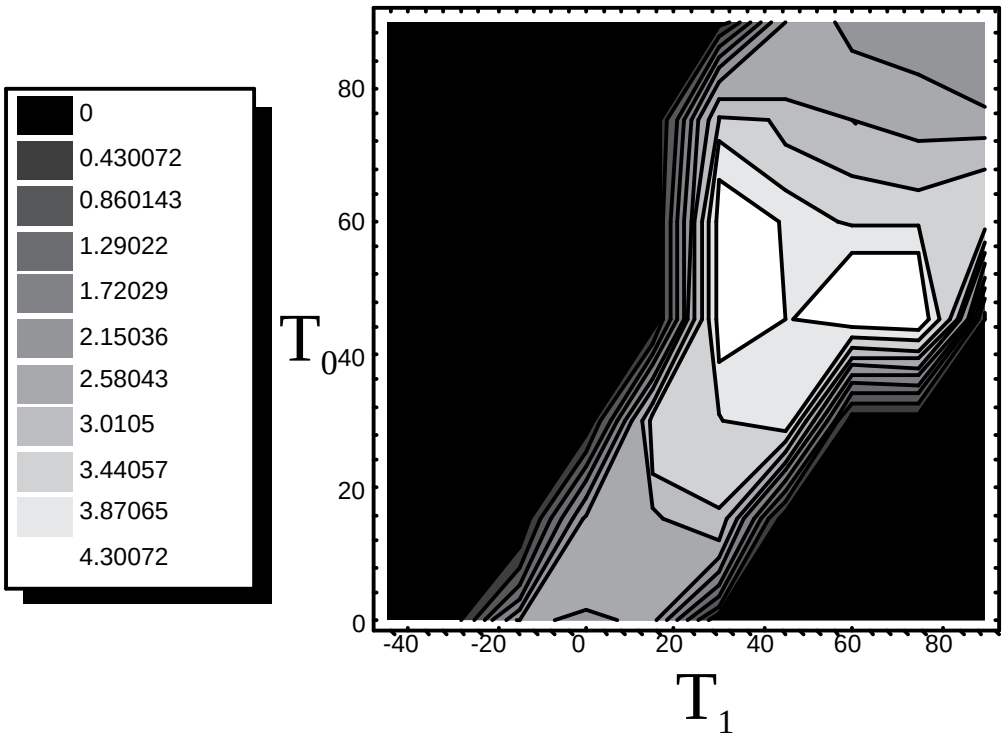

Figure 6.44: $\overline{N}^{av}_{xycr}$ for $[90 \pm \langle T_0|T_1\rangle]_{9s}$ made by the parallel fiber method

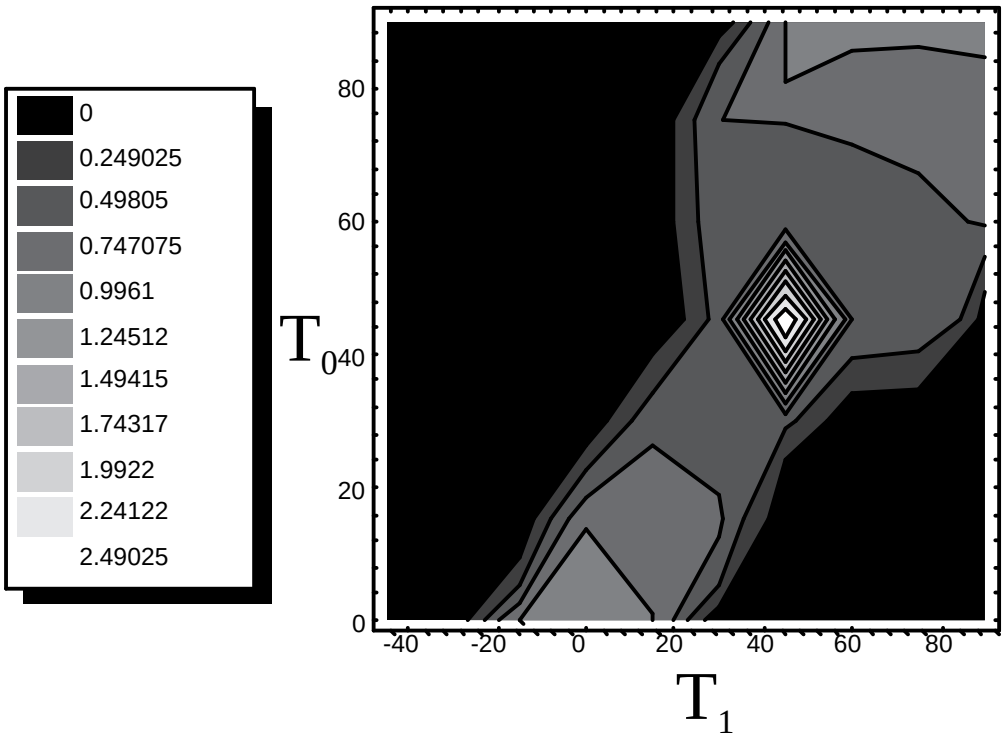

Figure 6.45: $\overline{N}^{av}_{xycr}$ for $[45 \pm \langle T_0|T_1\rangle]_{9s}$ made by the parallel fiber method

to a $[0/90]_{9}s$ straight fiber laminate.) This laminate was the only one not to have a significant dependence on the shear sign. Despite being independent on the sign of the shear loading, the performance of the parallel fiber $[45 \pm \langle 45|45\rangle]_{9s}$ was dismal compared to $[\pm 45]_{9s}$ as shown by a 38% decrease in shear buckling load.

Critical Shear Buckling Load for Parallel Fiber $[\pm(45\langle \mathbf{T_0}|\mathbf{T_1}\rangle)]_{\mathbf{9s}}$

The normalized critical shear buckling loads for the parallel fiber $[\pm(45\langle T_0|T_1\rangle)]_{9s}$ are shown in Figure 6.46. The largest critical shear buckling load for this type of laminate is $[\pm(45\langle 0|15\rangle)]_{9s}$ with 4.287, a 7.5% increase over $[\pm 45]_{9s}$. While this increase is almost as large as the $[90 \pm \langle 45|75\rangle]_{9s}$, it is not close to the shifted fiber $[\pm(45\langle 15|60\rangle)]_{9s}$ laminate with $\overline{N}^{av}_{xycr} = 4.996$. The reason for this is that the shifted fiber laminate, as was the case for uniaxial loading, is able to redistribute the applied loading to a greater degree compared to the parallel fiber case.

6.3 Equivalent Shear Stiffness

The equivalent shear stiffness of variable-stiffness laminates, Equation (6.10), will be presented for shifted and parallel fiber laminates of the form $[\phi \pm \langle T_0|T_1\rangle]_{9s}$ where $\phi = 0^0, 45^o, 90^o$. and $[\pm(45\langle T_0|T_1\rangle)]_{9s}$. In each case, the values of T_0 and T_1 will vary from 0^o to 90^o and -45^o to 90^o, respectively. The goal of this section is to compare the relative resistance of the variable-stiffness laminates to the applied shear loading. As previously explained, the equivalent shear stiffness has been normalized so that if $\overline{G}^{eq}_{xy} = 1$, then the laminate has a shear stiffness equivalent to an all 0^o or 90^o laminate. The comparison, as was the case for the shear buckling of the shifted fiber laminates, will be against $[\pm 45]_{9s}$ since it not only has the largest critical shear buckling load but also the largest normalized equivalent shear stiffness of 6.755.

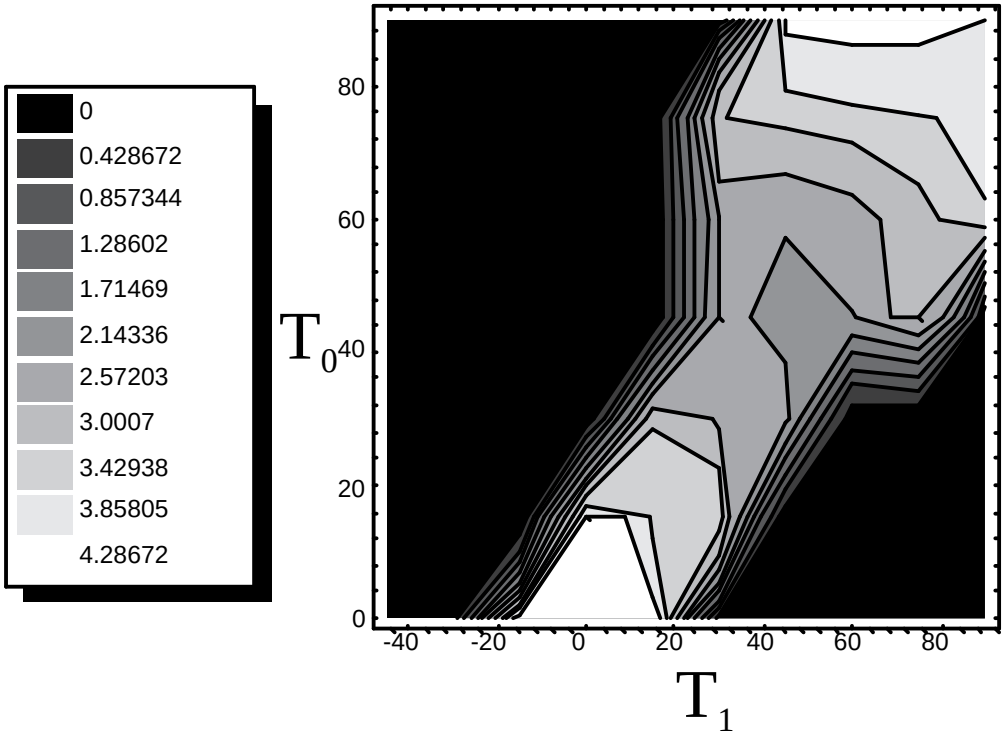

Figure 6.46: $\overline{N}^{av}_{xycr}$ for $[\pm(45\langle T_0|T_1\rangle)]_{9s}$ made by the parallel fiber method

Only three examples of the equivalent shear stiffness will be presented. The reason for this is that the same trends are provided in each example. The three equivalent shear stiffness plots, Figures 6.47–6.49, are for shifted fiber laminates of the form $[0 \pm \langle T_0|T_1\rangle]_{9s}$ and $[90 \pm \langle T_0|T_1\rangle]_{9s}$ and parallel fiber laminates for the form $[45 \pm \langle T_0|T_1\rangle]_{9s}$, respectively. Regardless of the laminate being created using a shifted or parallel fiber method, the equivalent shear stiffness has a maximum value equivalent to the $[\pm 45]_{9s}$. This maximum value will only occur when the variable-stiffness laminate is describing a $[\pm 45]_{9s}$ laminate. One such laminate is the shifted fiber $[0 \pm \langle 45|45\rangle]_{9s}$. Therefore, the largest shear stiffnesses will occur for laminates with fiber orientations that are approximately 45^o from a geometric axis of the panel.

6.4 Performance Enhancements for Variable-Stiffness Laminates Under Shear Loading

Due to the complexity involved in the shear loading of variable-stiffness panels, only one method is presented for increasing the performance of variable-stiffness laminates under applied in-plane shear loading. The resulting largest critical buckling loads with $\pm 45^o$ plies on the surface for the four cases previously examined are given in Table 6.2. None of the laminates that were examined exceeded the performance offered by the shifted fiber $[\pm (45\langle 15|60\rangle)]_{9s}$ laminate. The primary reason for this is that the addition of the $\pm 45^o$ plies disturbed the load redistribution to such an extent as to negate benefits which accompany the increase in the D matrix terms. Since the other laminates do not exhibit the beneficial load redistribution to the degree that the $[\pm (45\langle 15|60\rangle)]_{9s}$ does, their buckling loads are improved by adding the $\pm 45^o$ at the surface which increase the D matrix.

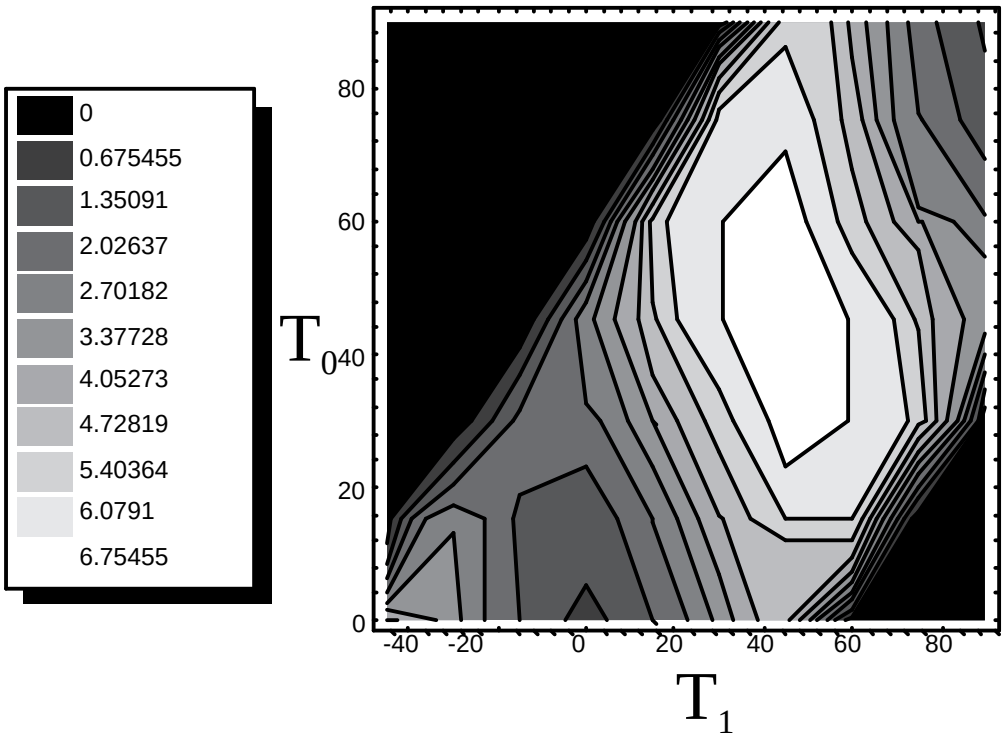

Figure 6.47: $\overline{G}_{xy}^{eq}$ for $[0 \pm \langle T_0 | T_1 \rangle]_{9s}$ made by the shifted fiber method.

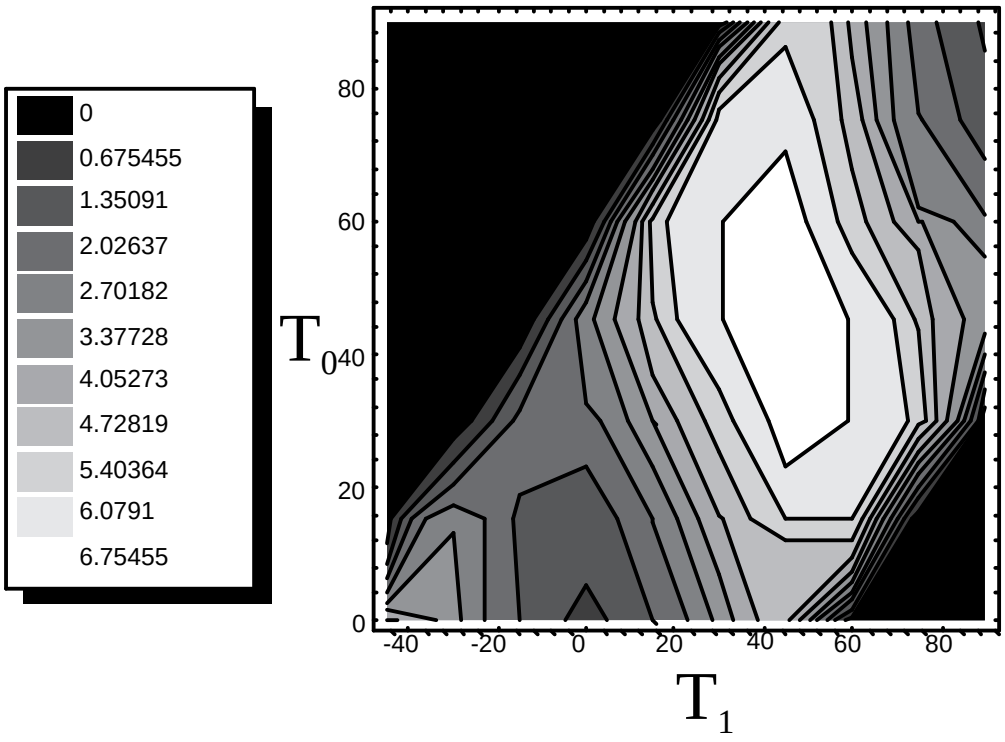

Figure 6.48: $\overline{G}_{xy}^{eq}$ for $[90 \pm \langle T_0|T_1\rangle]_{9s}$ made by the shifted fiber method.

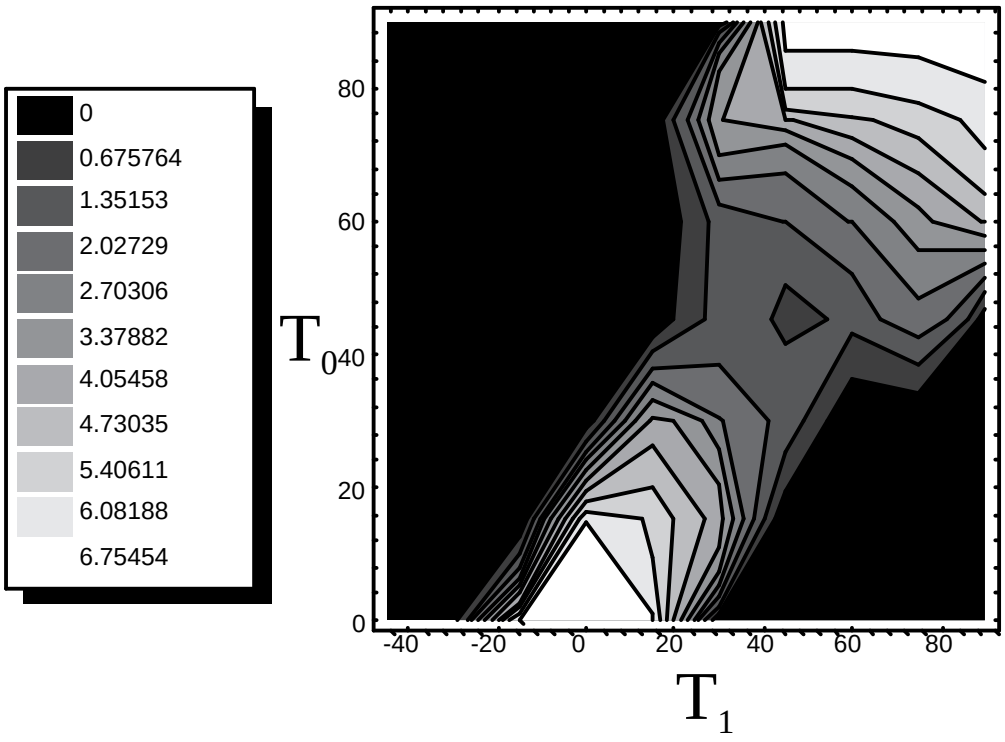

Figure 6.49: $\overline{G}_{xy}^{eq}$ for $[45 \pm \langle T_0|T_1\rangle]_{9s}$ made by the parallel fiber method.

Table 6.2: Critical buckling load for shifted fiber, variable stiffness laminates with $\pm 45^o$ plies placed on the surface of the laminate.

Laminate	$\overline{N}^{av}_{xycr}$
$[\pm (45\langle 15\vert 60\rangle)]_{9s}$	5.815
$[\pm 45/ (0 \pm \langle 0\vert 45\rangle)_8]_s$	4.726
$[\pm 45/ (90 \pm \langle 0\vert 45\rangle)_8]_s$	4.735
$[\pm 45/ (45 \pm \langle 30\vert 60\rangle)_8]_s$	3.255
$[\pm 45/ \pm (45\langle 15\vert 60\rangle)_8]_s$	5.320

The results from the addition of ± 45 plies on the surface of parallel fiber laminates are provided in Table 6.3. For parallel fiber laminates, the additional ± 45 plies on the surface were not able to increase the largest critical buckling load for three out of the four classes considered. The only improvement occurred in the $\phi = 45^o$ case which offered, by far, the lowest initial maximum buckling load. By adding these plies, the best laminates in each class, $[\pm 45/\left(0 \pm \langle 45|30\rangle\right)_8]_s$, $[\pm 45/\left(90 \pm \langle 45|75\rangle\right)_8]_s$, and $[\pm 45/ \pm \left(45\langle 0|15\rangle\right)_8]_s$, offer virtually identical critical shear buckling loads. However, each of these fell slightly short of the critical buckling load for the $[90 \pm \langle 45|75\rangle]_{9s}$.

6.5 Critical Buckling Loads of Variable-Stiffness Laminates Under Uniaxial and Shear Loadings

The design of a structure often involves multiple load scenarios such uniaxial, torsion, and bending. This section will show the buckling loads for variable-stiffness laminates under both uniaxial and shear loadings. The loads are assumed to occur at different times so interactive effects are not taken into account.

The comparison between laminates will begin by considering the straight fiber laminate with largest critical uniaxial and shear buckling loads, $[\pm 45]_{9s}$. Next, the shear buckling load will be determined for the variable-stiffness laminates which had the largest uniaxial buckling load. Then the laminates which have the largest shear buckling loads will be analyzed to determine their uniaxial buckling load. Table 6.4 summaries the results of this search. This table shows the difficulty in designing a variable-stiffness laminate for multiple load cases. The general trend is that the laminates which have excellent performance under one loading condition are deficient in the other. The primary reason for this is the manner in which the search for laminates was conducted.

Table 6.3: Critical buckling load for parallel fiber, variable stiffness laminates with $\pm 45^o$ plies placed on the surface of the laminate.

Laminate	$\overline{N}^{av}_{xycr}$
$[90 \pm \langle 45 \vert 75 \rangle]_{9s}$	4.301
$[\pm 45/\left(0 \pm \langle 45 \vert 30 \rangle\right)_8]_s$	4.227
$[\pm 45/\left(90 \pm \langle 45 \vert 75 \rangle\right)_8]_s$	4.276
$[\pm 45/\left(45 \pm \langle 45 \vert 45 \rangle\right)_8]_s$	2.961
$[\pm 45/ \pm \left(45 \langle 0 \vert 15 \rangle\right)_8]_s$	4.260

Table 6.4: Summary of gains in critical buckling loads of shifted and parallel fiber variable-stiffness laminates under (i) uniaxial and (ii) shear loading.

Laminate	Fiber Type	$\overline{N}^{av}_{xcr}$	% increase in $\overline{N}^{av}_{xcr}$	$\overline{N}^{av}_{xycr}$	% increase in $\overline{N}^{av}_{xycr}$
$[\pm 45]_{9s}$	straight	-1.768	—	3.988	—
$[\pm \left(45 \langle 15 \vert 60 \rangle\right)]_{9s}$	shifted	-0.878	-50	5.815	+46
$[90 \pm \langle 45 \vert 75 \rangle]_{9s}$	parallel	-1.764	-0.2	4.301	+8
$[0 \pm \langle 75 \vert 30 \rangle_3 / 90 \pm \langle 30 \vert 75 \rangle_6]_s$	shifted	-3.101	+75	3.385	-15
$[0 \pm \langle 45 \vert 30 \rangle]_{9s}$	parallel	-1.792	+1.4	4.253	+6.6

It was a manual search which attempted to use intuition to predict what type of laminae might help a given laminate. As such, the most complicated stacking sequence that was dealt with involved two stacks. Despite the shortcomings of this search procedure, the parallel fiber $[0 \pm \langle 45|30 \rangle]_{9s}$ laminate was able to increase both the critical buckling under uniaxial loads as well as under shear. While the margin was only a couple of percent, it does show the possibility offered by the use of spatially varying fiber orientations to increase the tailorability of composites.

Chapter 7

Conclusions

It is possible to use a tow placement machine to create a laminate composed of plies which have spatially varying fiber orientation. Two different methods, one of which was developed during this study, were described to model these spatially varying fiber paths. In each case, the resulting fiber paths were described using fiber orientation parameters. The first method involved shifting a curvilinear reference fiber path transverse to its axis of fiber orientation variation in order to create the remaining lamina fiber paths. The method introduced in this research takes the same reference fiber path and creates the other fiber paths in the ply so that they are parallel to it. These two methods are called the shifted fiber method and parallel fiber method, respectively. The modelling of the fiber paths for both of these methods made it possible to implement constraints based on manufacturing considerations. The primary manufacturing constraint utilized in the analysis provides a limit on the amount that an individual fiber path can be curved. This constraint proved to more restrictive for the parallel fiber case since it had to account for the curvature of every fiber path in a ply rather than simply the reference fiber path curvature as in the shifted fiber case.

It is necessary to solve the governing equations of equilibrium for laminated plates in order

to determine the stress and strain fields for variable-stiffness laminates under an applied loading condition. The resulting equations form a set of coupled, elliptical, partial differential equations with variable coefficients. The software program ELLPACK implemented an iterative solution procedure using collocation to approximate the in-plane displacements. Once these displacements were found, it was possible to determine the stress and strain distribution.

The two loading conditions examined were for a square, simply supported laminate under applied uniform end shortening and in-plane shear loading. The stiffness variation inherent in variable-stiffness laminates allow the laminates to redistribute the applied loading. This load redistribution can either transfer the primary loading away from a critical region in a panel or create beneficial stress distributions in the critical region. By transferring the loading towards the simply supported edges, the shift fiber $[90 \pm \langle 30|75 \rangle]_{9s}$ laminate was able increase the critical buckling load by 44% as well as the equivalent axial stiffness by 124% compared to a straight fiber $[\pm 45]_{9s}$ laminate. Improvement over straight fiber laminates was also found for the shear loading condition. In this case, the shifted fiber $[\pm (45\langle 15|60 \rangle)]_{9s}$ laminate increased the critical shear buckling load of the panel by 46% over $[\pm 45]_{9s}$. In each load condition, the parallel fiber laminates were able to increase the critical buckling load over $[\pm 45]_{9s}$. However, the increase was not nearly as significant as for the shifted fibers. The primary reason for this is that the stiffness changes for parallel fiber laminates are not as dramatic as for the shifted fiber case.

The goal of using the variable-stiffness concept was to extend the tailorability of composite materials by allowing the ply properties to vary as a function of location. This was met by both the shifted and parallel fiber variable-stiffness laminates.

Future Work

While an attempt has been made to thoroughly examine the response of variable-stiffness laminates to in-plane loading, other considerations still exist. One is that the ability to use intuition in the design of these variable-stiffness laminates will be dramatically reduced when a more complicated loading condition is examined. Therefore, numerical optimization would be needed to find the best performance that can be gained from the variable-stiffness laminates.

At this point, there appears to be enough potential benefits in the variable-stiffness design concept to warrant a testing program. It is important to gain data on the actual response of variable-stiffness laminates created by the tow placement machines in order to verify the gains predicted by the analysis. Also, the testing would help in the creation of additional constraints which result from the manufacturing process.

Improvements can also be made in the analysis procedure. One aspect which needs refinement is the modelling of the shifted fiber paths. If the paths are to be modelled as continuous fibers, then the resulting variation in thickness should be included in the analysis. A possible application for variable-stiffness laminates is dealing with stress concentrations since they have the ability to redistribute an applied loading. Also, the use of unsymmetric variable-stiffness laminates might offer interesting advantages by providing various degrees of bend-twist coupling.

Bibliography

[1] M. T. DiNardo and P. A. Lagace, "Buckling and Postbuckling of Laminated Composites with Ply Dropoffs." *AIAA Journal*, Vol. 27 No. 10, October, 1989, pp. 1392-1398.

[2] A. W. Leissa and A. F. Martin, "Vibration and Buckling of Rectangular Composite Plates with Variable Fiber Spacing." *Composite Structures*, Vol. 14, No. 4, 1990, pp. 339-357.

[3] M. W. Hyer and R. F. Charette, "Use of Curvilinear Fiber Format in Composite Structure Design." *AIAA Journal*, Vol. 29, No. 6, June 1991, pp. 1011-1015.

[4] D. O. Evans, M. M. Vanigila, and P.C. Hopkins, "Fiber Placement Process Study." *34th International SAMPE Symposium*, Vol. 34, Book 2, May, 1989, pp. 1822-1833.

[5] J. R. Barth, "Fabrication of Complex Composite Structures Using Advanced Fiber Placement Technology." *35th International SAMPE Symposium*, Vol. 35, Book 1, April, 1990, pp. 710-720.

[6] F. Bullock, S. Kowalski, and R. Young, "Automated Prepreg Tow Placement For Composite Structures." *35th International SAMPE Symposium*, Vol. 35, Book 1, April, 1990, pp. 734-743.

[7] M. L. Enders and P. C. Hopkins, "Developments in the Fiber Placement Process." *35th International SAMPE Symposium*, Vol. 35, Book 1, April, 1991, pp. 778-790.

[8] S. W. Kandebo, "V-22 Team Lowering Osprey Production Costs." *Aviation Week and Space Technology*, Vol. 139, No. 20, November 15, 1993, pp. 58-59.

[9] V. N. Parthasarathy, S. Kodiyalam, and J. E. Davis, "Optimization of Tow Fiber Paths for Composite Design." *Proceedings of the AIAA/ASME/ASCE/AHS/ASC 36th SDM Conference*, April 10-13, 1995, New Orleans, LA, pp.1031-1041.

[10] Gürdal, Z., and Olmedo, R. A., "Composite Laminates with Spatially Varying Fiber Orientations: Variable Stifness Panel Concept." *AIAA Journal*, Vol. 31, No. 4, April 1993, pp. 601-608.

[11] Olmedo, R., and Gürdal, Z., "Buckling Response of Laminates with Spatially Varying Fiber Orientations." *Proceedings of the AIAA/ASME/ASCE/AHS/ASC 34th SDM Conference*, April 19-21, 1993, La Jolla, CA, pp. 2261-2269.

[12] Jones, R. M., *Mechanics of Composite Materials.* Hemisphere, New York, 1975.

[13] Whitney, J. M., *Structural Analysis of Laminated Anisotropic Plates.* Technomic, Lancaster, PA, 1987.

[14] Rice, J. R., and Boisvert, R. F., *Solving Elliptic Problems Using ELLPACK.* Springer-Verlag, New York, 1985.

[15] Arora, J. S., *Introduction to Optimum Design.* McGraw-Hill, Inc., New York, 1989.

Vita

Chris Waldhart was born on January 12, 1972 to Thomas and Enid Waldhart at Central Baptist Hospital in Lexington, Kentucky. He lived in several houses in Lexington with his parents and sister, Ann. In the spring of 1990, he graduated from Lafayette Senior High School. The following fall he enrolled at Virginia Tech where he decided to major in ocean engineering. Four years and many assignments later, he completed the requirements to receive a bachelor degree in ocean engineering. That fall he began his pursuit of a Master of Science in Engineering Mechanics at Virginia Tech. This document represents the final step in the attainment of this degree. He is not sure where he fits in the grand scheme of things, but he believes that life will eventually find a way to knock him wherever he belongs.

Chris Waldhart

June 6, 1994